CIRCADIAN AND METABOLIC CONTROL OF MACROPHAGE ACTIVATION IN OBESITY

A Dissertation

by

HANG XU

Submitted to the Office of Graduate and Professional Studies of
Texas A&M University
in partial fulfillment of the requirements for the degree of

DOCTOR OF PHILOSOPHY

Chair of Committee,	Chaodong Wu
Committee Members,	Stephen B. Smith
	Rosemary Walzem
	Robert C. Alaniz
	Gladys Y. Ko
Head of Department,	Boon Chew

December 2016

Major Subject: Nutrition

ABSTRACT

Macrophage inflammatory status governs inflammatory responses in metabolic tissues including adipose and liver tissues, and critically contributes to the development of diet-induced obesity and systemic insulin resistance. Therefore, regulating macrophage proinflammatory or anti-inflammatory activation can help control the diet-induced inflammation in adipose tissue and systemic insulin resistance. To better understand the control of macrophage activation status, circadian clockworks and PFKFB3 were investigated in the context of diet-induced inflammation and insulin resistance.

Through in vivo studies of bone marrow-transplanted mice fed with high fat diet (HFD) for 12 weeks, and in vitro studies on bone marrow-derived macrophages (BMDM) and co-cultures of BMDM and adipocytes, the present study demonstrated that disruption of circadian genes *Period1* and *Period2* in macrophages increases their proinflammatory activation, and exacerbates diet-induced inflammation and insulin resistance. Through similar research methods, this research showed that PFKFB3 disruption in macrophages exacerbates diet-induced adipose tissue inflammation and insulin resistance. Taken together, both the circadian clock and PFKFB3 were shown to be key regulators of macrophage activation, evidenced by that either dysregulation of circadian clock or disruption of PFKFB3 contributes to the physiological cascade by which diet-induced obesity triggers macrophage proinflammatory activation, adipose tissue inflammation, and insulin resistance.

ACKNOWLEDGEMENTS

I would like to express my deepest gratitude to my committee chair, Dr. Chaodong Wu, my current committee members, Dr. Stephen B. Smith, Dr. Rosemary Walzem, Dr. Robert C. Alaniz, and Dr. Gladys Y. Ko, and my previous committee members, Dr. David N. McMurray, and Dr. Beiyan Zhou, for their guidance and support throughout the course of my graduate study and research.

I would like to thank all Wu lab members, Honggui Li, Xin Guo, Vera Halim, Cong Meng, Shih-Lung Woo, Ya Pei, Ting Qi, Ting Guo, Xiang Hu, Jiajia Zhao, Yan Zhao, Juan Zheng, Rachel Botchlett, and the department faculty and staff for making my time at Texas A&M University a great experience. Also, I would like to thank all of the friends who have given me encouragement, support and help in the 6-year journey of pursuing PhD.

Last but not the least, thanks to my husband, Junjie Song, who has been giving me unconditional love and great support. Also, thanks to my parents and parents in law for their love, care and encouragement.

NOMENCLATURE

AU	Arbitrary Units
BMAL1	Brain Muscle ARNT-Like Protein 1
BMDM	Bone Marrow-Derived Macrophage(s)
BMT	Bone Marrow Transplantation
CCG	Clock-Controlled Genes
CLOCK	Circadian Locomotor Output Cycles Kaput
Cry	Cryptochrome
Ctrl	Control
FAS	Fatty Acid Synthase
F-2, 6-P_2	Fructose 2,6-bisphosphate
GTT	Glucose Tolerance Test
HFD	High Fat Diet
IL-4	Interleukin-4
IL-1β	Interleukin-1β
IL-6	Interleukin-6
IL-10	Interleukin-10
iPFK2	Inducible 6-phosphofructo-2-kinase
ITT	Insulin Tolerance Test
JNK	c-Jun N-terminal Kinase
LFD	Low Fat Diet

LPS	Lipopolysacharride
Luc	Luciferase
MCP-1	Monocyte Chemotactic Protein-1
NF-κB	Nuclear Factor kB
Per	Period
PFK-2/FBPase	6-phosphofructo-2-kinase/fructose-2, 6-bisphosphatase
PPAR	Peroxisome Proliferator-activated Receptor
PPARα	Peroxisome Proliferator-activated Receptor Alpha
PPARγ	Peroxisome Proliferator-activated Receptor Gamma
ROS	Reactive Oxygen Species
RT-PCR	Reverse Transcription Polymerase Chain Reaction
6PFK1	6-phosphofructo-1-kinase
SREBP-1c	Sterol Regulatory Element-Binding Protein 1c
SVC	Stromal Vascular Cell(s)
TLR-4	Toll-Like Receptor-4
TNF α	Tumor Necrosis Factor α
TZDs	Thiazolidinediones
WT	Wild-Type

TABLE OF CONTENTS

Page

LIST OF FIGURES

Page

LIST OF TABLES

Page

1. INTRODUCTION AND LITERATURE REVIEW

1.1 Introduction

Over the past decades, research has shown that chronic low-grade inflammation is a common characteristic of obesity and a critical contributor to the development of non-infectious chronic diseases, such as type II diabetes, cardiovascular disease, and certain cancers [1, 2] (Fig. 1). In the process of inflammation, macrophages play a critical role. For example, it has been suggested that macrophage inflammatory status is a key determinant of systemic insulin resistance [3, 4]. It is well known that macrophage inflammatory status is under bi-directional control of macrophage polarization. On one hand, when undergoing classic proinflammatory, or M1 activation, macrophages display increased expression of proinflammatory cytokines, such as tumor necrosis factor alpha (TNFα) and interleukin-6 (IL-6). On the other hand, when undergoing M2 activation, macrophages produce anti-inflammatory factors, such as IL-10 and arginase I, which accounts for protection of overnutrition-induced insulin resistance [5-7]. As such, elucidating the mechanisms underlying macrophage inflammatory status appears to be a key to better understand the pathogenesis of inflammation in the context of systemic insulin resistance.

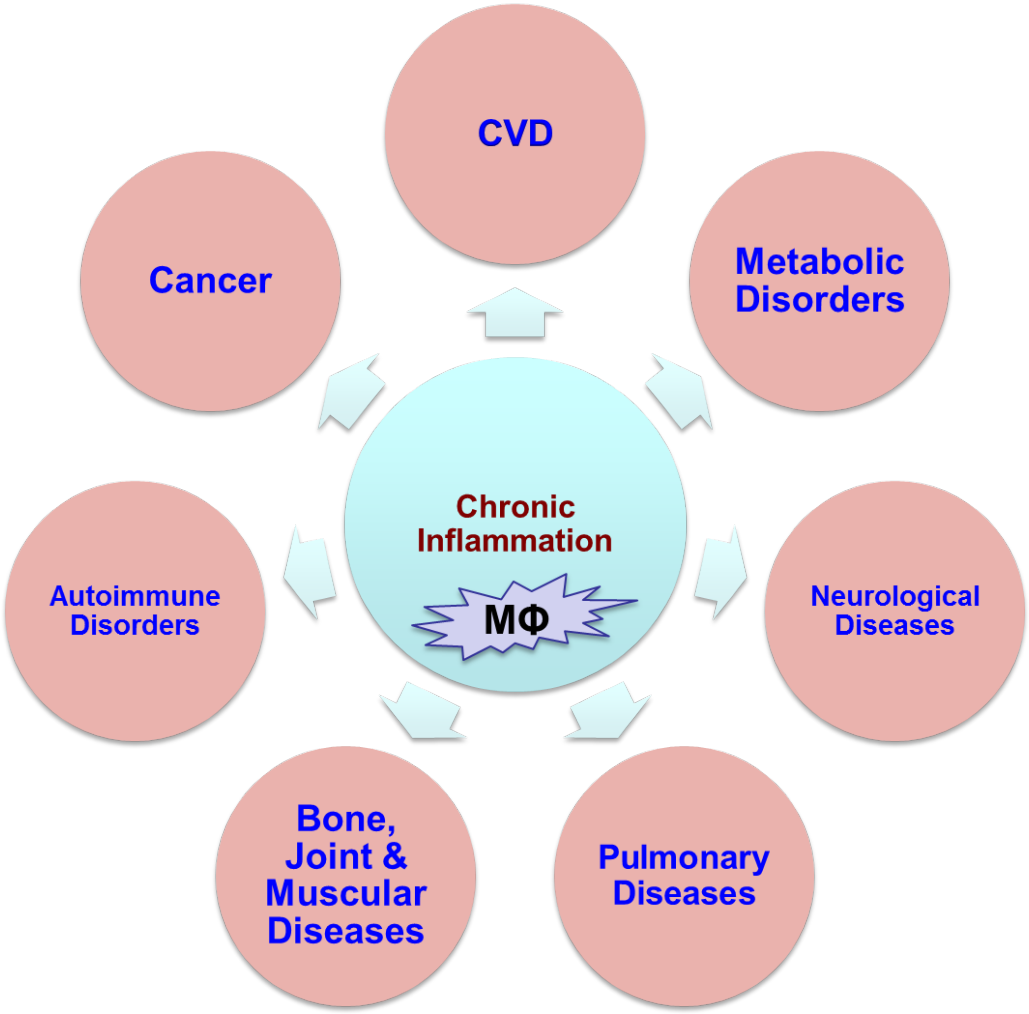

Figure 1. Chronic inflammation contributes to chronic diseases.

1.2 Literature Review

1.2.1 Obesity

Chronic diseases are the leading causes of death in the U.S. based on the 2010 data released by the Centers for Disease Control and Prevention. Heart disease, cancer, and stroke took the first, second, and fourth positions, respectively, and diabetes mellitus was ranked as the seventh leading cause of death [8]. Obesity is a key risk factor for the development of most chronic diseases. During obesity, fat accumulation and chronic low-grade inflammation interact, resulting in systemic insulin resistance [9]. Recently, accumulating evidence pointed out that fat deposition alone may not simply indicate insulin resistance. Instead, inflammatory responses in critical metabolic tissues, such as adipose and liver, are more important in causing systemic insulin resistance. My colleagues in the lab discovered that disruption of iPFK2 exacerbates diet-induced systemic insulin resistance and adipose tissue inflammatory response, even though less adiposity was observed when compared to HFD-fed WT (C57BL/6J) littermates [10]. It appears that controlling of inflammatory status can be crucial for improving systemic insulin resistance.

1.2.2 Macrophage

Macrophage activation plays a crucial role in regulating adipose tissue inflammation and metabolic disorders [11-15]. There are diverse macrophage phenotypes identified, but it is not well known about how one type of macrophages differs from the others, and whether different types of macrophages overlap in functional properties. Additionally,

the classification of macrophage phenotypes is still under development. The two most common macrophage phenotypes are the classically-activated M1 macrophages and the alternatively-activated M2 macrophages. Macrophage M1 activation (proinflammatory) is driven by Th1 cytokines, such as interferon gamma (IFN^{γ}) and TNFα, or by lipopolysaccharides (LPS) recognition [16-18]. M1 cells secrete proinflammatory cytokines, such as TNFα, IL-6, IL-1β [16-18]. M1 macrophages exhibit microbicidal properties and serve a defensive role in acute inflammatory response. However, prolonged or chronic inflammation is pathogenic and should be counteracted by protective mechanisms operated by anti-inflammatory M2 macrophages. Macrophage M2 activation (anti-inflammatory) is typically driven by Th2 cytokines, such as IL-4 and IL-13. Characterized by high endocytic clearance and anti-inflammatory capacities, M2 macrophages can promote repair of tissue damage and protect surrounding tissues from a detrimental immune response [19] (Fig. 2).

In classically-activated macrophages, nuclear factor kappa B (NF-κB) and/or c-Jun N-terminal kinase 1 (JNK1) signaling mediates the expression of proinflammatory cytokines. Under the condition of overnutrition, increased macrophage proinflammatory activation is a causal factor of insulin resistance [20]. In contrast, PPARγ is the known intracellular determinant that stimulates macrophage M2 activation [3, 4, 21, 22]. Increased M2 activation is associated with improvement of systemic insulin sensitivity and appears to protect against the development of obesity-associated metabolic diseases [3, 4].

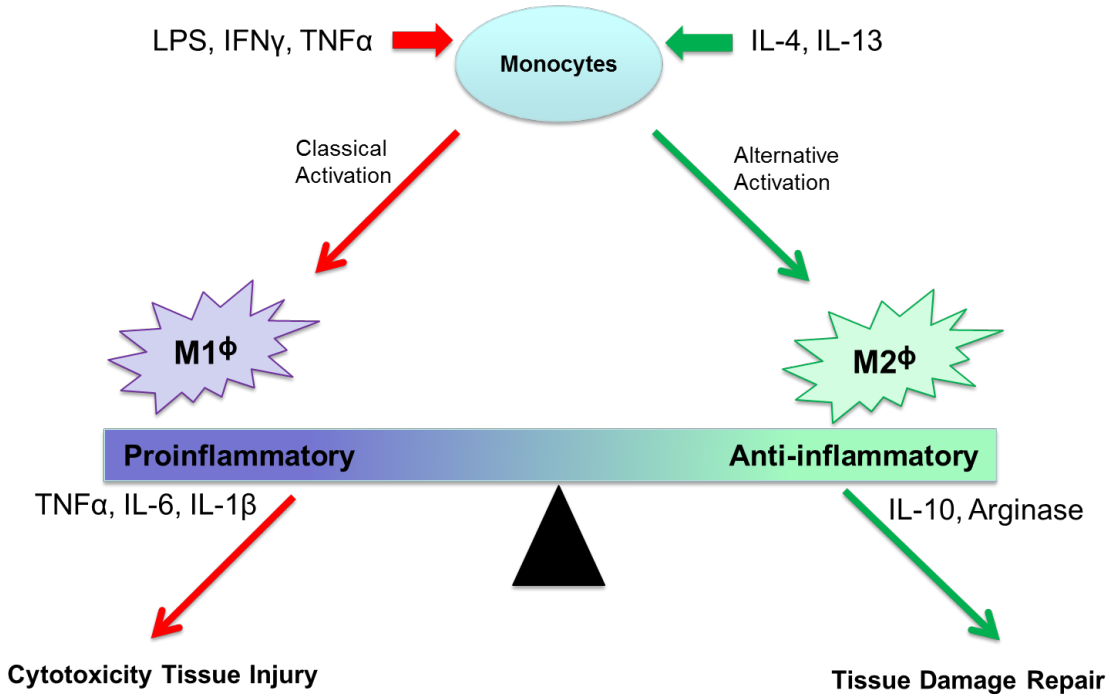

Figure 2. Macrophage proinflammatory (M1) activation and anti-inflammatory (M2) activation.

1.2.3 Circadian clocks

Many physiological processes display a 24-h rhythm, including fasting-feeding behavior, sleep-wake cycle, hormones level oscillation, and lipid/carbohydrate metabolism. [23] This 24-h rhythm is driven by an endogenous and entrainable circadian clock [23], which can also be adjusted to the local environment by external cues such as light-dark cycle and temperature [24]. When circadian rhythms are desynchronized by shift work, jet lag, and/or sleep disruption, human normal body weight regulation and glucose/lipid

homeostasis is profoundly affected [25-27]. Circadian dysregulation also is widely observed in obesity and metabolic syndrome. It has been demonstrated that HFD disrupts behavioral and molecular circadian rhythms in mice [28]. As many hormones involved in glucose homeostasis and insulin secretion are regulated by the circadian system [29, 30], the disruption of circadian rhythms leads to insulin resistance and obesity [31].

The core loop of circadian clock is responsible for rhythmic biological processes, existing in both brain and peripheral metabolic tissues, such as adipose, liver, and macrophage (Fig. 3). Within the core loop of the circadian clock, CLOCK-BMAL1 induces transcription of clock genes *Per1/Per2/Per3* and *Cry1/Cry2*, as well as clock-controlled genes. The protein products PERs and CRYs can form a complex in the cytoplasm, and it either translocates to nucleus to inhibit CLOCK-BMAL1 or is degraded after phosphorylation. This cycle typically takes 24 h. Thus, the circadian clock coordinates metabolic and immune processes in peripheral tissues in a day-night cycle through regulating transcription of genes involved, such as the gene of insulin in pancreas, leptin in adipose and cytokines in immune cells [23].

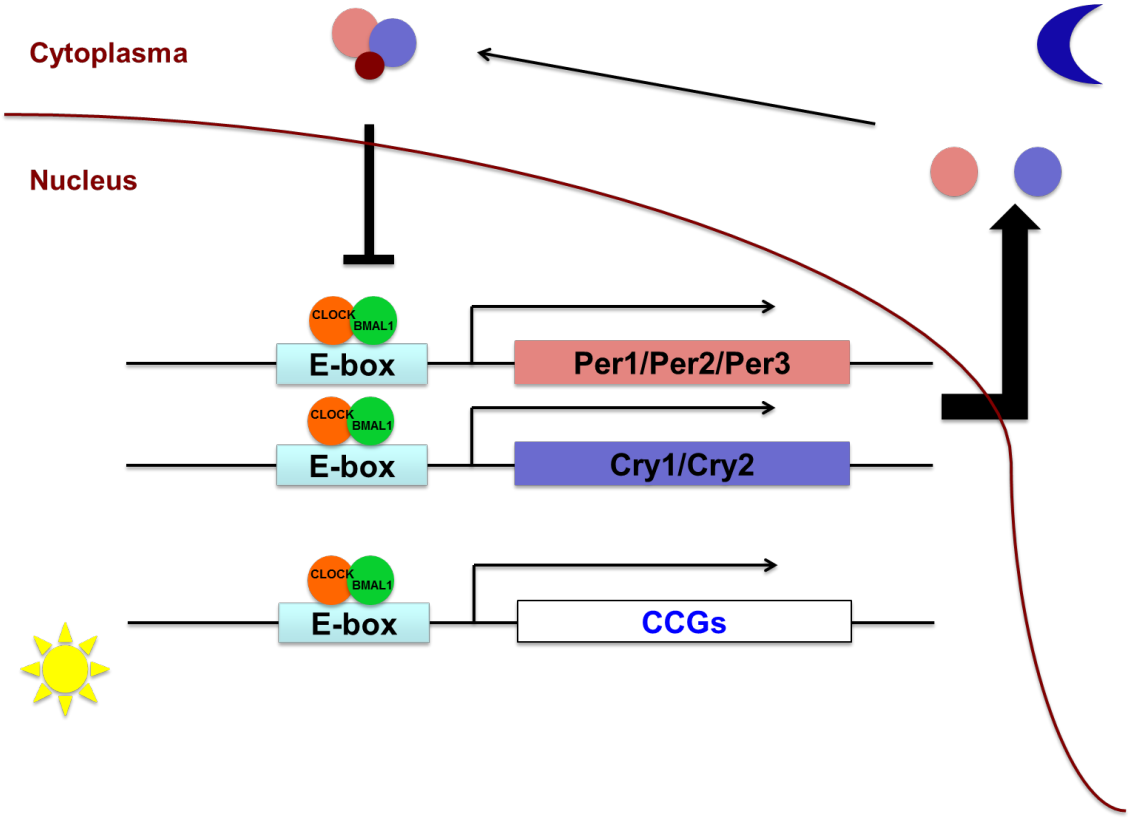

Figure 3. The core loop of circadian clocks is responsible for rhythmic biological processes. CCGs, clock-controlled genes.

1.2.4 PFKFB3/inducible 6-phosphofructo-2-kinase (iPFK2)

PFKFB3/iPFK2 is the key regulatory enzyme in the glycolytic pathway (Fig. 4). In glucose metabolism, fructose-2, 6-bisphosphate (F-2, 6-P_2) is a powerful activator of 6-phosphofructo-1-kinase (6PFK1), which is the rate-limiting enzyme of glycolysis. Meanwhile, F-2, 6-P_2 is also a powerful inhibitor of fructose-1, 6-bisphosphatase, which

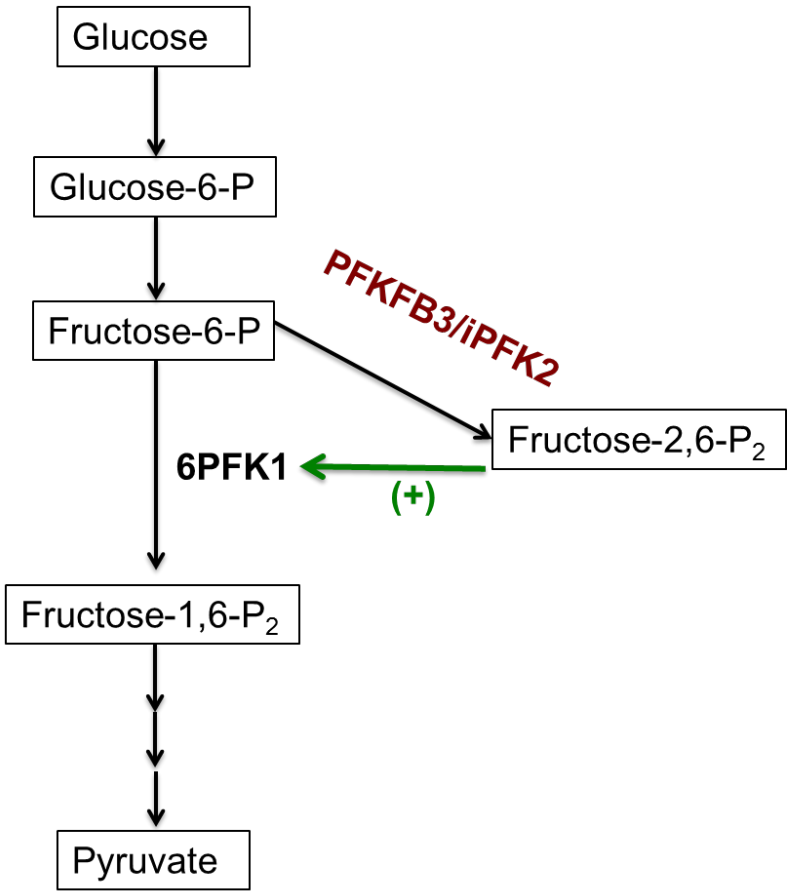

Figure 4. PRKFB3 in glycolysis pathway.

is the key enzyme of gluconeogenesis [32, 33]. The synthesis and degradation of F-2, 6-P_2 is catalyzed by 6-phosphofructo-2-kinase/fructose-2, 6-bisphosphatase (PFK-2/FBPase), which is a homodimeric bi-functional enzyme encoded by PFKFB gene, which include PFKFB1-4 encoding tissue-specific pfkfb isoenzymes [32-34]. The PFKFB3 gene encodes for the isoenzyme iPFK2 [35, 36] and is expressed in rapidly

proliferating cells, such as tumor cells, epithelial cells, and activated immune cells [35, 36]. Additionally, tissue distribution analysis has shown that PFKFB3 is highly expressed in adipose tissue and is expressed at very low levels in liver and muscle [10]. In macrophages, PFKFB3 is the predominant PFKFB gene and the expression is stimulated by LPS [37] and hypoxia [32], suggesting a role for PFKFB3 in macrophage inflammatory responses. Homozygous disruption of PFKFB3/iPFK2 results in lethal embryo, which indicates this gene is critical for fetus survivial. However, there are few published data that address the role of PFKFB3 in macrophage inflammatory status regulation and its relation to insulin resistance during obesity.

Previous studies of my colleagues in the lab have shown that HFD-fed global PFKFB3-disrupted mice gained less body weight and exhibited less adiposity when compared to WT mice after HFD feeding [10]. These HFD-fed PFKFB3-disrupted mice, however, displayed increased severity of systemic insulin resistance and adipose tissue dysfunction. This was evidenced by abnormal adipose tissue lipolysis, adipokine expression, proinflammatory responses, and impaired insulin signaling [10, 14]. Interestingly, increased adipose tissue inflammatory response and less macrophage infiltration in adipose tissue were observed concurrently in HFD-fed PFKFB3-disrupted mice, when compared with HFD-fed WT mice. This indicated that adipose tissue inflammatory response, rather than the number of infiltrated macrophages in adipose tissue, is more crucial in determining adipose tissue inflammation, insulin signaling and systemic insulin resistance.

Studies from others also suggested that macrophage inflammatory activation status is more important than the total number in adipose tissue for the inflammatory cytokines production. For example, mice lacking PPARγ in macrophages exhibited lower levels of macrophage infiltration in adipose tissue but displayed increased mRNA levels of IL-6, when compared to WT control [3, 38]. Rosiglitazone, as a PPARγ agonist, increased the total number of macrophages infiltrated in adipose tissue but decreased the expression of proinflammatory cytokines such as IL-18 [3, 38].

Additionally, researchers have demonstrated that iPFK2 is involved in the anti-diabetic effect of PPARγ activation in mice [15]. Considering the effect of PPARγ on macrophage activation, whether PFKFB3 is also involved in the process of macrophage activation in the context of systemic insulin resistance would be an interesting topic to investigate.

Therefore, my hypothesis is 1) circadian clock dysregulation enhances macrophage proinflammatory activation in diet-induced obesity, resulting in local and systemic insulin resistance; 2) PFKFB3 disruption enhances macrophage proinflammatory activation in diet-induce obesity, resulting in local and systemic insulin resistance.

2. CIRCADIAN CONTROL OF MACROPHAGE ACTIVATION*

2.1 Introduction

Obesity is highly associated with systemic insulin resistance and the consequential development of a wide variety of metabolic diseases including type 2 diabetes [39], fatty liver disease [40], and cardiovascular disease [41]. Over the past decade, adipose tissue inflammation has been increasingly regarded as a causal factor of obesity-associated insulin resistance [10, 12, 42-44]. As demonstrated in mice fed a high fat diet (HFD), adipose tissue develops low grade inflammation that is characterized by increased infiltration of immune cells and production of proinflammatory cytokines [12, 42]. The diet-induced proinflammatory signaling coupled with increased production of pro-hyperglycemic factors (*e.g.* free fatty acids and resistin) and decreased production of anti-hyperglycemic factors (*e.g.* adiponectin) that reflect inflammation-associated adipose tissue dysfunction [45-48] collectively impair insulin signaling in insulin-sensitive tissues including the liver and skeletal muscle, leading to systemic insulin resistance [49-54]. In contrast, treatment with thiazolidinediones or supplementation with fish oils ameliorates adipose tissue inflammation, which in turn contributes to the

---

* Reprinted from Xu H, Li H, Woo SL, Kim SM, Shende VR, Neuendorff N, Guo X, Guo T, Qi T, Pei Y, Zhao Y, Hu X, Zhao J, Chen L, Chen L, Ji JY, Alaniz RC, Earnest DJ, and Wu C. *Myeloid cell-specific disruption of Period1 and Period2 exacerbates diet-induced inflammation and insulin resistance.* This research was originally published in J Biol Chem, 2014. 289:16374-16388.

reversal of diet-induced adipose tissue dysfunction and systemic insulin resistance [55-57]. As such, obesity-associated inflammation is key to the regulation of systemic insulin sensitivity.

In relation to the link between inflammation and metabolic dysregulation in obesity, there is increasing evidence that dysregulated macrophage functional plasticity and versatility (polarization) is a key component of the mechanism by which inflammation in adipose and liver tissues mediates the development of obesity-associated insulin resistance and metabolic diseases. For example, in diet-induced obesity, adipose tissue macrophage infiltration is increased, and polarization is shifted toward the proinflammatory M1 activation, resulting in increased production of proinflammatory cytokines and potentiation of adipose tissue inflammation that contribute to impaired systemic insulin sensitivity [58]. Within macrophages, peroxisome proliferator-activated receptor γ and δ (PPAR γ / δ) are key transcription factors that stimulate macrophage alternative M2 (anti-inflammatory) activation [22, 59, 60]. Importantly, myeloid cell-specific disruption of PPARγ and/or PPARδ increases proinflammatory activation of adipose tissue macrophages and exacerbates obesity-associated insulin resistance [43, 59]. In contrast, the effect of PPARγ activation on reversing HFD-induced insulin resistance is mediated at least in part by stimulation of alternative activation of macrophages in adipose tissue [56]. Macrophage polarization is also regulated by Toll-like receptor 4 (TLR4) and/or c-Jun N-terminal kinase (JNK) such that their myeloid cell-specific disruption protects mice from diet-induced adipose tissue inflammation and systemic insulin resistance [61-63]. As such, these findings

demonstrate how the inflammatory status of macrophages governs the outcome of adipose tissue inflammation and systemic insulin sensitivity.

Circadian clocks in peripheral tissues and cells drive daily rhythms and coordinate many physiological processes including inflammation and metabolism. Recent observations suggest that circadian clock dysregulation plays a key role in the development of metabolic diseases including obesity and diabetes. Studies using mice with genetic mutation or deletion of core clock genes correspondingly indicate that global and adipocyte specific disruption of circadian clock function produces obesity or significant alterations in metabolism [64-66]. However, the specific mechanism underlying the link between circadian clock- and metabolic-dysregulated phenotypes is unknown. As key components of inflammation in obesity, macrophages contain cell-autonomous circadian clocks that have been shown to gate macrophage inflammatory responses including rhythms in lipopolysaccharide (LPS)-induced cytokine secretion [67, 68]. Because HFD induces adipose tissue circadian clock dysregulation in conjunction with adipose tissue macrophage proinflammatory activation [28] and environment-mediated circadian disruption amplifies macrophage proinflammatory responses [69], our hypothesis is that overnutrition causes circadian clock dysregulation, which in turn induces macrophage proinflammatory activation in adipose tissue so as to exacerbate inflammation and fat deposition, thus leading to systemic insulin resistance. To test this hypothesis, we conducted a series of experiments to determine whether 1) HFD induces circadian clock dysregulation along with proinflammatory activation in indigenous and adipose tissue macrophages, 2) genetic disruption of the clock

mechanism using mice with targeted mutations of the clock genes *Period1* (*Per1*) and *Per2* (*Per1*^{ldc}/*Per2*^{ldc}) alters macrophage proinflammatory status, 3) PPARγ plays a role in the proinflammatory activation of *Per1*/*2*-disrupted macrophages, and 4) adoptive transfer or co-culture of *Per1*/*2*-disrupted macrophages potentiates inflammatory responses and pathophysiology of adipose tissue in diet-induced obesity or adipocytes *in vitro*.

2.2 Materials and Methods

2.2.1 Animal experiments

Animals used in this study were derived from wild-type (WT) C57BL/6J mice and 129J mice obtained from The Jackson Laboratory (Bar Harbor, ME) and from breeding pairs of homozygous *mPer2*^{Luc} knockin mice (C57BL/6J background; generously provided by Dr. Joseph Takahashi, UT Southwestern Medical School, Dallas, TX) and homozygous mutant mice with targeted disruption of the clock genes, *Per1* and *Per2* (*Per1*^{ldc}/*Per2*^{ldc}; generously provided by Dr. David Weaver, University of Massachusetts Medical School, Worcester, MA). In homozygous *mPer2*^{Luc} mice, a luciferase (Luc) gene was fused in-frame to the C terminus of the endogenous mPER2 coding sequence so as to enable continuous recording of *Per2* oscillations via luciferase bioluminescence [70]. Establishment, genotyping, and phenotype of *Per1*^{ldc}/*Per2*^{ldc} mutant mice (129J background) have been described previously [71]. *Per1*^{ldc}/*Per2*^{ldc} mice are distinguished by a loss of circadian rhythmicity as well as altered expression

and circadian regulation of other clock genes [71]. In different peripheral tissues, *Per1*^{ldc}/*Per2*^{ldc} mutant mice consistently showed increased BMAL1 (600%) and increased CLOCK (65%) protein levels relative to WT controls.[5] All mice were maintained on a 12:12-h light-dark cycle (lights on at 06:00). At 5–6 wk of age, male wild-type C57BL/6J mice were fed an HFD (60% fat calories, 20% protein calories, and 20% carbohydrate calories) or a low fat diet (LFD, 10% fat calories, 20% protein calories, and 70% carbohydrate calories) for 12 wk as previously described [10, 44] (nutrient composition listed in Table. 1). After the feeding regimen, mice were fasted for 4 h before sacrifice for collection of blood and tissue samples [72, 73]. Epididymal, mesenteric, and perinephric fat depots were dissected and weighed as abdominal fat mass [73]. After weighing, adipose tissue and liver samples were either fixed and embedded for histological and immunohisto-chemical analyses or frozen in liquid nitrogen and stored at 80 °C for further analyses. Some mice were fasted similarly and used for insulin and glucose tolerance tests and/or and insulin signaling analyses as described below. To examine the dietary effect on *in vivo* circadian clock rhythmic in relation to obesity-associated metabolic phenotypes, *mPer2*^{Luc} mice were subjected to HFD feeding. Briefly, female homozygous *mPer2*^{Luc} mice at 5–6 wk of age were fed an HFD for 12 wk. Ageand gender-matched *mPer2*^{Luc} mice were fed an LFD and used as controls. After the feeding regimen *mPer2*^{Luc} mice were subjected to the same assays used for C57BL/6J mice. Additionally, both HFD-fed and LFD-fed *mPer2*^{Luc} mice were subjected to examination of wheel-running locomotor activity rhythms as

	LFD 3.85 kcal/gm		HFD 5.24 kcal/gm	
Macronutrients	**gm%**	**kcal%**	**gm%**	**kcal%**
Protein	19.2	20	26	20
Carbohydrate	67.3	70	26	20
Fat	4.3	10	35	60
Total		100		100
Ingredients	**gm**	**kcal**	**gm**	**Kcal**
Casein, 80 Mesh	200	800	200	800
L-Cystine	3	12	3	12
Corn Starch	315	1260	0	0
Maltodextrin 10	3	140	125	500
Sucrose	350	1400	68.8	275
Cellulose, BW200	50	0	50	0
Soybean Oil	25	225	25	225
Lard	20	180	245	2205
Mineral Mix S10026	10	0	10	0
DiCalcium Phosphate	13	0	13	0
Calcium Carbonate	5.5	0	5.5	0
Potassium Citrate, 1 H2O	16.5	0	16.5	0
Vitamin Mix V10001	10	40	10	40
Choline Bitartrate	2	0	2	0
FD&C Yellow Dye #5	0.05	0	0	0
FD&C Blue Dye #1	0	0	0.05	0
Total	1055.05	4057	773.85	4057

Table 1. Macro- and micronutrient composition of low-fat and high-fat diets.

previously described [74]. Some age-matched female *mPer2*^{Luc} mice were fed *ad libitum* and used for isolation of bone marrow cells.

To address a role for circadian clock rhythmic dysregulation in altering macrophage activation in relation to metabolic homeostasis, *Per1*^{ldc}/*Per2*^{ldc} mice were used for the present study. Accordingly, *Per1*^{ldc}/*Per2*^{ldc} mice (129J background) and wild-type 129J mice were maintained on a 12:12-h light-dark cycle (lights on at 06:00) and fed *ad libitum*. At 5– 6 wk of age, male *Per1*^{ldc}/*Per2*^{ldc} mice and wild-type 129J mice were anesthetized by ketamine (100 mg/kg)/xylazine (10 mg/kg of body weight). Immediately after euthanasia, *Per1*^{ldc}/*Per2*^{ldc} mice and wild-type 129J mice were subjected to isolation of bone marrow cells as previously described [60, 62]. The isolated bone marrow cells were used for *in vitro* analyses and served as donor cells for bone marrow transplantation (BMT). Briefly, male wild-type C57BL/6J recipient mice at 5–6 wk of age were lethally irradiated and subjected to BMT to generate chimeric mice using the established method [60, 61]. Wild-type C57BL/6J mice that were transplanted with donor cells from *Per1*^{ldc}/*Per2*^{ldc} mice were referred to as BMT-*Per1*^{ldc}/*Per2*^{ldc} mice. Wild-type C57BL/6J mice that were transplanted with donor cells from wild-type 129J mice were referred to as BMT-WT mice. After recovery for 4 wk, all chimeric mice were subjected for HFD feeding for 12 wk followed by metabolic assays. All study protocols were reviewed and approved by the Institutional Animal Care and Use Committee of Texas A&M University.

2.2.2 Macrophage differentiation and characterization

Bone marrow cells were isolated from the tibias and femurs of LFD- and/or HFD-fed *mPer2*^{Luc} mice as previously described [59]. After differentiation with Iscove's modified Dulbecco's medium containing 10% fetal bovine serum and 15% L929 culture supernatant for 8 d, bone marrow-derived macrophages (BMDMs) were subjected to inflammatory assays and circadian rhythm analyses using a lumicycle. Similarly, bone marrow cells were isolated from chow diet-fed *Per1*^{ldc}/*Per2*^{ldc} mice and 129J WT control mice and differentiated into BMDM for FACS analyses using flow cytometry with fluorescence-conjugated antibodies against F4/80 and CD11b as well as CD11c and CD206. For PPAR rescue experiment, *Per1*^{ldc}/*Per2*^{ldc} BMDM were treated with a PPAR 2-expressing lentiviral vector or a control vector for 24 h according to procedures provided with commercial kits (GenTarget Inc, San Diego, CA). WT BMDM (129J background) were treated similarly with a control vector and served as the control (Ctrl). Untreated WT BMDM were also included as controls. After incubation for an additional 24 h, the treated BMDM were subjected to inflammatory analyses. To examine macrophage proinflammatory activation, BMDM were treated with LPS (100 ng/ml) or PBS for 30 min before cell harvest to examine the inflammatory signaling using Western blot analyses. Some cells were treated with or without LPS at the same dose for 6 h before harvest of RNA samples. Some cells were subjected to FACS analyses as described below.

2.2.3 Confirmation of Per1/2 disruption

Genomic DNA was prepared from the tails of *Per1*^{ldc}/*Per2*^{ldc} mice and 129J wild-type mice as well as bone marrow cells, bone marrow-derived macrophages, and adipose tissue and liver samples of chimeric mice and subjected to PCR genotyping using previously described methods [75].

2.2.4 Insulin and glucose tolerance tests

Mice were fasted for 4 h and intraperitoneally injected with insulin (1 unit/kg of body weight) or D-glucose (2 g/kg of body weight). For insulin tolerance tests, blood samples (5 ul) were collected from the tail vein before and at 15, 30, 45, and 60 min after the bolus insulin injection. Similarly, for glucose tolerance tests blood samples were collected from the tail vein before and at 30, 60, 90, and 120 min after the glucose bolus injection [10, 44].

2.2.5 Measurement of metabolic parameters

The levels of plasma glucose, triglycerides, and free fatty acids were measured using metabolic assay kits (Sigma and BioVision, Mountain View, CA). The levels of plasma insulin were measured using ELISA kits (Crystal Chem Inc., Downers Grove, IL).

2.2.6 Isolation of stromal vascular cells from adipose tissue

Adipose tissue stromal vascular cells (SVCs) were isolated using the collagenase digestion method as previously described [10, 56]. After digestion and centrifugation,

the pelleted cells were collected as SVC. Adipose tissue SVC from *mPer2*^{Luc} mice were subjected to bioluminescence analysis as previously described [75]. SVC from HFD-fed BMT-*Per1*^{ldc}/*Per2*^{ldc} and BMT-WT mice were subjected to FACS analyses and other assays.

2.2.7 Circadian properties of mPer2Luc SVC and BMDM cells

SVC and BMDM prepared from LFD- and/or HFD-fed *mPer2*^{Luc} mice were suspended in supplemented Dulbecco's modified Eagle's medium (DMEM) (for SVC) or Iscove's modified Dul becco's medium (for BMDM) and then plated on 35-mm culture dishes (Corning). For both cell types, the medium was changed 24 h after plating so as to reduce the FBS concentration to 5%, and about 12 h later cultures were exposed to medium containing 50% adult horse serum for 2 h. Thereafter, serum-shocked SVC and BMDM were maintained in serum- free recording medium containing 0.1 mM beetle luciferin (Promega), 25 units/ml penicillin, and 25 g/ml streptomycin for bioluminescence analysis as described previously [74]. Individual cultures were sealed airtight with sterile glass coverslips (VWR) and sterile silicon grease (Dow Corning). The temporal patterns of mPER2::LUC bioluminescence were analyzed using an automated 32-channel luminometer (LumiCycle; Actimetrics, Wilmette, IL) that was maintained within a standard cell culture incubator at 35 °C. Bioluminescence from individual cultures was continuously recorded with a photomultiplier tube (PMT) for 70 s at intervals of 10 min. Because of the transient induction of bioluminescence after the medium change at the initiation of this analysis, the first cycle was excluded from data

analysis. Bioluminescence data were analyzed using the Lumicycle Analysis program (Actimetrics). For each raw data set, baseline drift was removed by fitting a polynomial curve with an order equal to one less than the number of recorded cycles. Rhythm parameters were determined from baseline-subtracted data using Levenberg-Marquardt algorithm (damped Sine) fit.

2.2.8 Flow cytometry analysis

Tibias/femurs were obtained from LFD- or HFD-fed *mPer2*^{Luc} (*n* 3) and from chow diet- fed *Per1*^{ldc}/*Per2*^{ldc} mice and 129J wild-type mice (*n* 3) and pooled to obtain sufficient BMDM. Epididymal fat pads were obtained from HFD-fed BMT-*Per1*^{ldc}/*Per2*^{ldc} mice and BMT- WT mice to prepare SVC samples (*n* 4–6). BMDM and adipose tissue SVC were stained with fluorescence-tagged antibodies (anti-F4/80 and anti-CD11b for macrophages and anti- CD11c and anti-CD206 for macrophage activation as previously described [76]) and subjected to FACS analyses using BD FACS Aria II flow cytometer (BD Biosciences) that is operated by Texas A&M Health Science Center College of Medicine Cell Analysis Facility. Briefly, the harvested cells were analyzed based on FSC-A and SSC-A. Live cells were then examined for F4/80 (FITC) and CD11b allophycocyanin (APC) expression. Mature macrophages (F4/80 CD11b cells) were then gated for CD11c (phycoerythrin (PE)/Cy7) and CD206 (PE) expression (macrophage polarization). Mature macrophages that were positive for CD11c but negative for CD206 were considered as M1 macrophages (F4/80 CD11b CD11c CD206 cells).

2.2.9 Co-culture of macrophages and adipocytes

BMDM were prepared from *Per1*^{ldc}/*Per2*^{ldc} and 129J wild-type control mice. Adipocytes were differentiated from 3T3-L1 cells in DMEM supplemented with 10 g/ml insulin, 1 M dexamethasone, and 0.5 mM 3-isobutyl-1-methyl-xanthine for 48 h followed by incubation for an additional 6 – 8 d in growth medium supplemented with 10 g/ml insulin [10, 77]. After differentiation, adipocytes were co-cultured with BMDM at a ratio of 10:1 based on the published method [60]. To examine changes in inflammatory signaling, the cells were treated with or without LPS (10 ng/ml) for 30 min before cell harvest. Some cells were treated with or without insulin (100 nM) for 30 min before harvest for determination of changes in insulin signaling. Cell lysates were prepared and used to examine inflammatory and insulin signaling using Western blot analyses. Additionally, some co-culture cells were treated with or without LPS (10 ng/ml) for 6 h and subjected to preparation of RNA samples to quantify gene expression using real-time reverse transcription PCR.

2.2.10 Western blots

Lysates were prepared from frozen tissue samples and cultured cells using the lysis buffer containing 50 mm HEPES (pH 7.4), 1% Triton X-100, 50 mm sodium pyrophosphate, 0.1 m sodium fluoride, 10 mm EDTA, 10 mm sodium orthovanadate, 10 g/ml aprotinin, 10 g/ml leupeptin, 2 mm benzamidine, and 2 mm phenylmethylsulfonyl fluoride. The levels of JNK1/2, phospho-JNK1/2, nuclear factor B (NF- κB) p65, phospho-p65 (Ser-536), Akt1/2, phospho-Akt (Ser-473), and PPAR in cell lysates (15 or

50 g/lane) were analyzed using 8% Tris-glycine gels and rabbit anti-serum as a primary antibody at a 1:1000 dilution. The blot was followed by a 1:10,000 dilution of goat anti-rabbit horseradish peroxidase- conjugated secondary antibody kit (Immobilon^{TM} Western; EMD Millipore, Billerica, MA) as previously described [73]. GAPDH or -actin was used as a loading control. The maximum intensity of each band was quantified using ImageJ software. Ratios of PJNK1/JNK1 and phospho-p65/p65 as well as phospho-Akt/Akt were normalized to GAPDH or -actin and adjusted relative to the average of control (PBS)-treated LFD, wild type, *Per1*^{ldc}/*Per2*^{ldc}, BMT-WT, or Adi/wild type, which was arbitrarily set as 1 (arbitrary units).

2.2.11 RNA isolation, reverse transcription, and real-time PCR

The total RNA was isolated from frozen tissue samples and cultured/isolated cells. Reverse transcription was performed using the GoScript^{TM} Reverse Transcription System (Promega), and real-time PCR analysis was performed using SYBR Green (ABI Prism 7200 Sequence Detection System; Applied Biosystems) [78, 79]. The mRNA levels were analyzed for interleukin-1 (IL-1), IL-6, tumor necrosis factor (TNF), IL-10, arginase1, monocyte chemoattractant protein 1 (MCP1), TLR4, adiponectin, hormone-sensitive lipase, resistin, sterol regulatory element-binding protein 1c (SREBP1c), acetyl-CoA carboxylase 1, fatty acid synthase (FAS), glucokinase, and glucose-6-phosphatase in tissue and/or cell samples. A total of 0.1 g of RNA was used for the determination. Results were normalized to 18 S ribosomal RNA or -actin mRNA and

plotted as relative expression to the average of control (PBS)-treated LFD, wild type, *Per1*^{ldc}/*Per2*^{ldc}, BMT-WT, or Adi/wild-type, which was arbitrarily set as 1.

2.2.12 Statistical methods

Numeric data are presented as the means S.E. Statistical significance was assessed by unpaired, two-tailed analysis of variance or Student's *t* tests. Differences were considered significant at the two-tailed p 0.05.

2.3 Results

2.3.1 HFD feeding induces adiposity, adipose tissue inflammation, systemic insulin resistance, and circadian clock dysregulation

Consistent with established observations [10, 12, 42], HFD-fed C57BL/6J mice displayed increased adiposity, adipose tissue inflammation, and systemic insulin resistance (Fig. 5).

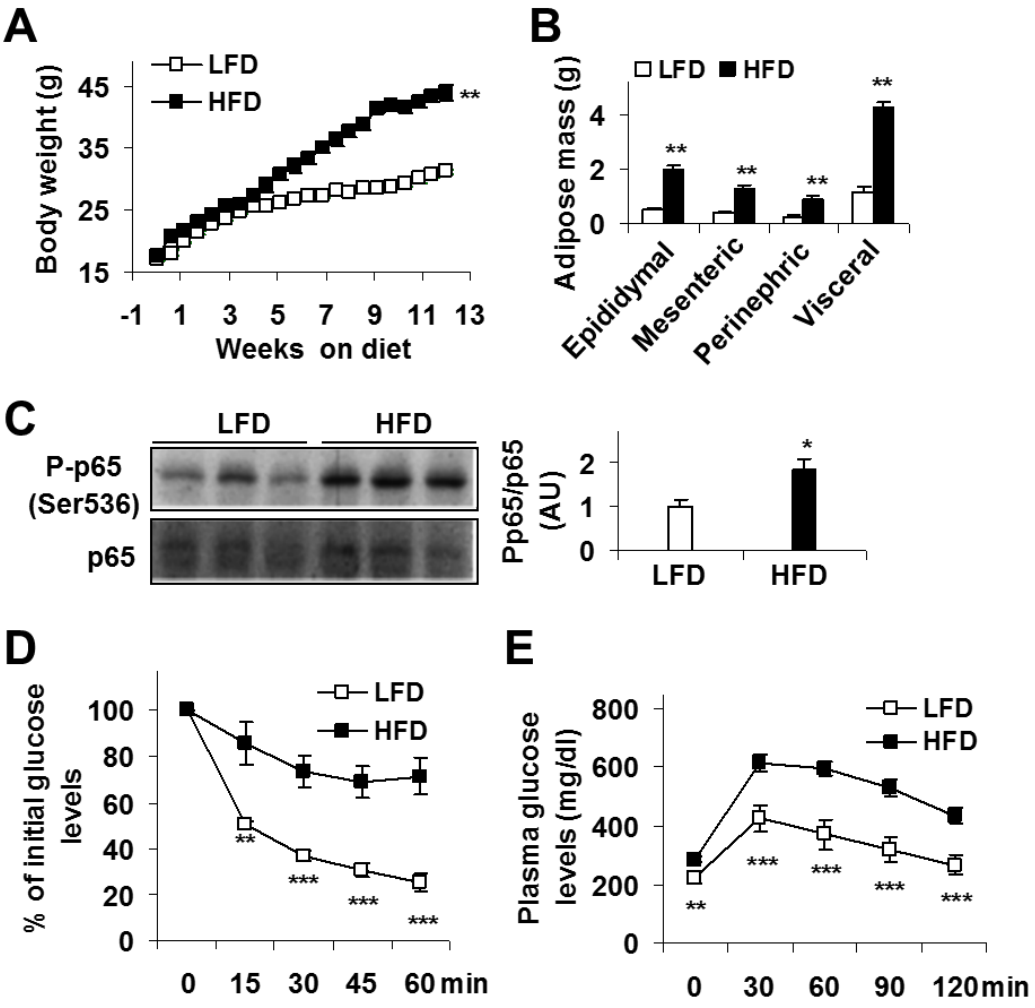

Figure 5. HFD feeding induces adiposity, adipose tissue inflammation, and systemic insulin resistance.

At 5 – 6 wk of age, *C57BL/6J male* mice were fed a high-fat diet (HFD) or low-fat diet (LFD) for 12 wk (n = 5 – 10). (A) Body weight was recorded weekly during the feeding regimen. (B) Adipose mass. Abdominal fat mass (visceral fat) was the sum of epididymal, mesenteric and perinephric fat mass. (C) Adipose tissue inflammatory signaling. The levels of total and phosphorylated NF-κB p65 were examined using Western blot analyses and quantified using densitometry. (D) Insulin tolerance tests. (E) Glucose tolerance tests. Data are means ± SE in line and bar graphs. *, $P < 0.05$; **, $P < 0.01$; and ***, $P<0.001$ HFD vs. LFD (C) for the same time point (A, D and E) or the same fat pad (B). For B and C, mice were fasted for 4 hour starting at the same time of the day prior to tissue collection or physiological assays. For D and E, mice were fasted for 4 hour starting at the same time of the day prior to be given a peritoneal injection of insulin (1 U/kg) (D) or glucose (2 g/kg) (E). AU, arbitrary units.

To address a possible link between metabolic phenotype and alterations in circadian clock functions, homozygous mPer2^{Luc} knockin mice (C57BL/6J background) (Fig. 6) were subjected to an identical feeding regimen. After HFD feeding for 12 wk, mPer2^{Luc} mice exhibited a marked increase in body weight and abdominal fat mass compared with LFD-fed mice (Fig. 7).

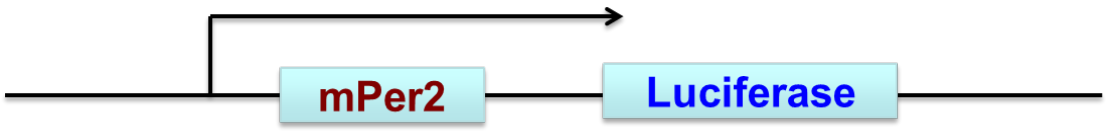

Figure 6. Homozygous mPer2Luc knockin mice.
The expressed PERIOD2::LUCIFERASE fusion protein is used as a real-time reporter of circadian dynamics in mice.

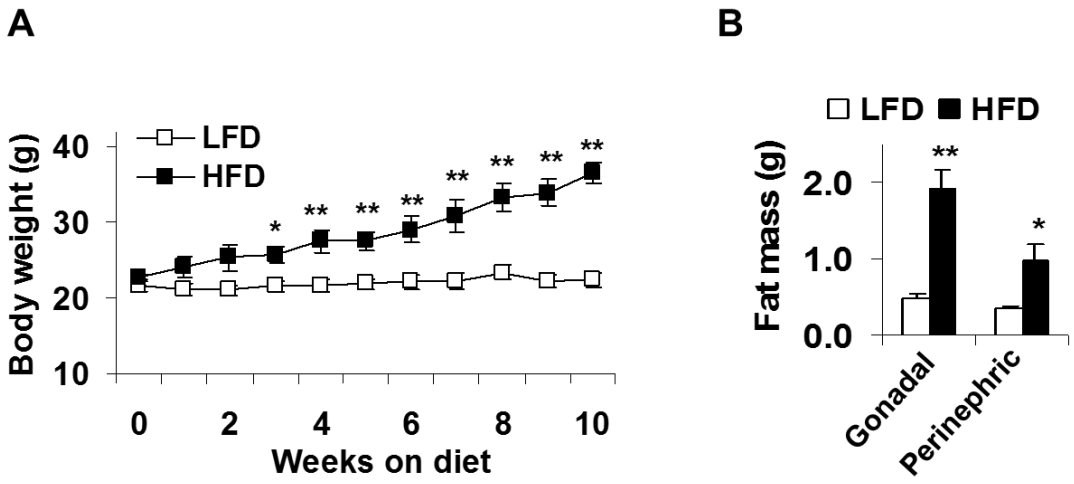

Figure 7. HFD feeding to mPer2Luc mice induces adiposity.
At 5 – 6 wk of age, *mPer2*^{Luc} mice were fed a high-fat diet (HFD) or low-fat diet (LFD) for 12 wk (n = 5 – 10). (A) Body weight was recorded weekly during the feeding regimen. (B) Adipose mass. Abdominal fat mass was calculated from the sum of gonadal and perinephric fat content. Data are means ± SE in line and bar graphs. *, $P < 0.05$; **, $P < 0.01$ HFD vs. LFD for the same time point (A) or the same fat pad (B). For B, mice were fasted for 4 hour starting at the same time of the day prior to tissue collection or physiological assays.

Consistent with HFD-fed C57BL/6J mice, HFD-fed mPer2^{Luc} mice exhibited a significant increase in the severity of insulin resistance and glucose intolerance indicated by insulin and glucose tolerance tests, respectively (Fig. 8). Additionally, HFD-fed mPer2^{Luc} mice displayed a significant increase in the period of the circadian rhythm of wheel-running behavior (Fig. 9).

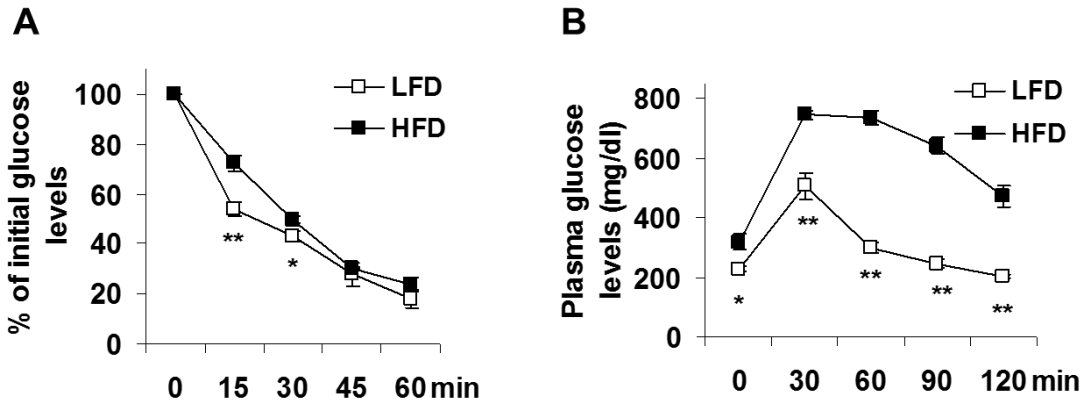

Figure 8. HFD feeding to mPer2Luc mice induces systemic insulin resistance. At 5 – 6 wk of age, *mPer2*^{Luc} mice were fed a high-fat diet (HFD) or low-fat diet (LFD) for 12 wk (n = 5 – 10). (A) Insulin tolerance tests. (B) Glucose tolerance tests. Data are means ± SE in line and bar graphs. *, $P < 0.05$; **, $P < 0.01$ HFD vs. LFD for the same time point. Mice were fasted for 4 hour starting at the same time of the day prior to be given a peritoneal injection of insulin (1 U/kg) (A) or glucose (2 g/kg) (B).

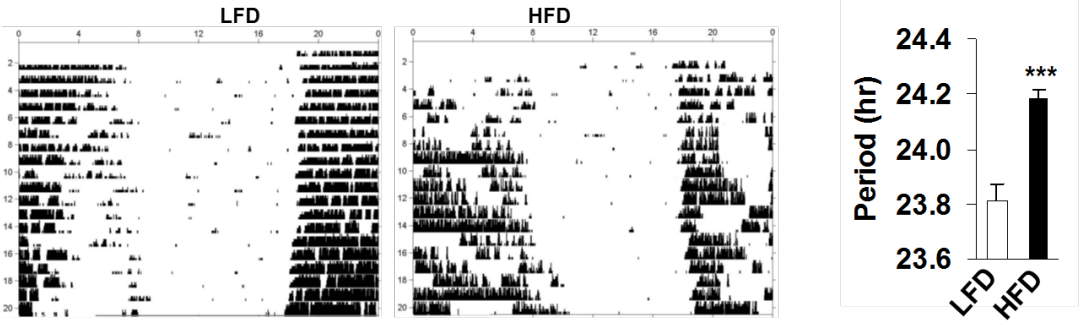

Figure 9. HFD feeding to mPer2^{Luc} mice induces circadian clock dysregulation. At 5 – 6 wk of age, *mPer2*^{Luc} mice were fed a high-fat diet (HFD) or low-fat diet (LFD) for 12 wk (n = 5 – 10). Representative circadian rhythms of wheel-running activity in LFD- and/or HFD-fed mice during exposure to constant darkness. Bar graph depicts differences in the free-running period of the activity rhythm between treatment groups. Data are means ± SE in line and bar graphs. ***, $P < 0.001$ HFD vs. LFD (right panel). The rhythm data were generated by the collaborator Dr. Earnest's lab.

2.3.2 HFD feeding lengthens the period of clock gene oscillations in adipose tissue SVC and BMDM and increases macrophage proinflammatory activation

Given the role of macrophages in inflammation [10, 12], we analyzed circadian oscillations of the clock gene Per2 in adipose tissue SVC, the immune cell-containing fraction of collagenase-digested visceral fat that has been widely used to examine the inflammatory status of adipose tissue macrophages [12, 59], and BMDM derived from mPer2^{Luc} mice (Fig. 10).

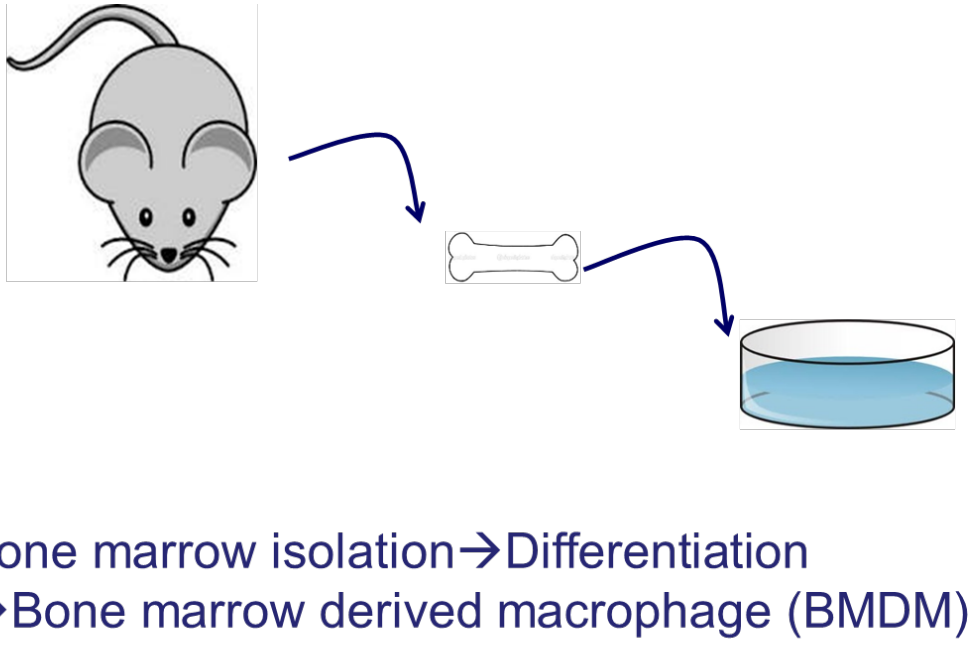

Figure 10. Preparation of BMDM.

SVC cultures from LFD-fed mice exhibited robust mPER2::LUC rhythms with a circadian period of 25.06 ± 0.4h (Fig. 11A). However, SVC cultures from HFD-fed mice were characterized by mPER2::LUC rhythms in which the period was significantly increased by ~9h (Fig. 11A). Similarly, the period of BMDM rhythms in mPER2::LUC bioluminescence was significantly increased in cultures from HFD-fed mPer2Luc mice relative to those from LFD-fed mice (Fig. 11B). BMDM cultures from HFD-fed mPer2Luc mice were also distinguished by robust decreases in the amplitude of the mPER2::LUC rhythm (Fig. 11B).

When the inflammatory status was analyzed under basal conditions (PBS-treated), the phosphorylation of JNK1 (p46, the key JNK isoform that mediates proinflammatory signaling) and NF-kB p65 (Ser-536) in BMDM from HFD-fed mPer2Luc mice did not significantly differ from that in BMDM from LFD-fed mice. However, upon LPS treatment, the phosphorylation of JNK1 and NK-kB p65 (Ser-536) in BMDM from HFD-fed mPer2Luc mice was significantly increased by 2.1- and 1.6 fold, respectively, compared with that in BMDM from LFD-fed mice (Fig. 12A). Moreover, under both basal and LPS-treated conditions, IL-1b, IL-6, and TNFa mRNA levels in BMDM from HFD-fed mPer2Luc mice were increased significantly relative to their respective levels in BMDM from LFD-fed mice (Fig. 12B).

Thus, overnutrition increases macrophage proinflammatory activation in concert with its effects on altering the timekeeping function of the macrophage circadian clockworks.

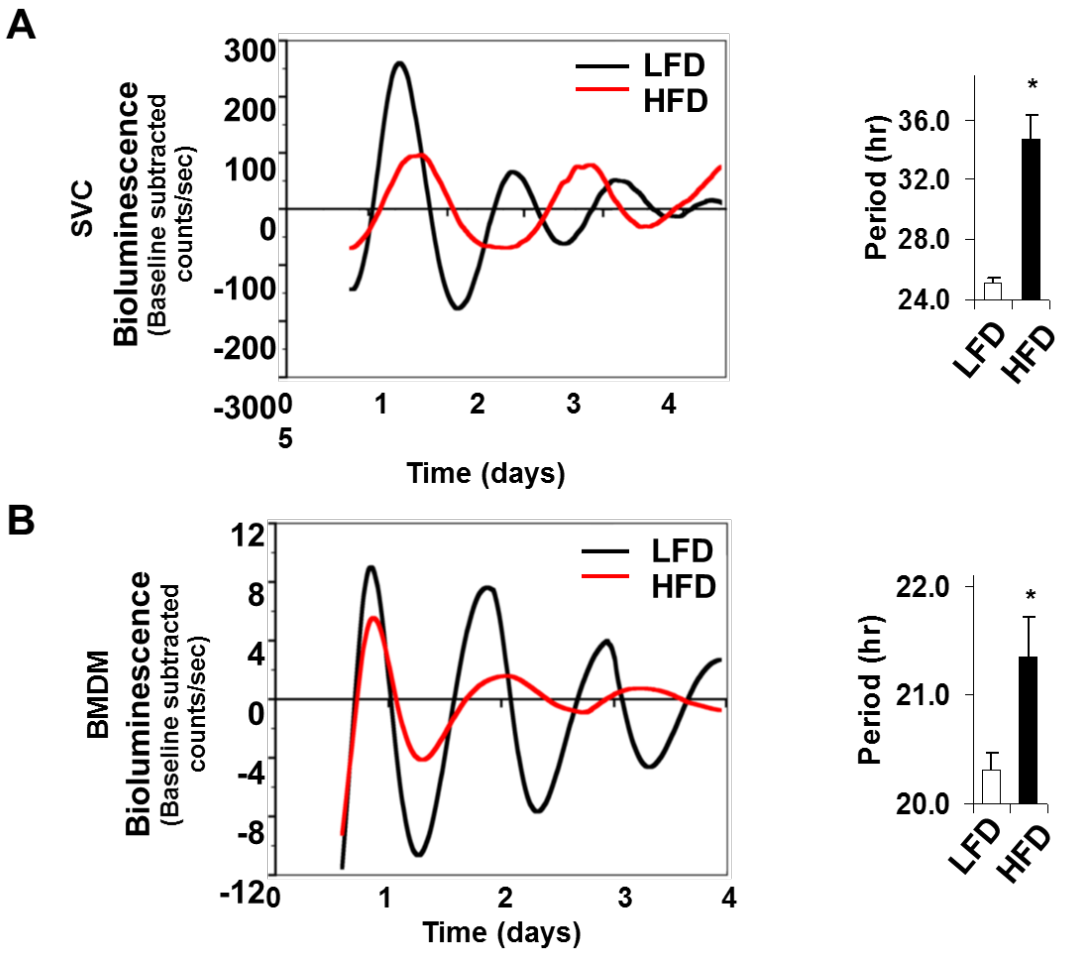

Figure 11. Overnutrition lengthens the period of clock gene oscillations in adipose tissue SVC and in BMDM.
At 5 – 6 wk of age, *mPer2*^{Luc} mice were fed an HFD or LFD for 12 wk (n = 5 – 6). Representative recordings of ensemble PER2::LUC bioluminescence (expressed as detrended baseline subtracted counts per second) from cultured adipose tissue stromal vascular cells (SVC) (A) or bone marrow-derived macrophages (BMDM) (B). Bar graphs depict group differences in PER2::LUC rhythm period between treatment groups. For bar graphs, data are means ± SE. *, $P < 0.05$ HFD vs. LFD. The bioluminescence data were generated by the collaborator Dr. Earnest's lab.

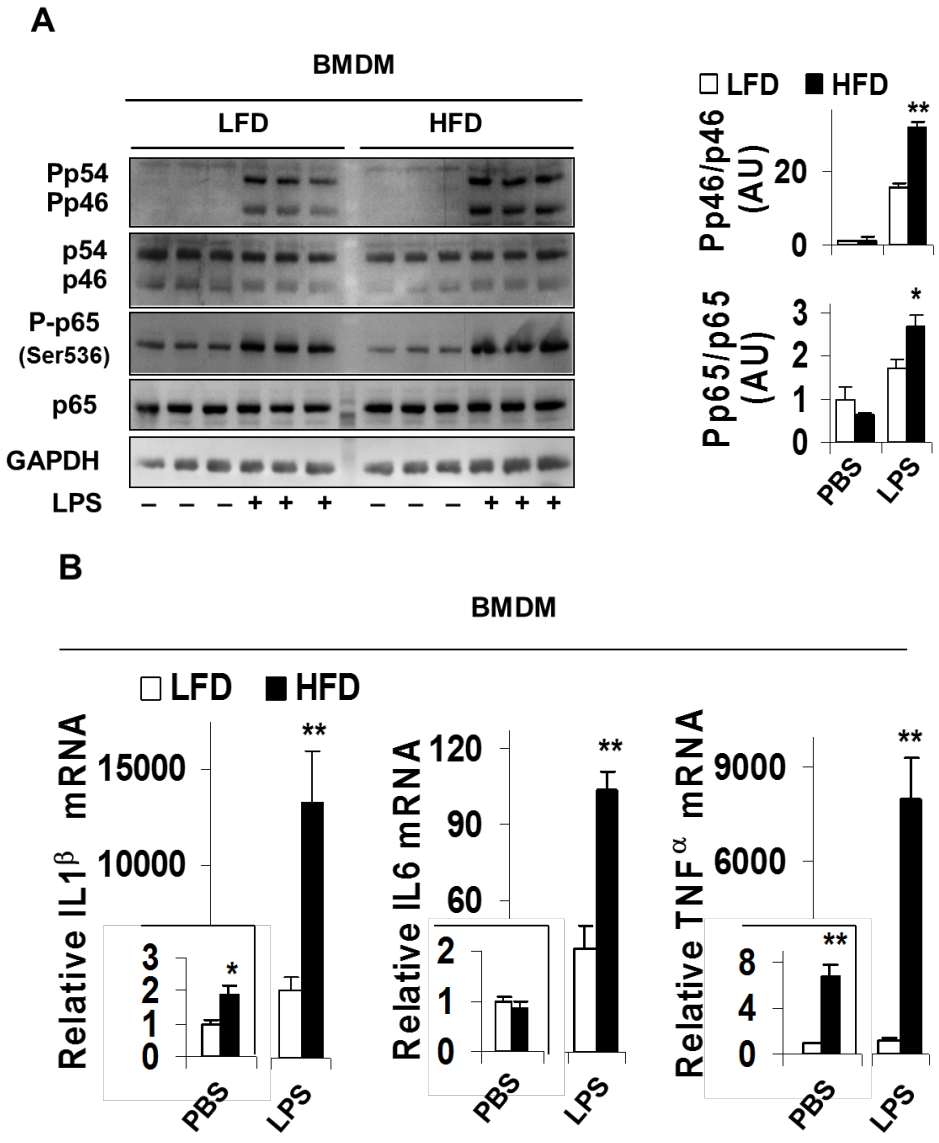

Figure 12. Overnutrition enhances macrophage proinflammatory responses. At 5 – 6 wk of age, *mPer2*^{Luc} mice were fed an HFD or LFD for 12 wk (n = 5 – 6). (A) Macrophage inflammatory signaling. Prior to harvest, BMDM were treated with LPS (100 ng/ml) or PBS for 30 min. The levels of JNK1 (p46), phospho-JNK1, NF-κB p65, and phospho-p65 (Ser-536) were examined using Western blot analyses and quantified using densitometry. (B) Macrophage IL-1β, IL-6, and TNF-α mRNA expression. Prior to harvest, BMDM were treated with LPS (100 ng/ml) or PBS for 6 hr. IL-1β and TNF-α mRNA levels were quantified using real-time PCR and plotted as relative expression. For bar graphs, data are means ± SE. *, $P < 0.05$ and **, $P < 0.01$ HFD vs. LFD under the same condition (PBS or LPS). AU, arbitrary units.

2.3.3 Circadian clock disruption increases macrophage proinflammatory activation

To address a direct role for circadian clock disruption in altering macrophage inflammatory status, BMDM obtained from mutant mice with targeted disruption of the clock genes Per1 and Per2 ($Per1^{ldc}/Per2^{ldc}$, 129J background), which are characterized by a loss of circadian rhythmicity [71], and BMDM from WT 129J mice were subjected to FACS analyses (Fig. 13).

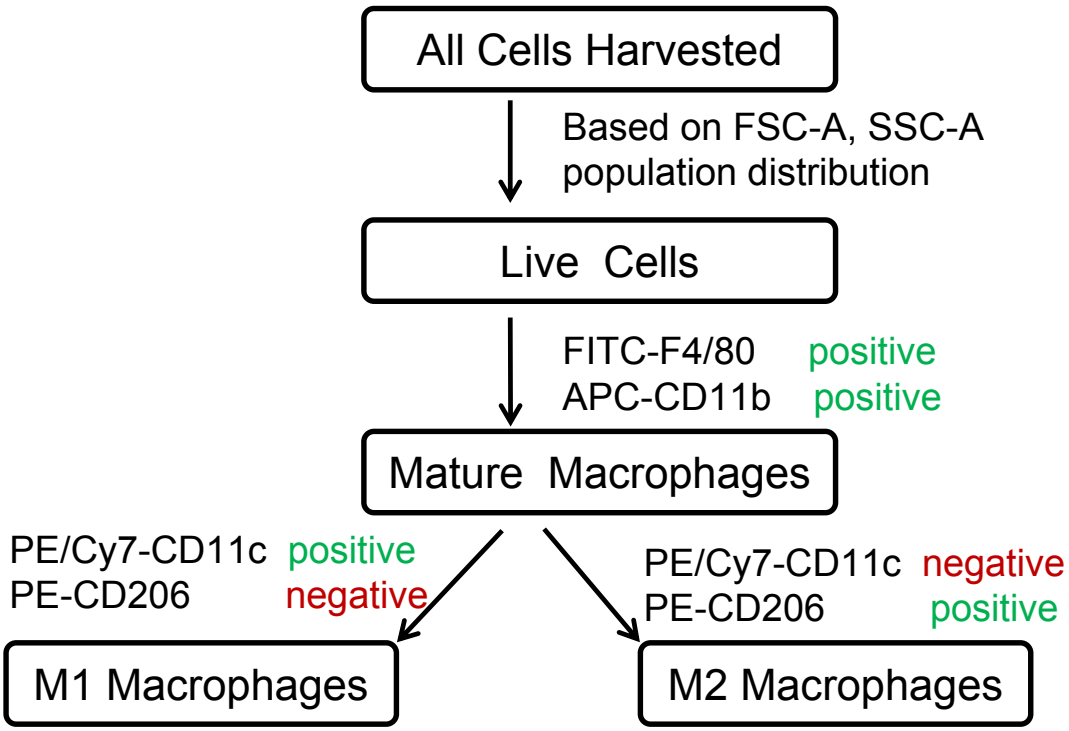

Figure 13. Flow chart of the FACS analysis for macrophage M1/M2 activation.

Among the analyzed cells, >95% of a total of 20,000-30,000 cells were mature macrophages ($F4/80^{+}CD11b^{+}$ cells) (Fig. 14A, quantitative data not included). Mature macrophages were then examined for activation status based on CD11c and CD206 expression (Fig. 14B top panel). Compared with controls, BMDM from Per1ldc/Per2ldc mutant mice displayed a significantly higher percentage of proinflammatory (M1) macrophages ($F4/80^{+}CD11b^{+}CD11c^{+}CD206^{-}$ cells) and no difference in percentage of anti-inflammatory (M2) macrophages ($F4/80^{+}CD11b^{+}CD11c^{-}CD206^{+}$ cells)(Fig. 14B bottom panel).

When inflammatory signaling was examined under basal conditions (PBS-treated), BMDM levels of JNK1 phosphorylation remained low with no genotype-based differences (Fig. 15A. However, in response to LPS, the phosphorylation of JNK1 in BMDM from Per1ldc/Per2ldc mice was significantly increased compared with that in BMDM from WT mice. Additionally, under both basal and LPS-treated conditions, NF-kB p65 (Ser-536) phosphorylation in BMDM from Per1ldc/Per2ldc mice was significantly higher than that in BMDM from WT mice. Among proinflammatory cytokines that were examined, IL-1b and TNFa mRNA expression in BMDM under both basal and LPS-treated conditions differed in accord with genotype (Fig. 15B). Compared with controls, BMDM from Per1ldc/Per2ldc mice exhibited significant increases in both basal and LPS-induced expression of IL-1b and TNFa mRNA. The levels of IL-6 mRNA did not differ between genotypes.

Thus, circadian clock malfunction associated with targeted disruption of Per1 and Per2 recapitulates macrophage proinflammatory activation induced by overnutrition.

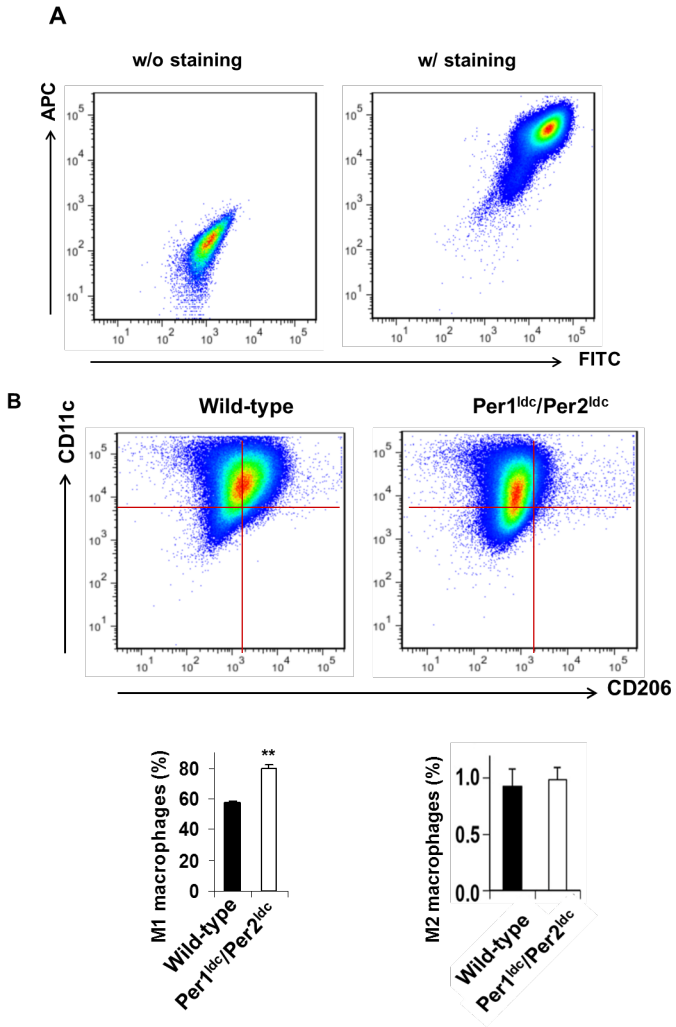

Figure 14. Per1/2 disruption increases macrophage proinflammatory activation. BMDM were prepared from chow diet-fed wild-type mice and *Per1*^{ldc}*/Per2*^{ldc} mice with targeted disruption of the clock genes Per1 and Per2 (n = 4 – 6). (A) Representative plots of macrophage purity and gating. BMDM were included without (left panel) or with (right panel) FITC-labeled anti-F4/80 and APC-labeled anti-CD11b antibodies and examined for FITC and APC intensities. (B) BMDM were examined for F4/80 and CD11b expression. Mature macrophages (F4/80$^+$ CD11b$^+$ cells) were then gated for CD11c and CD206 expression. Panels in (B), representative plots of proinflammatory (M1) macrophages (F4/80$^+$ CD11b$^+$ CD11c$^+$ CD206$^-$ cells) and anti-inflammatory (M2) macrophages (F4/80$^+$ CD11b$^+$ CD11c$^-$ CD206$^+$ cells); bar graph in (B), left panel for the percentages of M1 macrophages (upper left quadrant of panels in B) in mature macrophages and right panel for M2 macrophages (bottom right quadrant of panels in B). For bar graphs in (B), data are means ± SE. **, P < 0.01 *Per1*^{ldc}*/Per2*^{ldc} vs. wild-type.

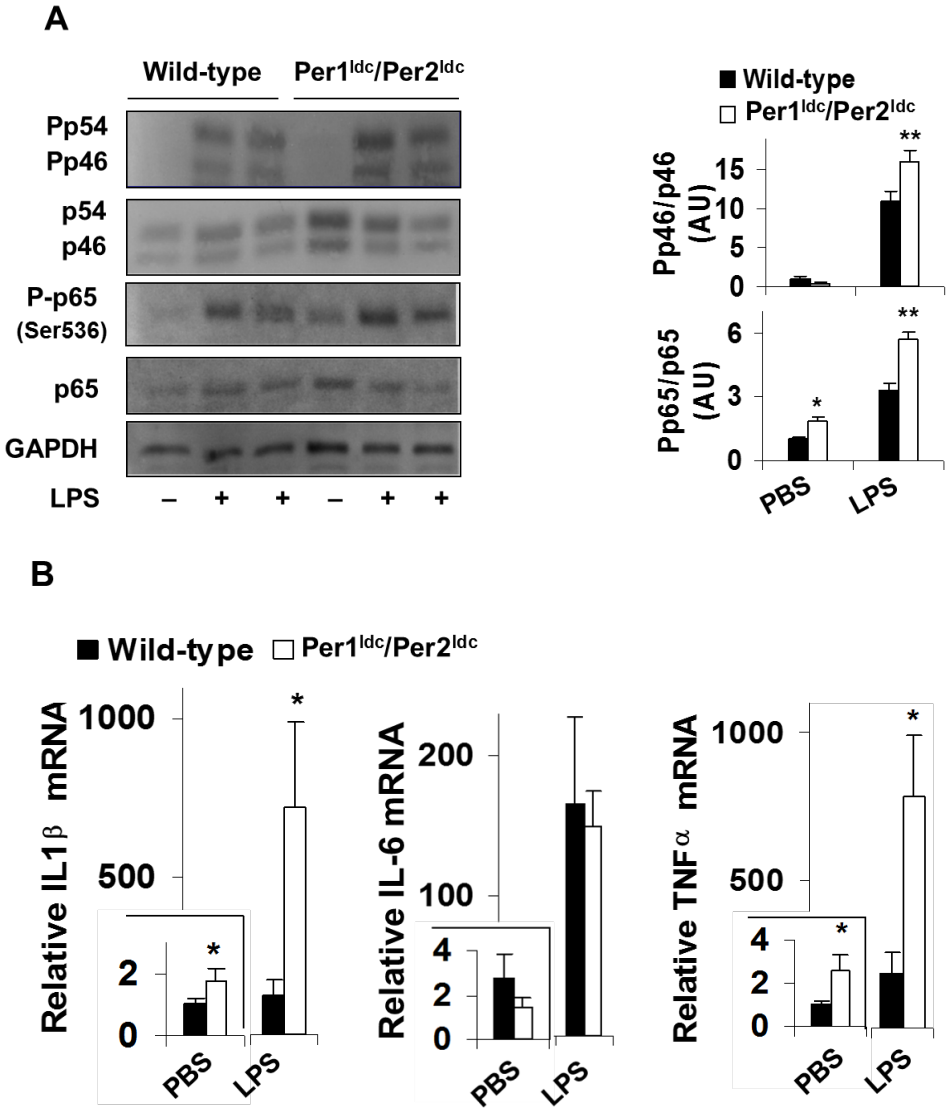

Figure 15. Per1/2 disruption increases macrophage proinflammatory responses. BMDM were prepared from chow diet-fed wild-type mice and *Per1^{ldc}/Per2^{ldc}* mice with targeted disruption of the clock genes Per1 and Per2 (n = 4 – 6). (A) Macrophage inflammatory signaling. Prior to harvest, BMDM were treated with LPS (100 ng/ml) or PBS for 30 min. The levels of total and phosphorylated JNK1 (p46) and NF-κB p65 were examined using Western blot analyses and quantified using densitometry. (B) Macrophage mRNA levels of proinflammatory cytokines. Prior to harvest, BMDM were treated with LPS (100 ng/ml) or PBS for 6 hr. The mRNA levels of IL-1β, IL-6, and TNFα were quantified using real-time PCR and plotted as relative expression. For bar graphs, data are means ± SE. *, $P < 0.05$ and **, $P < 0.01$ *Per1^{ldc}/Per2^{ldc}* vs. wild-type under the same condition (PBS or LPS). AU, arbitrary units.

2.3.4 PPARγ2 overexpression ameliorates Per1/2 disruption-associated macrophage proinflammatory activation

In subsequent mechanistic analyses, we next examined the expression of PPARγ because activation of this transcription factor stimulates macrophage alternative (anti-inflammatory) activation [56, 59], and its promoter region contains multiple E-boxes that bind the basic helix-loop-helix protein complexes formed by the core elements of the molecular clock brain muscle ARNT-like protein 1 (BMAL1) and circadian locomotor output cycles kaput (CLOCK) [80].

PPARγ protein levels in BMDM from Per1ldc/Per2ldc mice were significantly decreased by 40-60% relative to that observed in untreated and control vector-treated WT BMDM (Fig. 16). To address the potential involvement of PPARγ in Per1/2 regulation of macrophage activation, we next determined whether overexpression of PPARγ2, one of the two PPARγ isoforms that effectively mediates PPARγ actions [81], ameliorates the inflammatory status of BMDM from Per1ldc/Per2ldc mice. In comparison with cultures infected with a control vector, PPARγ2 overexpression in Per1ldc/Per2ldc-derived BMDM significantly increased PPARγ content by 2.5-fold (Fig. 16).

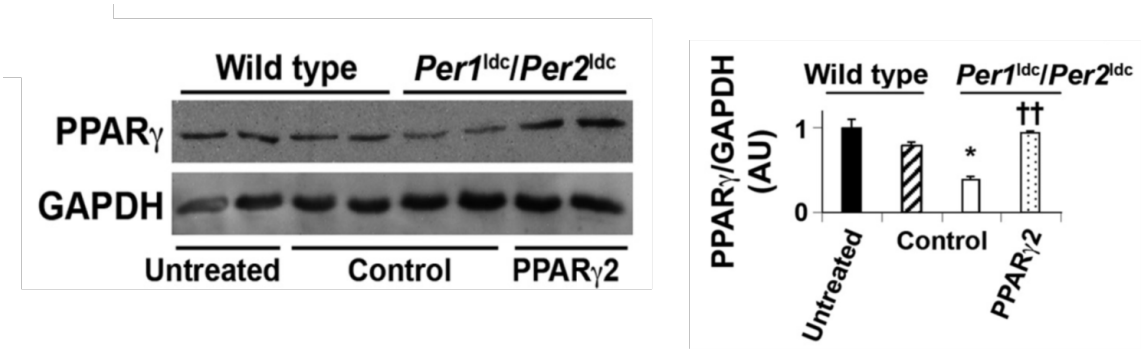

Figure 16. Per1/2 disruption decreased PPARγ protein levels.
BMDM were prepared from chow diet-fed wild-type mice and *Per1*^{ldc}/*Per2*^{ldc} mice with targeted disruption of the clock genes *Per1* and *Per2* (n = 4 – 8). Lysates of untreated macrophages, as well as PPARγ2-expressing-lentivirus- and/or control-lentivirus-treated macrophages were examined for PPARγ content. For the bar graph, PPARγ content was examined using Western blot analyses and quantified using densitometry. *Per1*^{ldc}/*Per2*^{ldc} -BMDM were infected with a lentivirus containing the cDNA of human PPARγ2 or a control lentivirus at 6 d after differentiation for 24 hr. Control vector-treated WT BMDM were included for comparison. The infected cells were incubated for an additional 48 hr and subjected to the pertinent assays. For bar graph, data are means ± SE. *, $P < 0.05$ *Per1*ldc/*Per2*ldc vs. wild-type for infected cells; †† $P < 0.01$ *Per1*^{ldc}/*Per2*^{ldc} +PPARγ2 vs. *Per1*^{ldc}/*Per2*^{ldc}. AU, arbitrary units.

Meanwhile, PPARγ2 overexpression in Per1ldc/Per2ldc-derived BMDM significantly reduced the phosphorylation of JNK1 and NF-kB p65 (Ser-536) in response to LPS-treatment, compared with cultures infected with a control vector (Fig. 17A)

When expression of inflammatory cytokines was examined, IL-1b and TNFa mRNA levels were similar under basal conditions in Per1ldc/Per2ldc controls and PPARγ2-overexpressing Per1ldc/Per2ldc BMDM. However, the LPS-mediated induction of IL-1b and TNFa, but not IL-6, mRNA levels in PPARγ2-overexpressing

Per1ldc/Per2ldc BMDM was significantly decreased relative to that found in control-treated Per1ldc/Per2ldc BMDM (Fig. 17B).

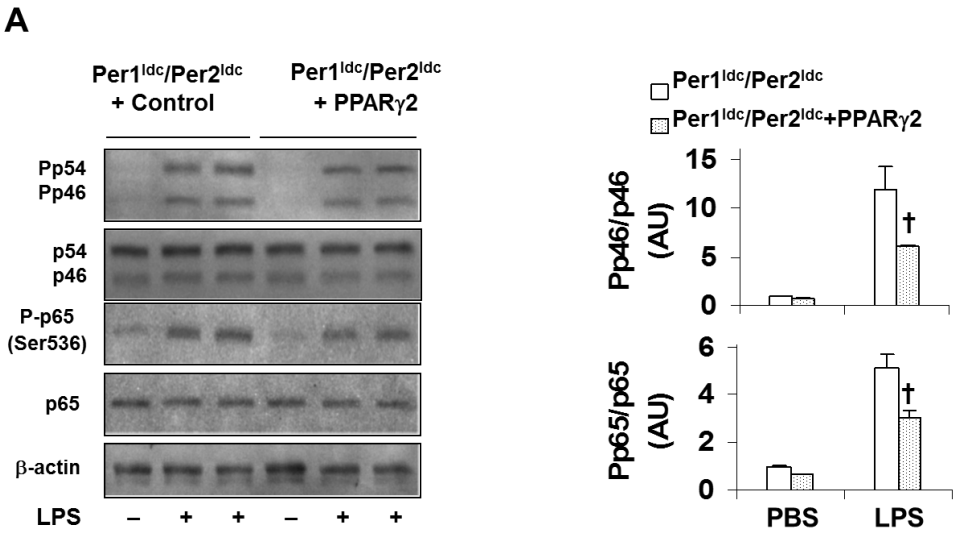

Figure 17. PPARγ2 overexpression ameliorates Per1/2 disruption-associated macrophage proinflammatory activation.
BMDM were prepared from chow diet-fed wild-type mice and *Per1*^{ldc}*/Per2*^{ldc} mice with targeted disruption of the clock genes *Per1* and *Per2* (n = 4 – 8). (A) Macrophage inflammatory signaling. Prior to harvest, BMDM were treated with LPS (100 ng/ml) or PBS for 30 min. The levels of total and phosphorylated JNK1 (p46) and NF-κB p65 were examined using Western blot analyses and quantified using densitometry. (B) Macrophage levels of IL-1β, IL-6, and TNFα mRNA. Prior to harvest, BMDM were treated with LPS (100 ng/ml) or PBS for 6 hr. The mRNA levels of cytokines were quantified using real-time PCR and plotted as relative expression. (C) The percentages of M1/M2 macrophages were examined using FACS analysis. *Per1*^{ldc}*/Per2*^{ldc} -BMDM were infected with a lentivirus containing the cDNA of human PPARγ2 or a control lentivirus at 6 d after differentiation for 24 hr. Control vector-treated WT BMDM were included for comparison. The infected cells were incubated for an additional 48 hr and subjected to the pertinent assays. For bar graphs, data are means ± SE. *, $P < 0.05$ and **, $P < 0.01$ *Per1*ldc/*Per2*ldc vs. wild-type for infected cells (C) under the same condition (B); †, $P < 0.05$ and †† $P < 0.01$ *Per1*^{ldc}*/Per2*^{ldc} +PPARγ2 vs. *Per1*^{ldc}*/Per2*^{ldc} (C) under LPS-treated condition (A and B). AU, arbitrary units.

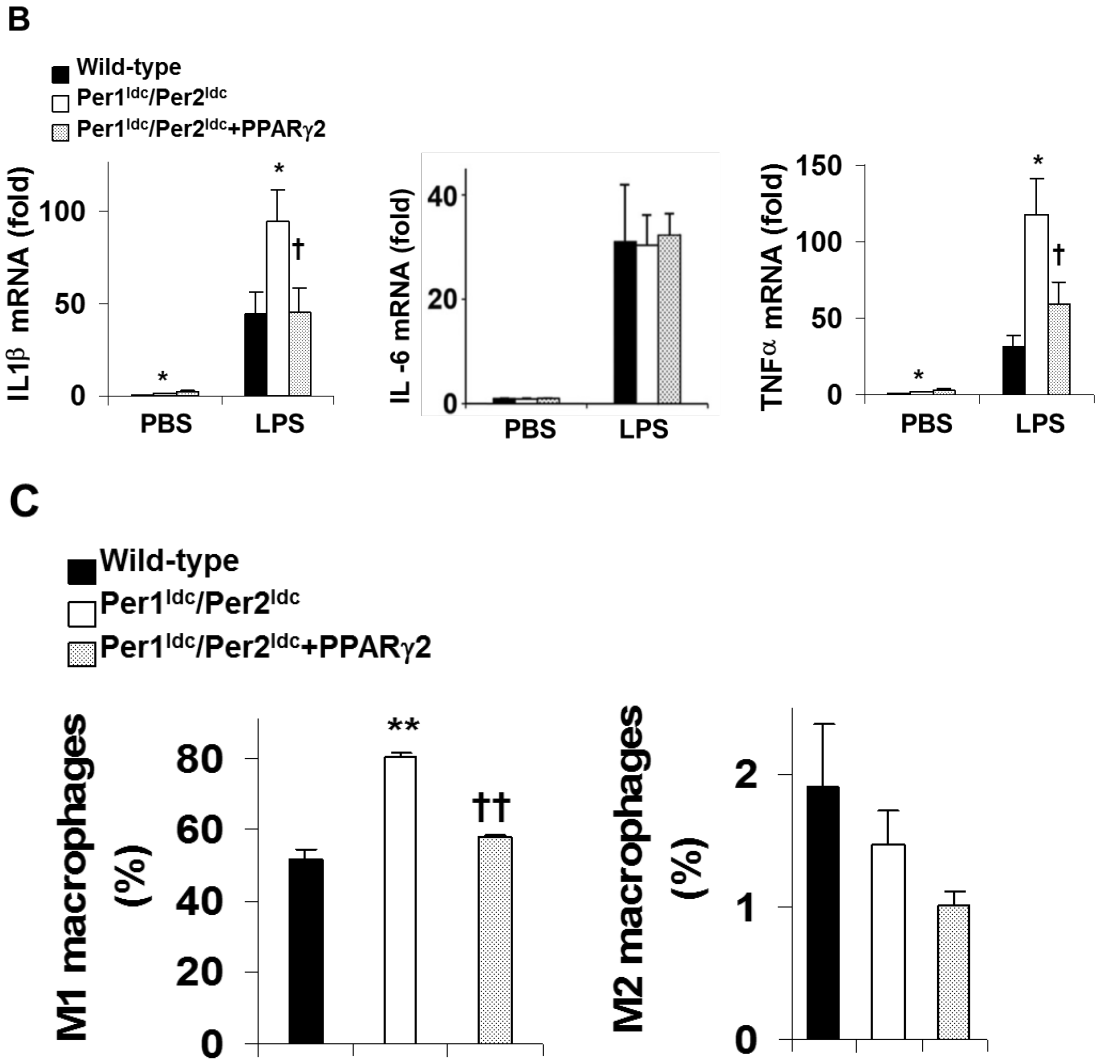

Figure 17 Continued.

Consistent with these observations, FACS analysis revealed that among analyzed mature macrophages, Per1ldc/Per2ldc controls showed a higher percentage of M1 macrophages compared with WT control cells. Importantly, PPARγ2 overexpression in

per1ldc/Per2ldc BMDM induced a significant decrease in the percentage of M1 macrophages relative to that observed in control-treated cells (Fig. 17C). Among three groups of BMDM (control-treated WT, control-treated Per1ldc/Per2ldc, PPARγ2-overexpressing Per1ldc/Per2ldc), the percentages of M2 macrophages did not differ significantly. Thus, PPARγ may play a role in the mechanism by which Per1/2 disruption up-regulates macrophage proinflammatory activation.

2.3.5 Confirmation of myeloid ccell-specific disruption of Per1/2

The inflammatory status of macrophages governs the outcome of adipose tissue inflammation and thereby systemic insulin sensitivity [58, 60]. To address the impact of macrophage-specific circadian clock on HFD-induced adipose tissue inflammation, bone marrow cells were isolated from per1ldc/Per2ldc mutant and WT mice and then transplanted into lethally irradiated WT recipient (C57BL/6J) mice (BMT) (Fig. 18). After HFD feeding for 12 wk and subsequent and metabolic characterization, bone marrow cells, BMDM, and adipose-derived SVC as well as adipose and liver tissues from chimeric mice were genotyped to identify WT and targeted alleles (Per1, Per2) and confirm bone cell repopulation.

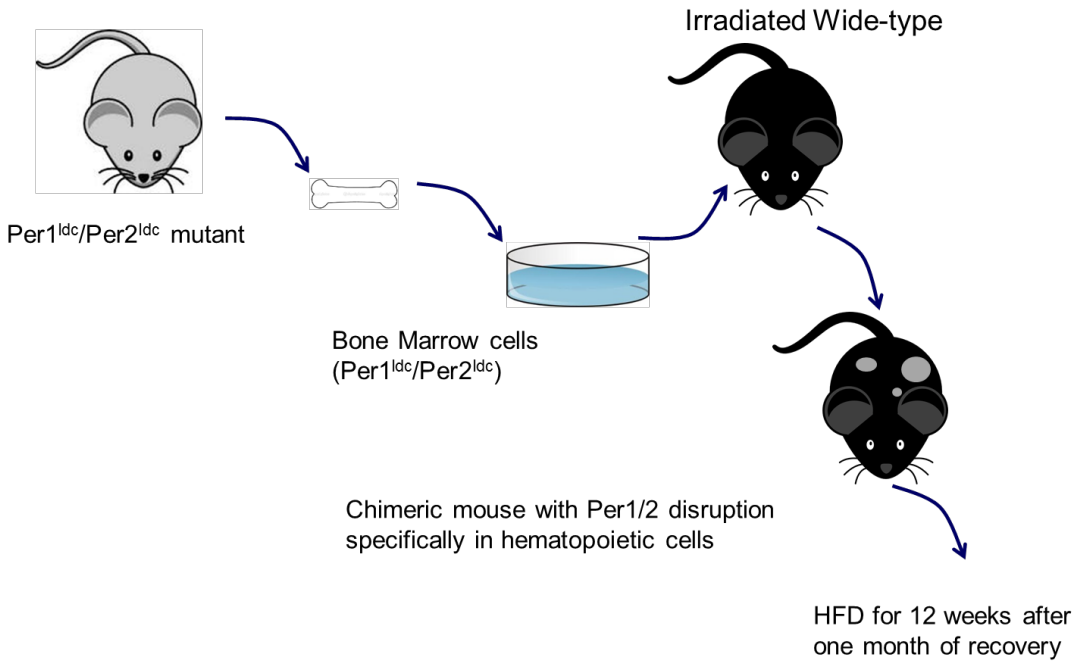

Figure 18. Bone marrow transplantation to form BMT-WT and BMT-Per1ldc/Per2ldc chimeric mice.

In BMT-WT mice (recipients, WT C57BL/6J mice; donors, WT 129J mice), genotyping of all genomic DNA samples revealed PCR products for only WT alleles (Fig. 19) In contrast, genomic DNA from all of these tissues/cells except BMDM in BMT-Per1ldc/Per2ldc mice (recipients, WT C57BL/6J mice; donors, Per1ldc/Per2ldc mice) showed PCR products for WT and mutant alleles. Genotyping of BMDM genomic DNA from BMT-Per1ldc/Per2ldc mice only yielded PCR products for mutant alleles (Fig. 19B). These results demonstrate the success of adoptive transfer of Per1/2-disrupted myeloid cells to WT recipient mice.

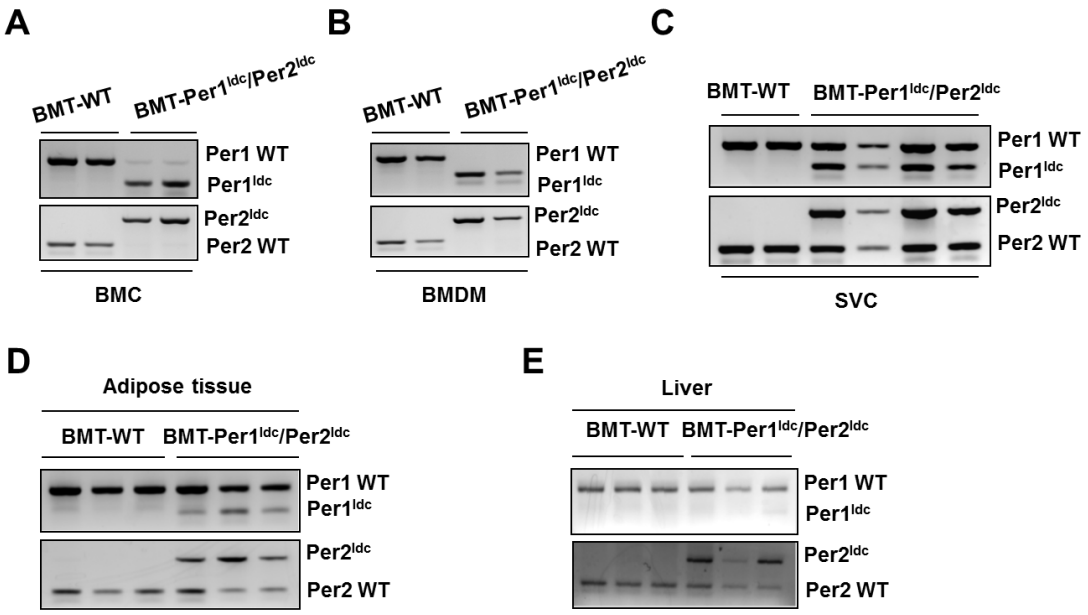

Figure 19. Confirmation of bone marrow cell repopulation.
Bone marrow cells from wild-type (WT) 129J mice and *Per1*^{ldc}*/Per2*^{ldc} (129J background) mice were transplanted into lethally irradiated male WT C57BL/6J mice (at 5 – 6 wk of age). After recovery for 4 wk, chimeric mice (BMT-WT and BMT-*Per1*^{ldc}*/Per2*^{ldc}) were fed an HFD for 12 wk. After the feeding regimen, genomic DNA was isolated from both isolated cells and tissue samples obtained from all chimeric mice and then subjected to PCR genotyping analyses to identify WT and targeted alleles (*Per1*, *Per2*) and confirm bone cell repopulation. The amplified band of smaller size (~ 235bp, top panel) signifies the *Per1* targeted alleles whereas the PCR product of larger size (~ 403bp, bottom panel) denotes the *Per2* targeted alleles in (A) Bone marrow cells; (B) Bone marrow-derived macrophages (BMDM); (C) Adipose tissue stromal vascular cells (SVC); (D) Adipose tissue; and (E) Liver. The confirmation data were generated by the collaborator Dr. Earnest's lab.

2.3.6 Myeloid cell-specific Per1/2 disruption exacerbates adipose tissue inflammation in obesity

When adipose tissue inflammatory status was examined, the phosphorylation of JNK1 and NF-kB p65 (Ser-536) in HFD-fed BMT-Per1ldc/Per2ldc mice was significantly

increased (Fig. 20A) compared with that in HFD-fed BM-WT. Additionally, adipose tissue IL-1b, IL-6 and TNFa mRNA levels in HFD-fed BMT-Per1ldc/Per2ldc mice were significantly higher than their respective levels in HFD-fed BMT-WT mice (Fig. 20B), whereas BMT genotype had no significant effect on the mRNA levels of arginase 1 and IL-10, which are indicative of macrophage alternative activation.

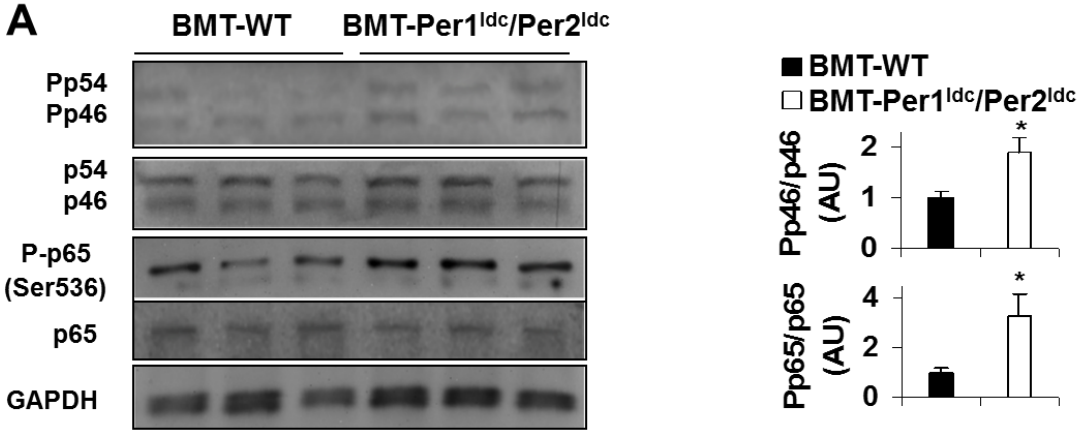

Figure 20. Myeloid cell-specific Per1/2 disruption exacerbates HFD-induced adipose tissue inflammation.
Chimeric mice (BMT-WT and BMT- *Per1*^{ldc}*/Per2*^{ldc}) were fed an HFD for 12 wk (n = 6 – 10). Prior to tissue collection, mice were fasted for 4 hr starting at the same time of the day. (A) Adipose tissue inflammatory signaling. The levels of total and phosphorylated JNK1 (p46) and NF-κB p65 were examined using Western blot analyses and quantified using densitometry. (B) Adipose tissue expression of genes related to macrophage polarization. The mRNA levels of cytokines and arginase1 were quantified using real-time PCR and plotted as relative expression. For bar graphs, data are means ± SE. *, P<0.05 and **, P<0.01 BMT *Per1*^{ldc}*/Per2*^{ldc} vs. BMT-WT (A) for the same gene (B). AU, arbitrary units.

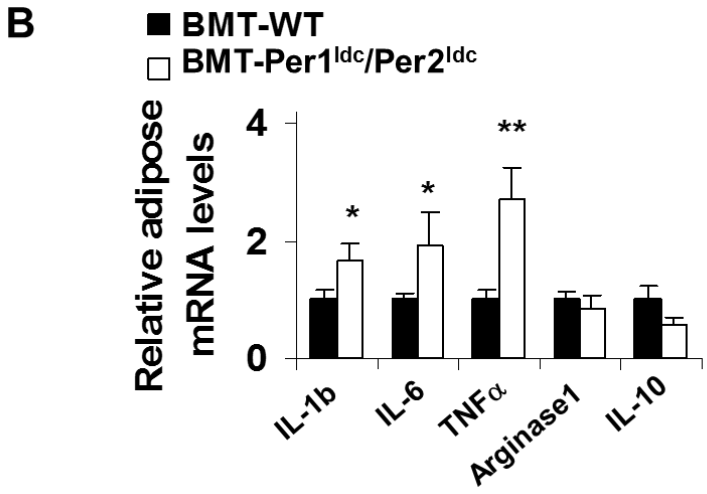

Figure 20 Continued.

Next, adipose-derived SVC were subjected to FACS analyses. After HFD feeding, SVC of BMT-Per1ldc/Per2ldc mice displayed a 1.8-fold increase in mature macrophages ($F4/80^+$ $CD11b^+$ cells) compared with those of BMT-WT mice (Fig. 21A). Upon analyzing the inflammatory status of the mature macrophages, adipose tissue SVC isolated from BMT-Per1ldc/Per2ldc mice showed a 2-fold increase in the overall percentage of proinflammatory macrophages ($F4/80^+$ $CD11b^+$ $CD11c^+$ $CD206^-$ cells) relative to that observed in BMT-WT mice (Fig. 21B). In contrast, the percentage of M2 macrophages in adipose tissue SVC did not differ between the WT and mutant groups. Thus, myeloid cell-specific Per1/2 disruption increases adipose tissue infiltration of proinflammatory macrophages, thereby exacerbating HFD-induced adipose tissue inflammatory responses.

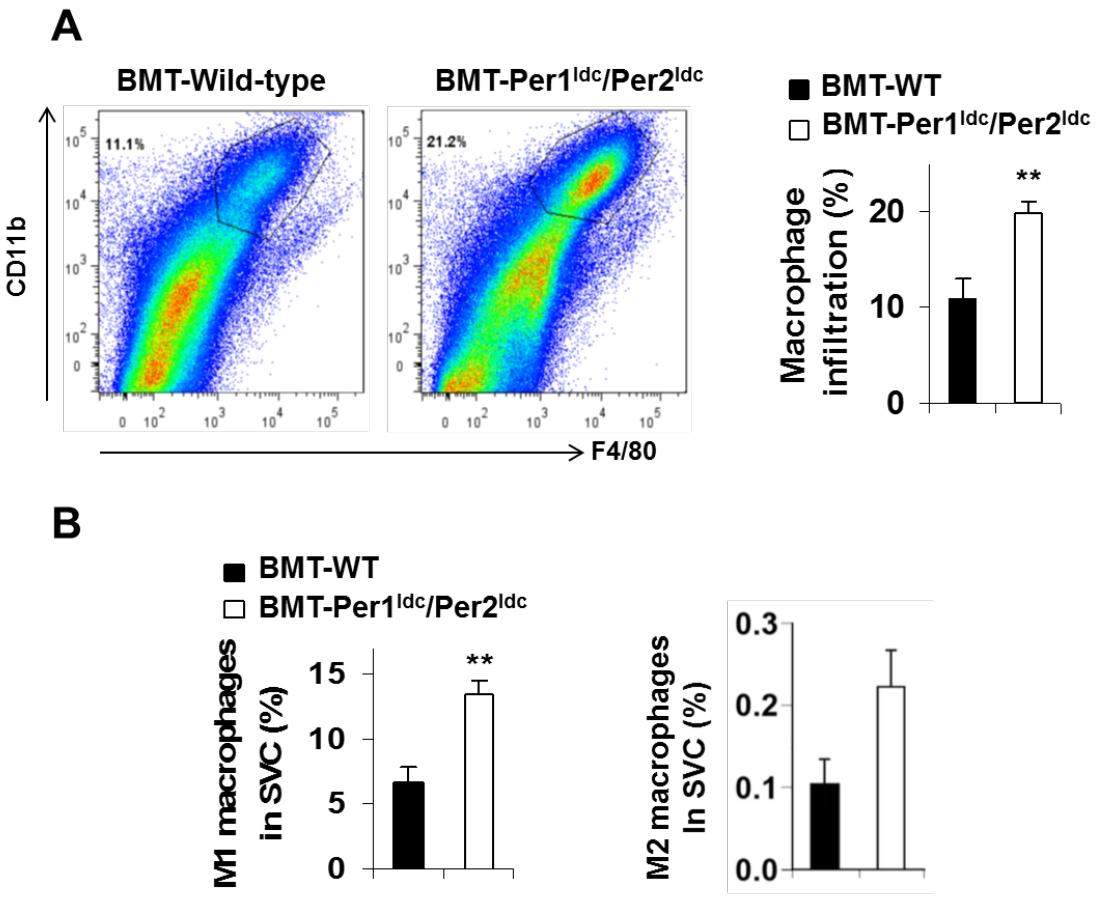

Figure 21. Myeloid cell-specific Per1/2 disruption exacerbates adipose tissue macrophages proinflammatory activation.
Chimeric mice (BMT-WT and BMT- *Per1*^{ldc}*/Per2*^{ldc}) were fed an HFD for 12 wk (n = 6 – 10). Prior to tissue collection, mice were fasted for 4 hr starting at the same time of the day. (A) FACS analyses of macrophage infiltration in epididymal fat pads of HFD-fed chimeric mice. Left two panels, representative images of adipose tissue stromal vascular cells (SVC) that were quantified for F4/80 and CD11b expression; right panel, percentages of mature macrophages (F4/80^{+} CD11b^{+} cells). (B) Quantification of proinflammatory (M1) macrophages (F4/80^{+} CD11b^{+} CD11c^{+} CD206^{-} cells), and anti-inflammatory (M2) macrophages (F4/80^{+} CD11b^{+} CD11c^{-} CD206^{+} cells) in SVC isolated from adipose tissue of HFD-fed chimeric mice. For bar graphs, data are means ± SE. **, P<0.01 BMT *Per1*^{ldc}*/Per2*^{ldc} vs. BMT-WT.

2.3.7 Myeloid cell-specific Per1/2 disruption exacerbates adiposity and adipose tissue dysfunction

Next, we examined the effects of myeloid cell-specific circadian clock disruption on adipose tissue metabolic responses in WT recipients. In response to HFD feeding, BMT-Per1ldc/Per2ldc mice gained much more abdominal fat mass and displayed a greater increase in adiposity than BMT-WT mice (Fig. 22, A and B). Consistent with these changes, the size of most adipocytes in adipose tissue was larger in BMT-Per1ldc/Per2ldc mice than in BMT-WT mice (Fig. 22C)

Locally, adipose tissue of HFD-fed BMT-Per1ldc/Per2ldc mice showed a significant decrease in insulin-induced Akt phosphorylation (Ser-473) relative to that observed in HFD-fed BMT-WT mice (Fig. 23A), and this decrease was accompanied by decreased adipose tissue expression of mRNAs encoding adiponectin, and adipokine that improves systemic insulin sensitivity, and hormone-sensitive lipase (Fig. 23B), a rate-determining enzyme that controls adipose tissue fat deposition by hydrolyzing triglycerides stored in adipose tissue lipid droplets. Compared with HFD-fed BMT-WT mice, HFD-fed BMT-Per1ldc/Per2ldc mice also showed a significant increase in adipose tissue mRNA levels of resistin, an adipokine that promotes systemic insulin resistance (Fig. 23B); although adipose tissue mRNA levels of MCP1, whose increase in adipocytes attracts macrophage infiltration, and TLR4, an inflammatory receptor, did not differ between HFD-fed BMT-Per1ldc/Per2ldc mice and BMT-WT mice.

Together, these results indicate that myeloid cell-specific Per1/2 disruption potentiates HFD-induced adipose tissue dysfunction.

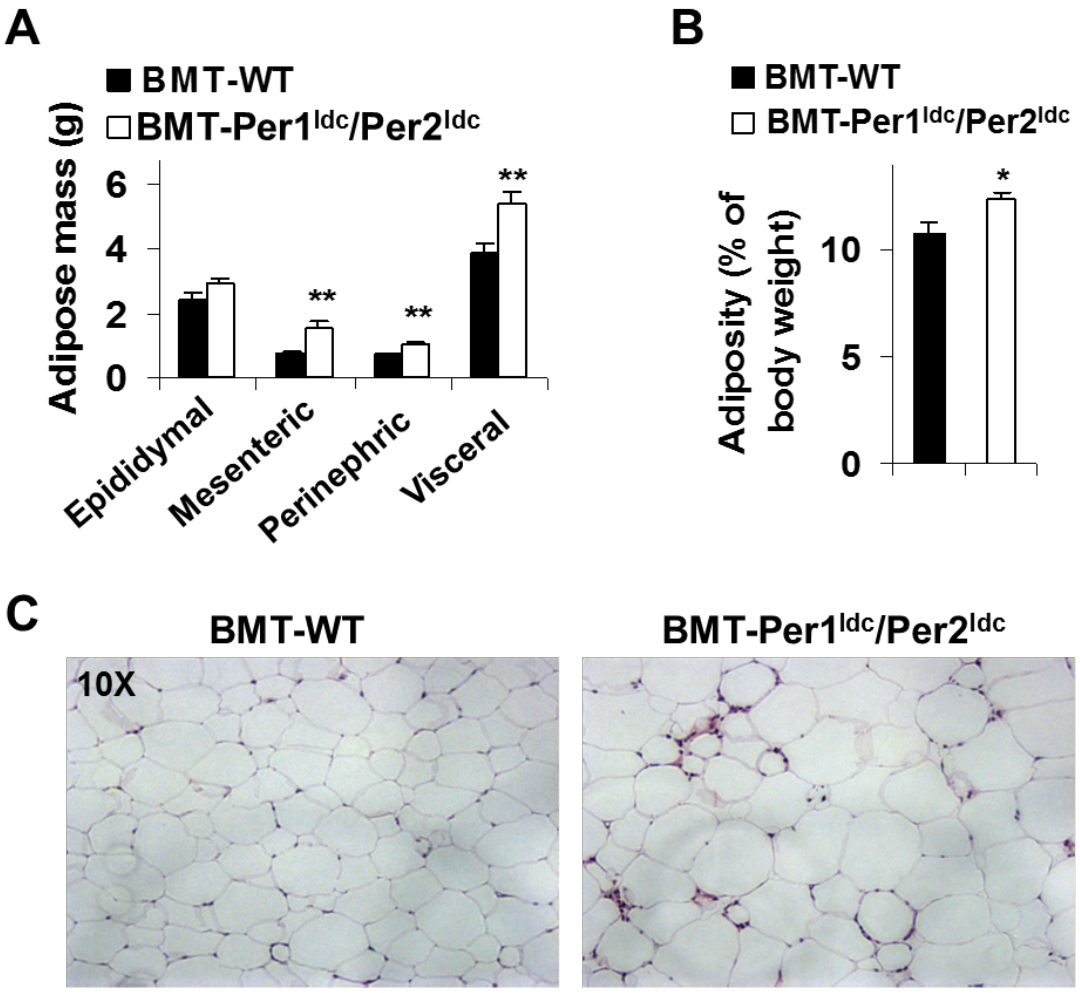

Figure 22. Myeloid cell-specific Per1/2 disruption exacerbates HFD-induced adiposity.

Chimeric mice (BMT-WT and BMT- *Per1*^{ldc}*/Per2*^{ldc}) were fed an HFD for 12 wk (n = 6 – 10). Prior to tissue collection or insulin injection, mice were fasted for 4 hr starting at the same time of the day. (A) Adipose mass. Abdominal fat mass was calculated as the sum of epididymal, mesenteric, and perinephric fat content. (B) Adiposity was calculated by normalizing abdominal fat content to body weight. (C) H&E staining of adipose tissue. For bar graphs (A and B), data are means ± SE. *, $P < 0.05$ and **, $P < 0.01$ BMT- *Per1*^{ldc}*/Per2*^{ldc} vs. BMT-WT (B) for the same fat pad (A).

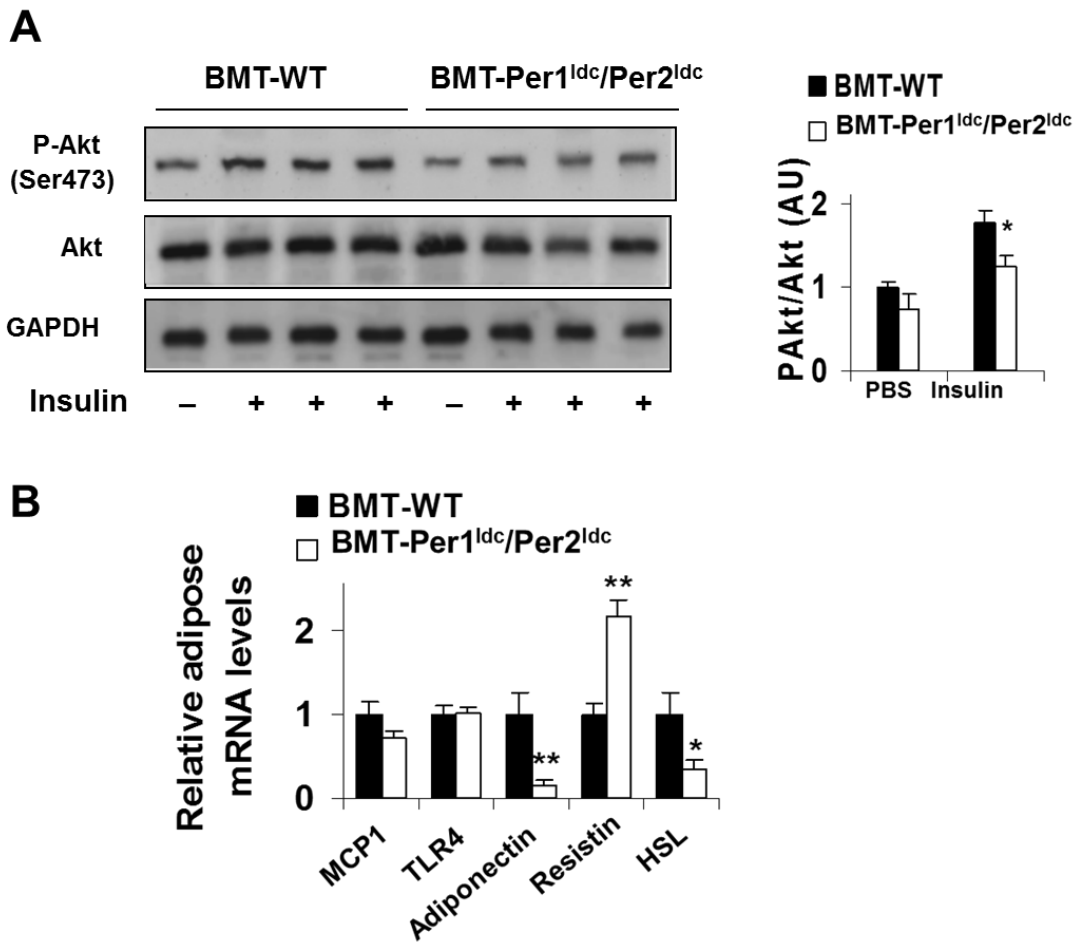

Figure 23. Myeloid cell-specific Per1/2 disruption exacerbates HFD-induced adipose tissue insulin resistance.
Chimeric mice (BMT-WT and BMT- *Per1*^{ldc}*/Per2*^{ldc}) were fed an HFD for 12 wk (n = 6 – 10). Prior to tissue collection or insulin injection, mice were fasted for 4 hr starting at the same time of the day. (A) Adipose tissue insulin signaling. After fasting, HFD-fed chimeric mice were given a bolus injection of insulin (1 U/kg body weight) or PBS into the portal vein. The levels of total and phosphorylated Akt1/2 were examined using Western blot analyses and quantified using densitometry. (B) Adipose tissue gene expression. The adipose mRNA levels of genes involved in adipose tissue inflammatory and metabolic responses were quantified using real-time PCR and plotted as relative expression. For bar graphs (A and B), data are means ± SE. *, $P < 0.05$ and **, $P < 0.01$ BMT- *Per1*^{ldc}*/Per2*^{ldc} vs. BMT-WT under the same condition (Insulin in A) or for the same gene (B). AU, arbitrary units.

2.3.8 Per1/2-disrupted macrophages increase adipocyte inflammatory responses and impair adipocyte functions

Given the critical role of macrophages in initiating or exacerbating adipose tissue inflammation, we co-cultured macrophages and adipocytes at a 1:10 ratio to address the direct effects of circadian clock disruption on macrophages and/or macrophage factors that regulate adipocyte function. Compared with co-cultures containing adipocytes and WT BMDM (Adi/WT BMDM), adipocytes cultures with Per1ldc/Per2ldc BMDM (Adi/Per1ldc/Per2ldc BMDM) showed a much greater increase in NF-kB p65 (Ser-536) phosphorylation in response to LPS treatment (Fig. 24A).

Adipocytes cultured with Per1ldc/Per2ldc BMDM also exhibited a significant increase in IL-1b, IL-6, RNF-a, and resistin mRNA levels and a decrease in adiponectin mRNA levels compared with their respective levels in Adi/WT BMDM co-cultures (Fig. 24B), indicating increased production of pro-insulin resistant and pro-hyperglycemic factors.

When insulin signaling was analyzed, adipocytes cultured with Per1ldc/Per2ldc BMDM showed a significant decrease in insulin-induced Akt phosphorylation (Ser-473) compared with Adi/WT BMDM co-cultures (Fig. 24C). Taken together, these results suggest that Per1/2-disrupted macrophages directly increase adipocyte proinflammatory responses and decrease adipocyte insulin sensitivity.

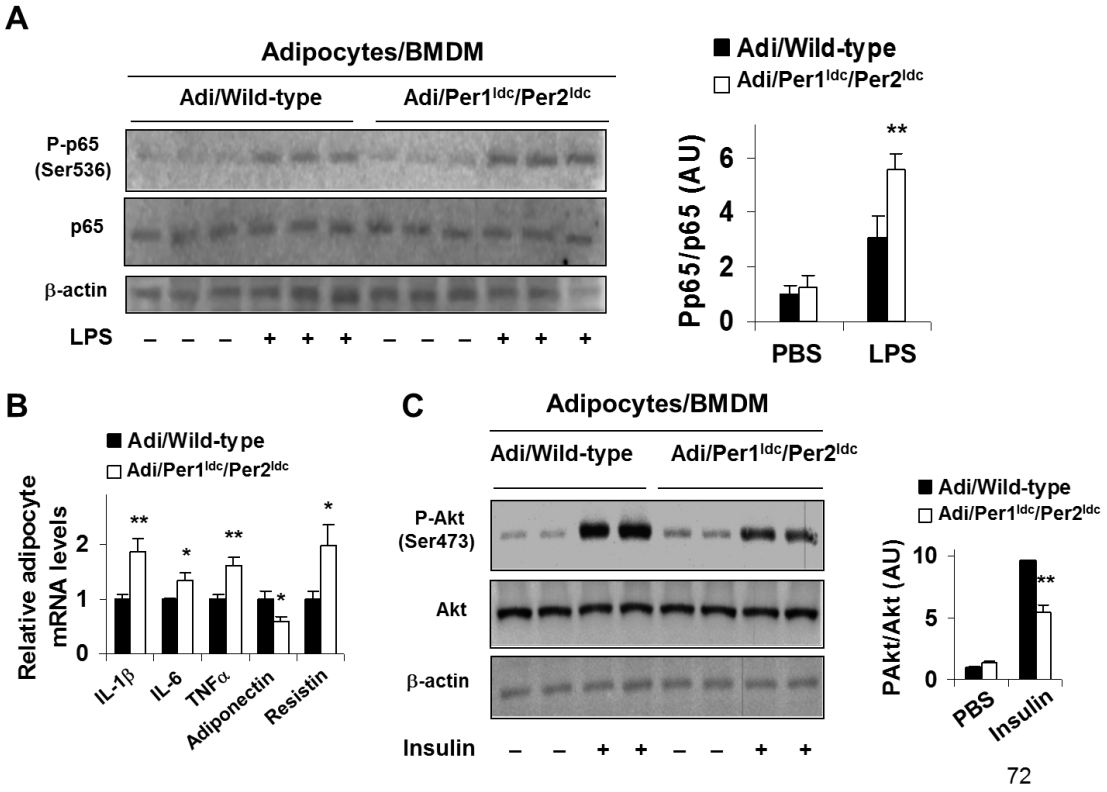

Figure 24. Per1/2-disrupted macrophages increase adipocyte inflammatory responses and impair adipocyte insulin signaling in co-cultures.
Adipocytes were co-cultured with macrophages differentiated from bone marrow cells of wild-type (Adi/Wild-type) or *Per1^{ldc}/Per2^{ldc}* mice (Adi/ *Per1^{ldc}/Per2^{ldc}*) at a 10:1 ratio (adipocytes: macrophages) for 48 hr (n = 4–6). **(A)** NF-κB signaling of co-cultured adipocytes. Prior to harvest, adipocyte-macrophage co-cultures were treated with LPS (100 ng/ml) or PBS for 30 min. The levels of total and phosphorylated NF-κB p65 were examined using Western blot analyses and quantified using densitometry. **(B)** Cytokine and adipokine mRNA levels in co-cultured adipocytes were quantified using real-time PCR and plotted as relative expression. **(C)** Insulin signaling of co-cultured adipocytes. Prior to harvest, the co-cultures were treated with insulin (100 nM) or PBS for 30 min. The levels of total and phosphorylated Akt1/2 were examined using Western blot analyses and quantified using densitometry. For bar graphs, data are means ± SE. *, $P < 0.05$ and **, $P < 0.01$ Adi/ *Per1^{ldc}/Per2^{ldc}* vs. Adi/Wild-type under the same condition (LPS in A; Insulin in C) for the same gene (B). AU, arbitrary units.

2.3.9 Myeloid cell-specific Per1/2 disruption exacerbates diet-induced insulin resistance and glucose intolerance

Macrophage-driven adipose tissue inflammation contributes to the development of systemic insulin resistance [62, 63]. We examined systemic pathophysiology. Before HFD feeding, the body weight of BMT-Per1ldc/Per2ldc mice did not differ from BMT-WT mice. After HFD feeding, BMT-Per1ldc/Per2ldc mice gained more body weight and consumed more food than BMT-WT mice (Fig. 25, A and B). However, feeding efficiency did not differ between two groups of chimeric mice (Fig. 25B).

Compared with HFD-fed BMT-WT mice, HFD-fed BMT-Per1ldc/Per2ldc mice exhibited a significant increase in plasma insulin and glucose levels (Fig. 25, C and D); however, plasma triglyceride and free fatty acid levels remained unchanged (data not shown). In addition, HFD-fed BMT-Per1ldc/Per2ldc mice displayed a significant increase in the severity of insulin resistance and glucose intolerance indicated by insulin and glucose tolerance testes, respectively (Fig. 25, E and F). Thus, disruption of myeloid cell-specific circadian clock mechanism is sufficient to exacerbate HFD-induced insulin resistance and metabolic dysregulation.

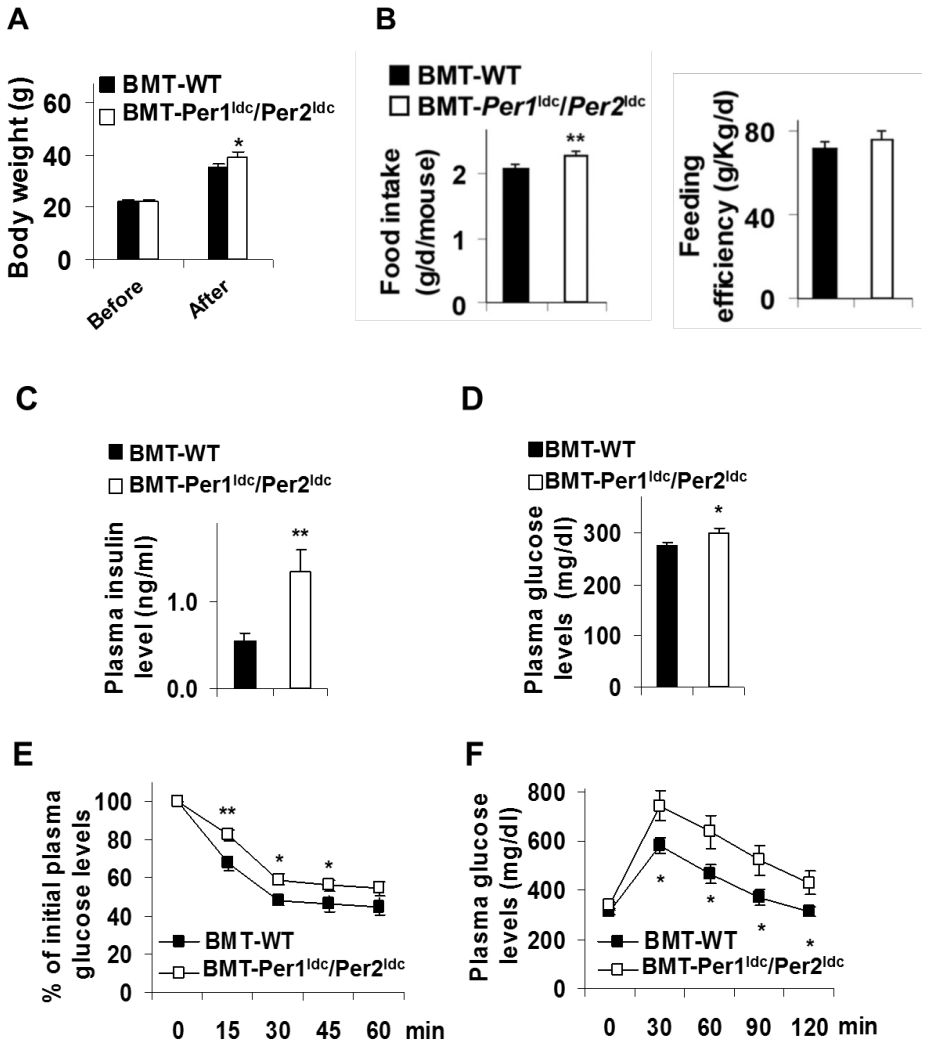

Figure 25. Myeloid cell-specific Per1/2 disruption exacerbates diet-induced insulin resistance and glucose intolerance.
Chimeric mice (BMT-WT and BMT- *Per1*^{ldc}/*Per2*^{ldc}) were fed an HFD for 12 wk (n = 6 – 10). **(A)** Body weight was monitored before and after HFD feeding. **(B)** Food intake was recorded during the feeding period and calculated as food consumption (g) per day per mouse. Right panel, feeding efficiency was calculated as the ratio of food intake to body weight. **(C)** Plasma levels of 19 insulin. **(D)** Plasma levels of glucose. **(E)** Insulin tolerance tests. **(F)** Glucose tolerance tests. For A – F, data are means ± SE. *, $P < 0.05$ and **, $P < 0.01$ BMT- *Per1*^{ldc}/*Per2*^{ldc} vs. BMT-WT (B – D) under the same condition (A) or time point (E and F). For C – F, HFD-fed chimeric mice were fasted for 4 hr starting at the same time of the day prior to tissue collection or physiological assays. For E and F, mice were given a peritoneal injection of insulin (1 U/kg) (E) or glucose (2 g/kg) (F).

2.3.10 Myeloid cell-specific Per1/2 disruption exacerbates liver inflammatory responses, insulin resistance, and metabolic dysregulation

During obesity, adipose tissue inflammation and dysfunction can produce distal effects on liver inflammatory and metabolic responses [77, 82], which in turn also contribute to the control of systemic insulin sensitivity and glucose homeostasis. Thus, we used the same BMT-WT and BMT-Per1ldc/Per2ldc mice to concurrently analyze the effect of myeloid cell-specific circadian clock disruption on liver responses. Compared with HFD-fed BMT-WT mice, HFD-fed BMT-Per1ldc/Per2ldc mice exhibited a significant increase in liver inflammatory responses, indicated by the increases in the phosphorylation of JNK1 (1.7-fold) and NF-kB p65 (2-fold) (Fig. 26A) and in the mRNA levels of IL-1b, IL-6, and TNFa (Fig. 26B).

Meanwhile, HFD-fed BMT-Per1ldc/Per2ldc mice displayed a significant increase in the liver weight (Fig. 26C) and a corresponding increase in the severity of hepatic steatosis (Fig. 26D).

When insulin signaling was analyzed, liver tissue from HFD-fed BMT-Per1ldc/Per2ldc mice showed significant decreases in insulin-induced Akt phosphorylation (Ser-473) (Fig. 26E). Consistent with increased severity of hepatic steatosis, HFD-fed BMT-Per1ldc/Per2ldc mice were distinguished from controls by a significant increase in liver mRNA levels of SREBP1c and FAS, which are, respectively, a critical transcription factor and a lipogenic enzyme that promotes lipogenesis and hepatic steatosis (Fig. 26F) relative to that found in control mice. These results indicate

that similar to adipose tissue, HFD-induced liver metabolic dysregulation is amplified by myeloid cell-specific Per1/2 disruption.

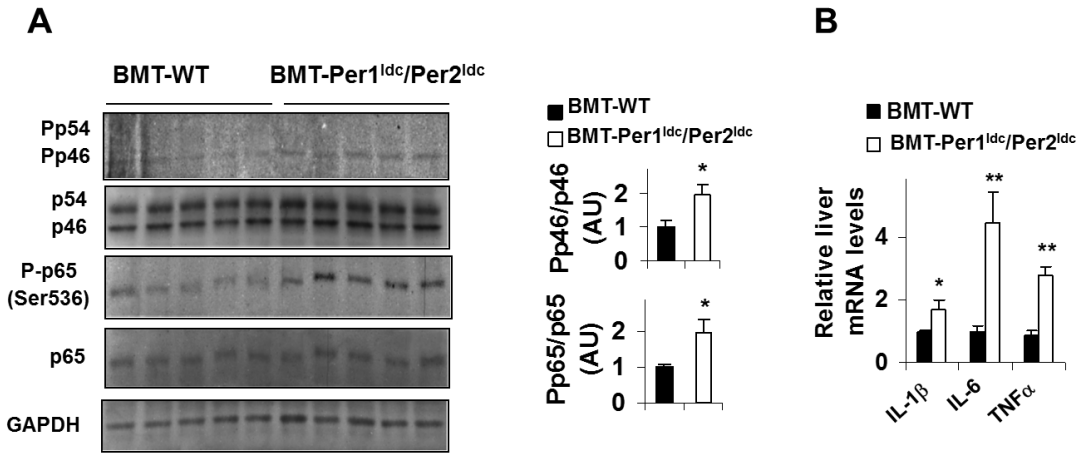

Figure 26. Myeloid cell-specific Per1/2 disruption exacerbates HFD-induced liver inflammatory responses and insulin resistance.
Chimeric mice (BMT-WT and BMT- *Per1*^{ldc}*/Per2*^{ldc}) were fed an HFD for 12 wk (n = 6 – 10). **(A)** Liver inflammatory signaling. The levels of total and phosphorylated JNK1 (p46) and NF-κB p65 were examined using Western blot analyses and quantified using densitometry. **(B)** Liver levels of proinflammatory cytokine mRNAs. **(C)** Liver weight. **(D)** Liver histology (H&E staining). **(E)** Liver insulin signaling. **(F)** Liver mRNA levels of key metabolic genes. For A – F, HFD-fed chimeric mice were fasted for 4 hr starting at the same time of the day prior to tissue collection (A – D, and F) or insulin injection (E). For B and F, liver mRNA levels of metabolic genes were quantified using real-time PCR and plotted as relative expression. For E, chimeric mice were given a bolus injection of insulin (1 U/kg body weight) or PBS into the portal vein. For bar graphs (A – C, E, and F), data are means ± SE. *, $P < 0.05$ and **, $P < 0.01$ BMT- *Per1*^{ldc}*/Per2*^{ldc} vs. BMT-WT (A – C) under same condition (Insulin in E) for the same gene (F). AU, arbitrary units.

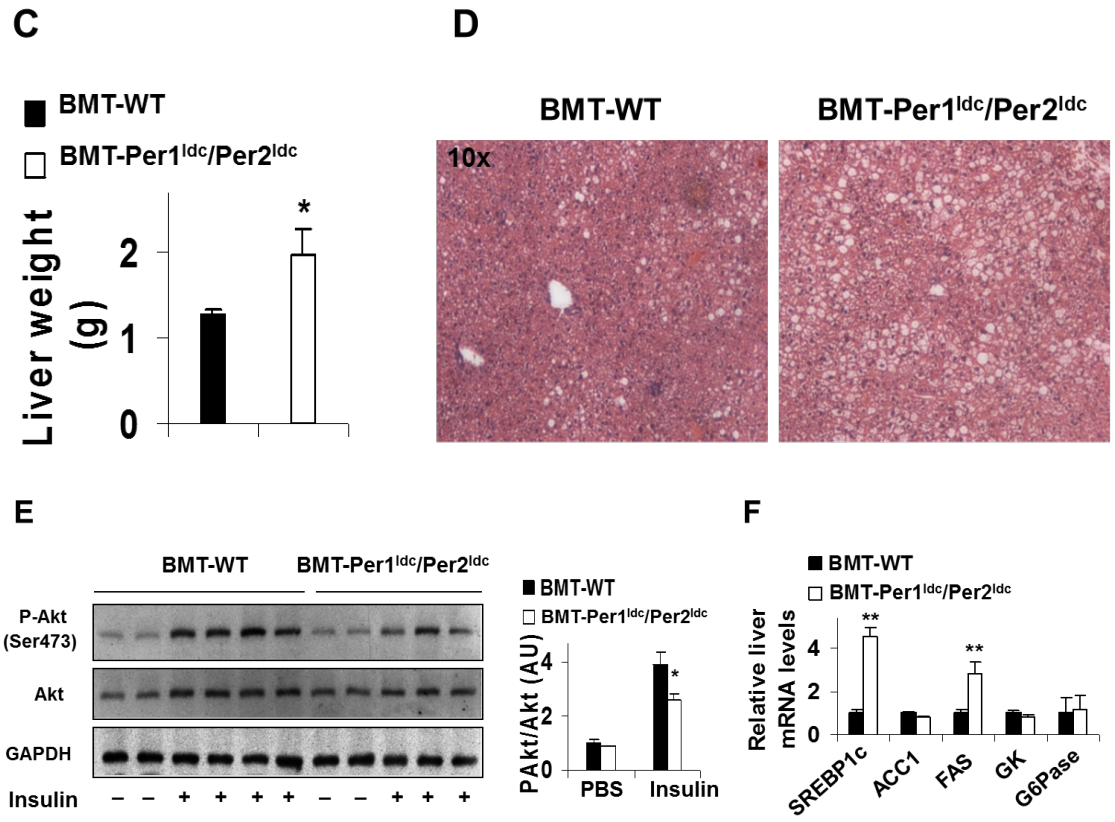

Figure 26 Continued.

2.4 Discussion

During obesity, macrophage proinflammatory activation initiates or aggravates inflammation in key metabolic organs including adipose and liver tissues, thereby leading to systemic insulin resistance. However, it remains to be elucidated exactly how overnutrition induces proinflammatory activation of macrophages, particularly in those found in adipose tissue where increased inflammation plays a causal role in the

pathogenesis of insulin resistance [10, 12, 42-44]. In parallel with this inductive effect on macrophage proinflammatory activation [12],HFD feeding has been shown to decrease the amplitude of adipose tissue clock gene rhythms in *Bmal1*, *Clock*, and *Per 2* expression [28] and to lengthen the period of the *Per2* rhythm in cultured adipose tissue [31]. Taken together, these observations suggest that dysregulation of peripheral circadian clocks may link diet-associated obesity to adipose tissue inflammation. In support of this putative association, the present study demonstrates that in HFD-fed mice where minor increases in period of the activity of rhythm were similar to those observed previously [28], overnutrition caused dysregulation of peripheral circadian clocks (*i.e.* substantial increases in the period of *Per 2* oscillations) specifically within key mediators of adipose tissue inflammation, macrophages in stromal vascular cells, and BMDM. Furthermore, the diet-related clock dysregulation in BMDM was accompanied by increased proinflammatory activation. It is noteworthy that our findings provide evidence for the direct link between circadian clock dysregulation and macrophage proinflammatory activation in diet-induced obesity. Specifically, clock-disrupted ($Per1^{ldc}/Per2^{ldc}$) macrophages are distinguished by enhanced proinflammatory activation, and myeloid cell-specific clock disruption ($Per1^{ldc}/Per2^{ldc}$) exacerbates diet-induced inflammation and insulin resistance in chimeric mice repopulated with only mutant bone marrow cells. As such, the current study indicates for the first time that dysregulation of the macrophage circadian clock (*e.g. Per1*/*2* disruption) is a critical factor in the mechanism through which overnutrition induces macrophage

proinflammatory activation, thereby leading to adipose tissue inflammation in the context of systemic insulin resistance and hyperglycemia.

Per1 and *Per2* are vital components of the circadian clock mechanism and function as negative regulators in feedback loops involving interactions between *Bmal1*, *Clock*, and the cryptochrome (*Cry1* and *Cry2*) genes [29]. Previously, genetic or environmental disruption of circadian clock function has been shown to alter macrophage proinflammatory responses. In macrophages, conditional targeting of Bmal1 abolishes the rhythmic gating of innate immune responses such that cytokine responsiveness to LPS stimulation remains constantly elevated [68]. Environmental disruption of circadian rhythms after weekly 6-h shifts in the light-dark cycle similarly exacerbates inflammatory responses of peritoneal macrophages to LPS challenge in the absence of sleep loss or stress effects [69]. In the present analysis of *Per1*ldc/*Per2*ldc mice that are characterized by a globally arrhythmic phenotype [71], circadian clock dysfunction did not influence macrophage differentiation, as the percentage of mature macrophages ($F4/80^+$ $CD11b^+$ cells) differentiated from bone marrow cells of *Per1*ldc/*Per2*ldc mice was identical to that found in wild-type mice. However, among mature macrophages, *Per1*/*2*-disrupted cells showed a much higher percentage of $CD11c^+$ $CD206^-$ cells, indicating increased macrophage proinflammatory activation. The macrophage inflammatory status was corroborated by the finding that *Per1*/*2* disruption increased JNK1 and NF-*κ*B p65 phosphorylation and IL-1β and TNFα expression in mature macrophages under LPS-stimulated conditions. Thus, *Per1*/*2* disruption-associated circadian dysfunction increases macrophage proinflammatory activation.

How the *Per1* and *Per2* genes regulate macrophage activation remains to be determined. It is possible that *Per1* and *Per2* modify inflammatory gene expression through their feedback regulation of CLOCK/BMAL1 transcriptional activity. Indeed, CLOCK has been shown to function as a positive regulator of the transcription factor NF-*κ*B, which is a critical determinant of inflammatory responses [83]. Consequently, the relative increases in CLOCK levels observed in peripheral tissues from mutant mice (data not shown) suggest that the loss of negative feedback regulation resulting from *Per1*/*2* disruption may further enhance the activation of NF-*κ*B and ultimately the induction of NF-*κ*B responsive genes such as IL-1β, TNFα, and other cytokines. Alternatively, *Per1* and *Per2* may alter macrophage inflammatory signaling through interactions with other components of the core or auxiliary feedback loops comprising the molecular clockworks because REV-ERBα has been shown to modulate macrophage TLR signaling [84] and function as an inhibitor of proinflammatory IL-6 release [68]. Given that active PPARγ promotes macrophage anti-inflammatory activation [56, 59, 85] and this transcription factor is a molecular target of insulin-sensitizing and anti-diabetic drugs [86], PPARγ may play a role in *Per1*/*2* regulation of macrophage activation. In fact, our data support this hypothesis because PPARγ levels were decreased in *Per1*/*2*-disrupted macrophages in conjunction with their enhanced proinflammatory activation and PPARγ 2 overexpression reversed, at least in part, this *Per1*/*2* disruption-associated shift in inflammatory status. Collectively, these observations suggest a novel mechanism for macrophage polarization in which the circadian clock normally acts through PPARγ to inhibit macrophage proinflammatory activation. Because the PPARγ promoter

contains multiple E-boxes [80], it will be important to determine whether negative feedback by *Per1* and/or *Per2* modulates CLOCK/BMAL1 regulation of E-box mediated transcription of PPARγ.

The significance of circadian clock function in macrophage activation was further manifested by the finding that adoptive transfer of *Per1*/*2*-disrupted myeloid cells to wild-type mice exacerbated HFD-induced inflammation and insulin resistance. Notably, BMT-*Per1*^{ldc}/*Per2*^{ldc} mice displayed marked increases in adipose tissue inflammatory responses as indicated by enrichment of mature proinflammatory macrophages in adipose tissue and increased inflammatory signaling and proinflammatory cytokine expression. Consequently, inflammation associated adipose tissue dysfunction (*i.e.* decreased insulin signaling and adipose tissue metabolic dysregulation) was markedly increased in BMT-*Per1*^{ldc}/*Per2*^{ldc} mice. Given the origin of the myeloid cells/macrophages, the increased severity of adipose tissue inflammatory responses and dysfunction in BMT-*Per1*^{ldc}/*Per2*^{ldc} mice solely reflects proinflammatory activation in clock-disrupted macrophages. This relation was substantiated by the finding that co-culture of adipocytes with *Per1*/*2*-disrupted macrophages increased adipocyte inflammatory response and decreased adipocyte insulin sensitivity. In similar fashion, *Per1*/*2*-disrupted macrophages appeared to mediate the increased severity of liver inflammatory responses and metabolic dysregulation. Altogether, these observations provide convincing evidence that macrophage circadian clock dysregulation is sufficient to potentiate overnutrition-induced inflammation in adipose tissue and the liver, thereby increasing systemic insulin resistance.

In summary, the present data unveil a novel mechanism for obesity-associated insulin resistance in which circadian clock dysregulation is a key factor that links overnutrition and macrophage proinflammatory activation to adipose tissue inflammation. At the cellular level, HFD-associated overnutrition modulates circadian clock function in macrophages, which in turn induces the proinflammatory activation of macrophages, especially those in adipose tissue. When activated, clock-disrupted macrophages are sufficient to exacerbate diet induced adipose tissue inflammation and systemic insulin resistance. Because adipose tissue inflammatory responses and corresponding insulin sensitivity in overnutrition-related obesity are differentially engaged by specific types of fatty acids found in HFDs, future studies are warranted to compare the effects of saturated and polyunsaturated fatty acids on macrophage and adipocyte circadian clocks. Thus, it will be important to determine whether saturated fatty acids that activate proinflammatory signaling pathways and lead to impaired insulin sensitivity (*e.g.* palmitate) also modulate the circadian timekeeping function of macrophage and adipocyte clocks and whether this circadian clock dysregulation is blocked or abated by polyunsaturated fatty acids that repress adipose tissue inflammatory responses and have a beneficial impact on insulin sensitivity.

3. PFKFB3 CONTROL OF MACROPHAGE ACTIVATION

3.1 Introduction

Chronic diseases are the leading causes of morbidity and mortality in the United States [87, 88]. The current body of knowledge suggests a critical role for macrophages in the control of systemic insulin resistance associated with chronic diseases [3, 4]. Overnutrition is a key causal factor that contributes to chronic metabolic disorders largely by induction of macrophage proinflammatory activation, however, the exact mechanisms by which nutrient metabolism regulates macrophage inflammatory status are poorly understood [11-15]. This opens up an area for overnutrition induced systemic insulin resistance prevention and/or treatment by means of altering macrophage inflammatory status.

PFKFB3, encoding for inducible 6-phosphofructo-2-kinase (iPFK2), is proposed to be a critical modulator of macrophage inflammatory status. As a key regulatory enzyme of glycolysis, PFKFB3/iPFK2 is also involved in the effect of PPARγ activation and appears play a role in macrophage activation [15]. Additionally, our lab has demonstrated that global PFKFB3 disruption exacerbates expression of proinflammatory cytokines such as TNFα and IL-6 in adipose tissue macrophages as well as adipocytes [10]. As such, elucidating the role of PFKFB3/iPFK2 in controlling the M1/M2 macrophage balance can contribute significantly to a better understanding of the underlying mechanisms of overnutrition-induced insulin resistance. This could offer better strategies for prevention and/or treatment of obesity-related diseases.

In this study, both integrative and cellular approaches were included to define a pivotal role played by PFKFB3 in modulating macrophages inflammatory properties. Our hypothesis is that PFKFB3 disruption enhances macrophage proinflammatory activation in diet-induced obesity, resulting in local and systemic insulin resistance. To test this hypothesis, we conducted a series of experiments to determine whether 1) disruption of PFKFB3 exacerbates macrophage proinflammatory activation (in vitro), 2) myeloid cell-specific disruption of PFKFB3 exacerbates diet-induced inflammation and insulin resistance (in vivo), and 3) PFKFB3-disrupted macrophage exacerbates adipocytes inflammatory responses and insulin resistance.

3.2 Materials and Methods

3.2.1 Animal experiments

Animals used in this study were derived from wild-type (WT) C57BL/6J mice obtained from The Jackson Laboratory (Bar Harbor, ME) and from breeding pairs of WT and PFKFB3$^{+/-}$ mice generated as previously described (Homozygous disruption of PFKFB3/iPFK2 is embryonic lethal)[89]. All mice were maintained on a 12:12-h light-dark cycle (lights on at 06:00). All mice were fed chow diet ad libitum except those that were used for dietary feeding study. At the age of 5-6 wk, male mice were used for both feeding and bone marrow isolation and macrophage activation analyses. For dietary feeding studies, mice were fed an high fat diet (HFD, 60% fat calories, 20% protein calories, and 20% carbohydrate calories) or a low fat diet (LFD, 10% fat calories, 20% protein calories, and 70% carbohydrate calories; Research Diets, Inc.) for 12 wk as

previously described[10, 44] (nutrient composition listed in Table. 1). During the 12-wk feeding period, body weight and food intake of the mice were recorded every week. After the feeding regimen, mice were fasted for 4 h before sacrifice for collection of blood and tissue samples [72, 73, 90]. Epididymal, mesenteric, and perinephric fat depots were dissected and weighted as visceral fat content[73]. After weighing, adipose tissue and liver samples were either fixed and embedded for histological and immunohisto-chemical analyses or frozen in liquid nitrogen and then stored at -80 °C for further analyses. Some mice were fasted similarly and used for insulin and glucose tolerance tests and /or insulin signaling analyses as described below. All study protocols were reviewed and approved by the Institutional Animal Care and Use Committee of Texas A&M University.

3.2.2 Determination of PFKFB3 mRNA and iPFK2 amount

PFKFB3 mRNA and iPFK2 amount in the adipose tissue and macrophages were determined using real-time PCR and Western blot, respectively, as described below.

3.2.3 Glucose and insulin tolerance tests

Glucose and Insulin tolerance tests were performed as previously described [91]. Mice were fasted for 4 h and intraperitoneally injected with D-glucose (2 g/kg of body weight) or insulin (1 unit/kg of body weight). For glucose tolerance tests, blood samples (5 ul) were collected from the tail vein before and at 30, 60, 90, and 120 min after the glucose

bolus injection. Similarly, for insulin tolerance tests, blood samples were collected from the tail vein before and at 15, 30, 45, 60 min after the bolus insulin injection.

3.2.4 Measurement of plasma glucose and insulin

The levels of plasma glucose were measured using glucose assay kit (Sigma and BioVision, Mountain View, CA). The levels of plasma insulin were measured using ELISA kits (Crystal Chem Inc., Downers Grove, IL).

3.2.5 Measurement of rates of glycolysis

Each well (6-well plate) of macrophages were incubated with medium supplemented with 1 μCi [3-^{3}H]-glucose for 3 h. After incubation, the medium was collected to determine the production of ^{3}H2O (in disintegration per minute (DPM)) as described [92]. Two sets of medium were collected after 3 hr incubation. One set was used to measure total DMP, which equals ^{3}H2O plus the left ^{3}H-glucose and other non-H2O metabolites. The other set was used air dry, and measured leftover DPM. The differences give the DPM of ^{3}H2O. Rates of glycolysis are expressed as nanomoles of glucose metabolized per 3 h per milligram of protein.

3.2.6 Histological and immunohisto-chemical analyses of adipose tissue

The paraffin-embedded adipose tissue blocks were cut into sections of 5-μm thickness and stained with hematoxylin and eosin. In addition, the sections were stained for the expression of F4/80 with rabbit anti-F4/80 (1:100) (AbD Serotec, Raleigh, NC) as

previously described [42, 93]. The fraction of F4/80-expressing cells for each sample is calculated as the sum of the number of nuclei of F4/80-expressing cells divided by the total number of nuclei in sections of a sample. Six fields per slide were included, and a total of 4-6 mice per group were used.

3.2.7 Isolation of stromal vascular cells (macrophages) from adipose tissue

Adipose tissue stromal vascular cells (SVCs) and adipocytes were isolated using the collagenase digestion method as previously described [56]. After digestion and centrifugation, the pelleted cells were collected as SVCs, and the floating cells were harvested as adipocytes.

3.2.8 Bone marrow isolation and macrophage differentiation

Bone marrow cells were isolated from the tibias and femurs of the WT mice as previously described [59, 62]. After erythrocyte lysis with ammonium chloride (Stem Cell Technologies), cells were induced for differentiation with Iscove's modified Dulbecco's medium containing 10% fetal bovine serum and 15% L929 culture supernatant for 8 d. The bone marrow-derived macrophages (BMDMs) were subjected to inflammatory response analysis and co-culture study.

3.2.9 Co-culture of macrophages and adipocytes

BMDMs prepared from PFKFB3$^{+/-}$ or WT mice were co-cultured with differentiated 3T3-L1 adipocytes as previously described [60, 91]. After differentiation for 8 d,

adipocytes were co-cultured with BMDMs at a ratio of 10:1 based on the published method [60, 94]. To determine changes in inflammatory signaling, some cells were treated with or without LPS (100 ng/ml) for 30 min before cell harvest. To examine changes in insulin signaling, some cells were treated with or without insulin (100 nmol/L) for 30 minutes before harvest. Cell lysates were prepared and used to examine inflammatory and insulin signaling by Western blots. Additionally, some co-cultured cells were treated with or without LPS (100 ng/ml) for 6 h and subjected to preparation of RNA samples to quantify gene expression using real-time PCR.

3.2.10 Bone marrow transplantation

Bone marrow transplantation analyses were performed as previously described [91]. 6-wk-old PFKFB3$^{+/-}$ male mice or WT littermates were used as donor. Male WT recipient mice at 5-6 wk of age were lethally irradiated and subjected to BMT to generate chimeric mice using the established method [60, 61]. WT mice that were transplanted with donor cells from PFKFB3$^{+/-}$ mice were referred to as BMT-PRKRB$^{+/-}$ mice. WT mice that were transplanted with donor cells from WT mice were referred to as BMT-WT mice. After recovery for 4 wk, recipient mice were then fed an HFD for 12 wk before metabolic assays and tissue collections. All study protocols were reviewed and approved by the Institutional Animal Care and Use Committee of Texas A&M University.

3.2.11 Western blots

Lysates were prepared from frozen tissue samples and cultured cells. Western blots were conducted as previously described [91]. The levels of protein iPFK2, JNK1/2, phosphor-JNK1/2, nuclear factor kB (NF-**κ**B) p65, hospho-p65, Akt, phosphor-Akt, and PPARγ in cell lysates were analyzed. GAPDH or b-actin was used as a loading control. The maximum intensity of each band was quantified using ImageJ software. Ratio of pJNK1/JNK1 and phosphor-p65/p65 as well as phosphor-Akt/Akt were normalized to GAPDH or b-actin and adjusted relative to the average of control (PBS)-treated LFD, WT, BMT-WT, or Adi/WT, which was arbitrarily set as 1 (arbitrary units, AU).

3.2.12 RNA isolation, reverse transcription, and real-time PCR

The total RNA was isolated from frozen tissue samples and culture/isolated cells. RNA isolation and real-time RT-PCR were conducted as previously described [91]. Reverse transcription was performed using the GoScript™ Reverse Transcription System (Promega), and real-time PCR analysis was performed using SYBR Green (LightCycler ® 480 system; Roche Life Science, Indianapolis, IN). The mRNA levels were analyzed for interleukin-1b (IL-1**β**), IL-6, tumor necrosis factor a (TNF**α**), IL-10, arginase1, monocyte chemoattractant protein 1 (MCP1), TLR4, adiponectin, and PFKFB3 in tissue and/or cell samples. A total of 0.1 ug of RNA was used for the determination. Results were normalized to 18 S ribosomal RNA and plotted as relative expression to the average of control (PBS)-treated LFD, WT, BMT-WT, or Adi/WT, which was arbitrarily set as 1.

3.2.13 Statistical methods

Numeric data are presented as means ± S.E. Statistical significance was assessed by unpaired, two-tailed analysis of variance or Student's t test. Differences were considered significant at the two-tailed $p<0.05$.

3.3 Results

3.3.1 PFKFB3 disruption decreases glycolysis in macrophages

At 5-6 wk of age, bone marrow cells were isolated from chow diet-fed male PFKFB3$^{+/-}$ mice and WT littermates. Bone marrow cells (BMC) and differentiated BMDM were used to measure the expression of PFKFB3. Compared to BMDM from WT controls, BMC and BMDM from PFKFB3$^{+/-}$ mice exhibited decreased PFKFB3 mRNA level (Fig. 27, A and B). Consistently, in PFKFB3 disrupted BMDM, the rate of glycolysis decreased significantly compared to WT macrophages (Fig. 27C).

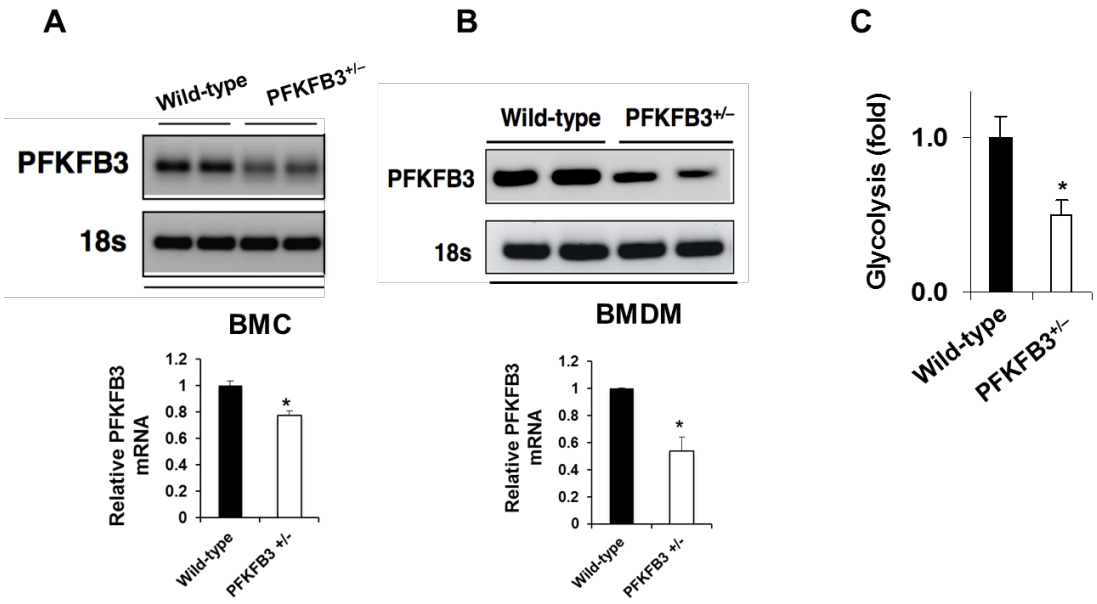

Figure 27. PFKFB3 disruption decreases glycolysis in macrophages.
BMC and BMDM were prepared from chow diet-fed wild-type mice and PFKFB3$^{+/-}$ mice with targeted disruption of heterozygous disruption of the gene PFKFB3 (n=3-6). (A) BMC mRNA level of PFKFB3. (B) BMDM mRNA level of PFKFB3. (C) Relative rates of glycolysis. For bar graphs, data are means ±SE. *, P< 0.05 PFKFB3$^{+/-}$ vs. wild-type.

3.3.2 PFKFB3 disruption exacerbates macrophage proinflammatory activation and impairs macrophage alternative activation

When inflammatory responses were analyzed, BMDM from PFKFB3$^{+/-}$ mice exhibited a significant increase in the phosphorylation of NF-**κ**B compared with BMDM from wild-type littermates (Fig. 28A).

Moreover, upon LPS stimulation, the BMDM M1 (proinflammatory) activation differed in accord with genotype. Under both basal and LPS-treated conditions, the mRNA levels of TNFα and IL-6 in PFKFB3$^{+/-}$ BMDM were significantly higher than their respective levels in WT BMDM, indicating that PFKFB3 disruption exacerbates macrophage proinflammatory activation (Fig. 28B). Upon IL-4 stimulation for BMDM M2 (anti-inflammatory) activation, under both basal and treated conditions, the mRNA levels of IL-6 and IL-1**β** in PFKFB3$^{+/-}$ BMDM were significantly higher than their respective levels in WT BMDM, indicating that PFKFB3 disruption hinders macrophage anti-inflammatory activation (Fig. 28C). The similar pattern was also observed in peritoneal macrophages when treated IL-4 (data not shown).

3.3.3 Myeloid cell-specific PFKFB3 disruption does not worsen diet-induced obesity

Macrophage inflammatory status governs adipose inflammation and contributes to the development of systemic insulin resistance [58, 60]. To address the impact of macrophage specific PFKFB3 on HFD-induced adipose tissue inflammation, Bone marrow cells of PFKFB3-disrupted mice and/or wild-type littermates were transplanted into lethally irradiated wild-type mice (BMT), noted as BMT- PFKFB3$^{+/-}$ mice

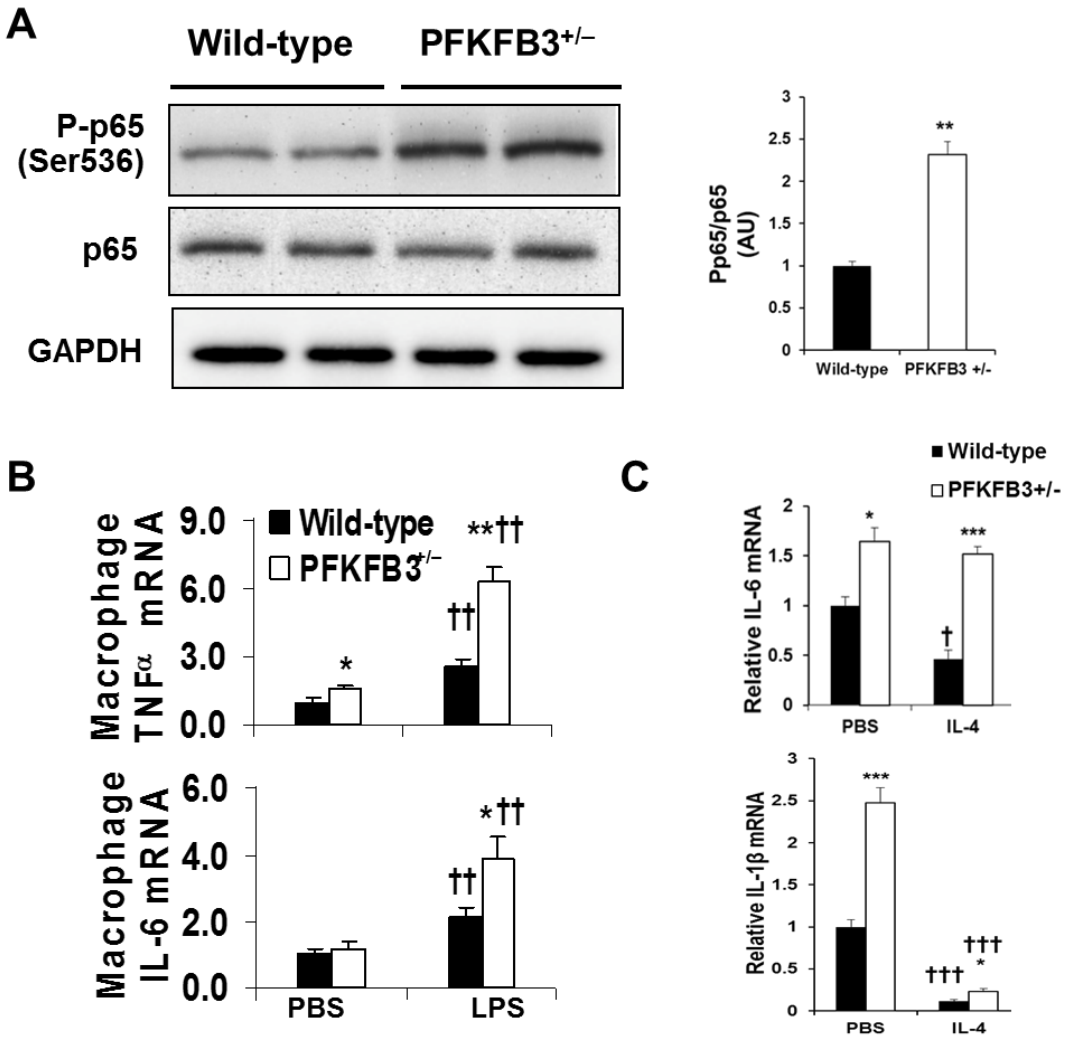

Figure 28. PFKFB3 disruption exacerbates macrophage proinflammatory activation and impairs macrophage alternative activation.
BMDM were prepared from chow diet-fed wild-type mice and PFKFB3$^{+/-}$ mice with targeted disruption of heterozygous disruption of the gene PFKFB3 (n=3-6). (A) The phosphorylation of NF-**κ**B p65, examined using western blot and quantified using Image-J. (B) The mRNA levels of proinflammatory cytokines. BMDM were treated with LPS (100 ng/ml) or PBS for 6h. The mRNA levels of TNF**α** and IL-6 were quantified using real-time PCR and plotted as relative expression. (C) The mRNA levels of anti-inflammatory cytokines. BMDM were treated with IL-4 (10 ng/ml) or PBS for 48 h. The mRNA levels of IL-6 and IL-1β were quantified using real-time PCR and plotted as relative expression. For bar graphs, data are means ±SE. *, P< 0.05; **, P< 0.01; and ***, P< 0.001 PFKFB3$^{+/-}$ vs. wild-type (A) under the same conditions (B, PBS or LPS; C, PBS or IL-4); †, P< 0.05; ††, P< 0.01; †††, P< 0.001 LPS vs. PBS (B) or IL-4 vs. PBS (C) for the same genotype. AU, arbitrary units.

(PFKFB3$^{+/-}$ →WT) and BMT-WT mice (WT→WT) respectively. After one month of recovery, the mice were fed with HFD for 12 wk.

Before and after HFD feeding, the body weight of BMT- PFKFB3$^{+/-}$ mice did not differ from BMT-WT mice. Mice in both groups gained similar body weight (Fig. 29A) and displayed comparable abdominal fat mass (Fig. 29B).

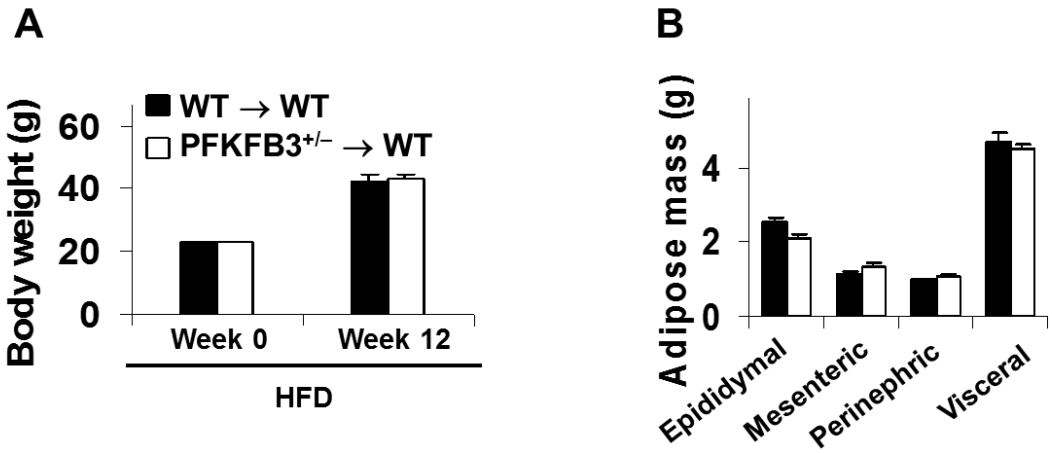

Figure 29. Myeloid cell-specific PFKFB3 disruption did not alter diet-induced obesity.
Chimeric mice BMT-WT (WT→WT) and BMT- PFKFB3$^{+/-}$ (PFKFB3$^{+/-}$ →WT) were fed an HFD for 12 wk (n=7-10). (A) Body weight was monitored before and after HFD feeding. (B) Adipose mass. Abdominal fat mass (visceral fat) was the sum of epididymal, mesenteric and perinephric fat mass. Data are means ±SE. For B HFD-fed chimeric mice were fasted for 4h starting at the same time of the day before tissue collection.

3.3.4 Myeloid cell-specific PFKFB3 disruption exacerbates diet-induced systemic insulin resistance

Even with comparable adiposity, HFD-fed BMT- PFKFB3$^{+/-}$ mice exhibited a significant increase in plasma insulin and glucose levels, compared with HFD-fed BMT-WT mice (Fig. 30, A and B). In addition, HFD-fed BMT- PFKFB3$^{+/-}$ mice displayed a significant increase in the severity of insulin resistance and glucose intolerance indicated by insulin and glucose tolerance testes, respectively (Fig. 30, C and D). Thus, myeloid cell-specific PFKFB3 disruption does not alter adiposity after HFD feeding, but exacerbates systemic insulin resistance.

3.3.5 Myeloid cell-specific PFKFB3 disruption exacerbates diet-induced adipose tissue inflammation and insulin resistance

Immunohisto-chemical analysis of adipose tissue sections suggested that there was more macrophage infiltration in adipose tissue from BMT- PFKFB3$^{+/-}$ mice compared with that in adipose tissue from BMT-WT mice (Fig. 31A). When inflammatory status was examined in adipose tissue, the phosphorylation of NF-**κ**B p65 was increased significantly in BMT- PFKFB3$^{+/-}$ mice compared with BMT-WT mice, both fed with HFD (Fig. 31B). Accordingly, BMT- PFKFB3$^{+/-}$ mice displayed decreased insulin sensitivity evidenced by decreased insulin-induced phosphorylation of Akt, when compared with BMT-WT mice (Fig. 31C). Thus, myeloid cell-specific PFKFB3 disruption increases macrophage infiltration in adipose tissue and inflammatory responses, and meanwhile exacerbates HFD-induced adipose tissue insulin resistance.

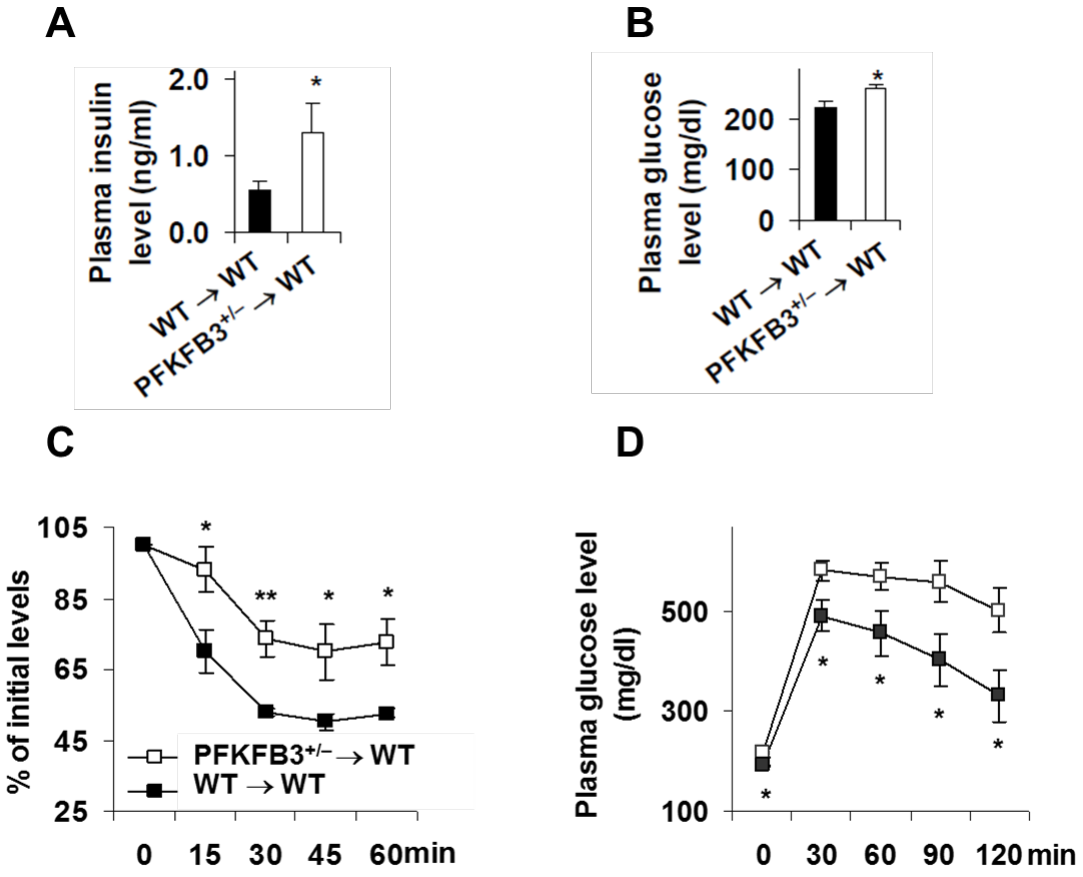

Figure 30. Myeloid cell-specific PFKFB3 disruption exacerbates diet-induced insulin resistance and glucose intolerance.
Chimeric mice BMT-WT (WT→WT) and BMT- PFKFB3$^{+/-}$ (PFKFB3$^{+/-}$ →WT) were fed an HFD for 12 wk (n=7-10). (A) Plasma levels of insulin. (B) Plasma levels of glucose. (C) Insulin tolerance test. (D) Glucose tolerance test. Data are means ±SE. *, P< 0.05; and **, P< 0.01 BMT- PFKFB3$^{+/-}$ vs. BMT-WT under the same conditions (A and B) or time points (C and D). HFD-fed chimeric mice were fasted for 4h starting at the same time of the day before tissue collection or physiological assays. For C and D, mice were given a peritoneal injection of insulin (1 unit/kg) (C) or glucose (2g/kg) (D).

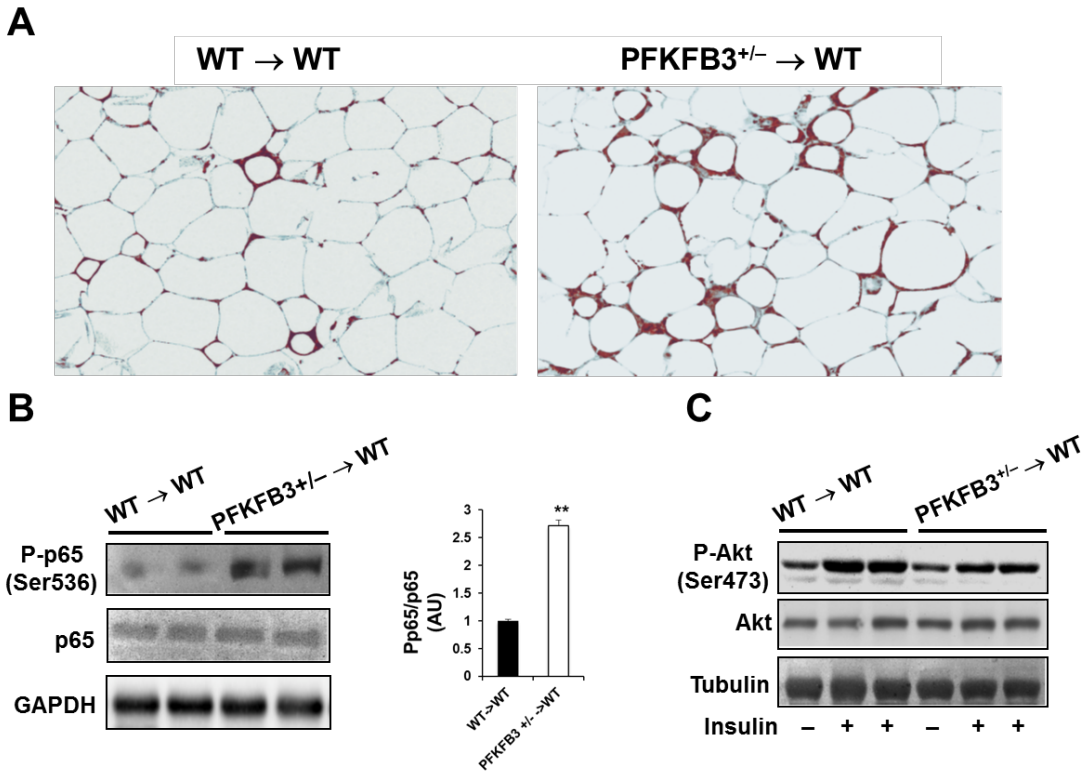

Figure 31. Myeloid cell-specific PFKFB3 disruption exacerbates obesity-associated adipose tissue inflammation and insulin resistance.
Chimeric mice BMT-WT (WT→WT) and BMT- PFKFB3$^{+/-}$ (PFKFB3$^{+/-}$ →WT) were fed an HFD for 12 wk (n=7-10). Before tissue collection or insulin injection, mice were fasted for 4h starting at the same time of the day. (A) F4/80 staining of adipose tissue. (B) Adipose tissue inflammatory signaling. The levels of total and phosphorylated NF-κB p65 were examined using western blot and quantified using Image-J. (C) Adipose tissue insulin signaling. After fasting, HFD-fed chimeric mice were given a bolus injection of insulin (1 unit/kg of body weight) or PBS into the portal vein. The levels of total and phosphorylated Akt were examined using western blot analyses and quantified by Image-J. For bar graphs (B), data are means ±SE. **, P< 0.01 BMT- PFKFB3$^{+/-}$ vs. BMT-WT. AU, arbitrary units.

Similarly, we observed significant increase of NF-κB p65 phosphorylation in liver from BMT- PFKFB3$^{+/-}$ mice compared with that in liver from BMT-WT mice (data

not shown). Additionally, insulin-induced phosphorylation of Akt decreased significantly in liver from BMT- PFKFB3$^{+/-}$ mice compared with that in liver from BMT-WT mice (data not shown). Thus, myeloid cell-specific PFKFB3 disruption increases liver inflammatory responses and impaired HFD-induced liver insulin sensitivity.

3.3.6 PFKFB3-disrupted macrophages increase adipocyte inflammatory responses and impair adipocyte insulin signaling

As macrophages play a pivotal role in initiating or exacerbating adipose tissue inflammation, next we wanted to address the direct effects of PFKFB3 disruption on macrophages and/or macrophage secreted factors that regulate adipocyte function. BMDM from PFKFB3$^{+/-}$ mice and WT mice were co-cultured with adipocytes at a 1:10 ratio, respectively. Compared with co-cultures containing adipocytes and WT BMDM, adipocytes co-cultured with PFKFB3$^{+/-}$ BMDM exhibited a significant increase in the phosphorylation of NF-**κ**B p65 and JNK in response to LPS treatment (Fig. 32A). When insulin signaling was analyzed, adipocytes co-cultured with PFKFB3$^{+/-}$ BMDM displayed a significant decrease in Akt phosphorylation (Ser473) induced by insulin compared with adipocytes co-cultured with WT BMDM (Fig. 32B). These results suggest that PFKFB3-disrupted macrophages directly increase adipocyte proinflammatory responses and decrease adipocyte insulin sensitivity.

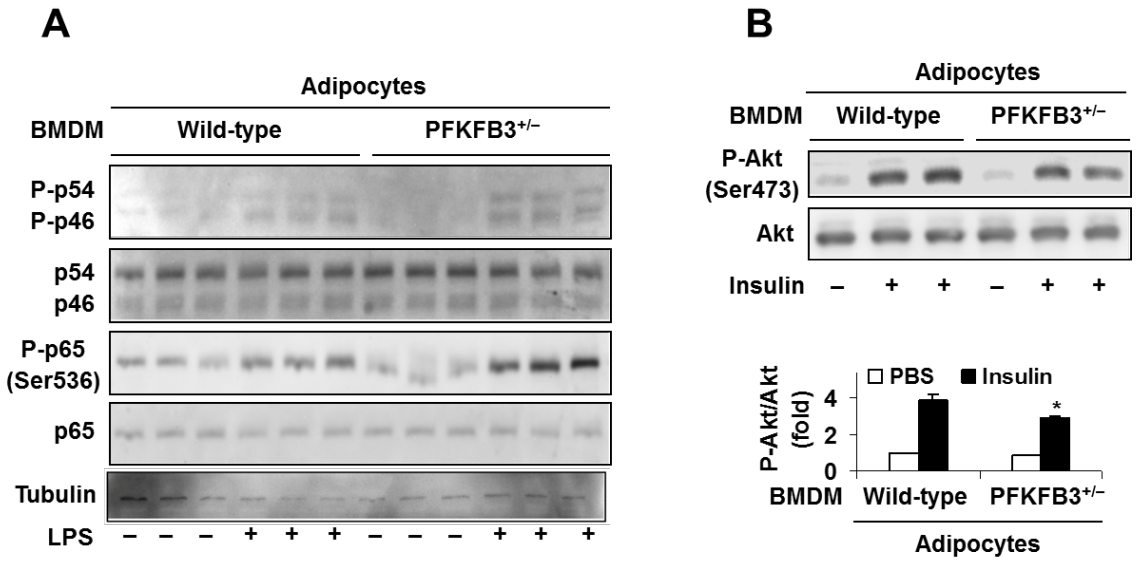

Figure 32. PFKFB3-disrupted macrophages increase adipocyte inflammatory responses and impair adipocyte insulin signaling.
Adipocytes were co-cultured with macrophages differentiated from bone marrow cells of wild-type or PFKFB3$^{+/-}$ mice at a 10:1 ratio for 48 h (n=4-6). (A) NF-κB and JNK signaling of co-cultured adipocytes. Co-cultures were treated with LPS (100 ng/ml) or PBS for 30 min before harvest. The levels of total and phosphorylated JNK1 (p46) and NF-κB p65 were examined using western blot analyses and quantified using Image-J. (B) Insulin signaling of co-cultured adipocytes. Co-cultures were treated with insulin (100 nM) or PBS for 30 min before harvest. The levels of total and phosphorylated Akt were examined using western blot and quantified by Image-J. For bar graphs (B), data are means ±SE. *, P< 0.05 Adi/ PFKFB3$^{+/-}$ vs. Adi/wild-type under the same conditions (insulin).

3.4 Discussion

In diet-induced obesity (DIO), macrophage proinflammation activation is a key contributor to the inflammation in key metabolic organs including adipose and liver tissues, resulting in systemic insulin resistance. Therefore, research has been widely conducted recently in the attempt to discover modulators of macrophage activation so as to control the inflammation and pathogenesis of insulin resistance. For example, it has been demonstrated that circadian control of macrophage activation plays an important role in diet-induced inflammation and insulin resistance [91]; miR-223 has been proved to be a regulator of macrophage activation in obesity-associated adipose tissue inflammation [95]. Interestingly, our previous research has suggested that PFKFB3 protects mice against diet-induced inflammation and insulin resistance [10, 77], and FKFB3 gene happens to be a circadian controlled gene. Thus, PFKFB3 is a good candidate to test if it is another modulator of macrophage activation.

In HFD-fed WT mice, PFKFB3 expression in adipose tissue decreased (data not shown) and inflammation increased at the same time, compared with LFD-fed WT mice. To test the causal effect, macrophages from PFKFB3-disrupted mice were examined. Compared to WT macrophages, PFKFB3-disrupted macrophages displayed higher proinflammatory activation and lower anti-inflammatory activation. Thus, PFKFB3 disruption directly affects macrophage activation and inflammatory status. Whether PFKFB3-disruption in macrophage is sufficient enough to bring about adipose tissue inflammation and systemic insulin resistance was investigated by bone marrow transplantation. We generated myeloid-specific PFKFB3-disrupted mice through BMT.

After HFD feeding, the adiposity in BMT- PFKFB3$^{+/-}$ mice was comparable with BMT-WT mice. However, we observed increased macrophage infiltration in adipose tissue, elevated inflammatory responses in adipose tissue and exacerbated systemic insulin resistance in BMT- PFKFB3$^{+/-}$ mice compared to BMT-WT mice. The following co-culture study suggested a direct effect of macrophage PFKFB3 disruption on exacerbating adipocytes inflammatory responses and insulin resistance.

How the PFKFB3 gene regulates macrophage activation status remains to be further determined. It is possible that when PFKFB3 is disrupted in macrophage, the rate of glycolysis decreases and ROS production increases, which in turn contribute to the proinflammatory responses in macrophages. The present study gained new insights of the role of PFKFB3 in regulating macrophage inflammatory status, and will provide essential information for the development of selective PFKFB3 activators in the prevention and/or treatment of overnutrition-induced systemic insulin resistance.

4. SUMMARY AND CONCLUSION

4.1 Summary

Macrophage activation status plays a critical role in chronic inflammation associated with obesity and insulin resistance. The presented study investigated the ways to modulate macrophage activation from circadian aspect and metabolic aspect in diet-induced obesity.

Upon HFD feeding, mice developed exacerbated adiposity, adipose tissue inflammation, systemic insulin resistance and circadian dysregulation. Interestingly, macrophages from HFD-fed mice also displayed increased circadian dysregulation and inflammatory responses compared to LFD-fed group. To address a direct role for circadian clock disruption in altering macrophage activation status, BMDM prepared from Per1/Per2-disrupted mice were examined. Compared to control cells, the Per1/Per2-disrupted macrophages exhibited a marked increase in proinflammatory activation (M1) even though maintaining comparable percentage of anti-inflammatory activation, which resulted in a significant increase of inflammatory signaling and proinflammatory cytokines expression. Meanwhile, PPARγ expression was decreased in Per1/Per2-disrupted macrophages, and overexpression of PPARγ2 rescued the exacerbated inflammatory status in Per1/Per2-disrupted macrophages. Next, in vivo BMT study was conducted to test if macrophage Per1/Per2 disruption is sufficient enough to bring about systemic insulin resistance. As expected, macrophages in adipose tissue from HFD-fed BMT-Per1^{ldc}/Per2^{ldc} mice exhibited more proinflammatory properties, compared to HFD-fed BMT-WT mice, resulting in exacerbated adipose

tissue inflammation and insulin resistance. Significantly, increased severity of systemic insulin resistance was observed in BMT-Per1^{ldc}/Per2^{ldc} mice after HFD feeding. Lastly, in vitro co-culture study was conducted to confirm the direct effect of macrophage Per1/Per2 disruption on increasing adipose tissue inflammation and insulin resistance.

The study about the role of PFKFB3 on macrophage activation was conducted similarly as above. Decreased glycolysis and increased inflammatory responses were observed in BMDM when PFKFB3 was disrupted. Additionally, it was shown that PFKFB3 disruption in macrophages is sufficient enough to bring about systemic insulin resistance using BMT mouse model. As indicated by the results from co-culture experiments, PFKFB3-disrupted macrophages can directly increase adipocyte inflammatory responses and disturb insulin signaling.

Taken together, either circadian dysregulation by disruption of clock genes Per1 and Per2, or PFKFB3 disruption can exacerbate macrophage proinflammatory activation, resulting in severe diet-induced adipose tissue inflammation and systemic insulin resistance.

4.2 Conclusion

The present study provided further evidence for the importance of macrophage inflammatory status in regulating adipose tissue inflammation and systemic insulin sensitivity in diet-induce obesity. This is supported by the findings that HFD-fed mice exhibited increased severity of adipose tissue inflammation and systemic insulin resistance, whenever macrophages were much more proinflammatory activated upon disruption of Per1/Per2 or PFKFB3. More importantly, this study gained new insights into the role of circadian and PFKFB3 in regulating macrophage activation status, which will promote the development of new evidence-based approaches for prevention and/or treatment of diet-induced systemic insulin resistance.

REFERENCES

1. Hotamisligil GS: **Inflammation and metabolic disorders.** *Nature* 2006, **444:**860-867.

2. Shoelson SE, Lee J, Goldfine AB: **Inflammation and insulin resistance.** *J Clin Invest* 2006, **116:**1793-1801. Erratum in: J Clin Invest. 2006,1116:2308.

3. Odegaard JI, Ricardo-Gonzalez RR, Goforth MH, Morel CR, Subramanian V, Mukundan L, Eagle AR, Vats D, Brombacher F, Ferrante AW, Chawla A: **Macrophage-specific PPARγ controls alternative activation and improves insulin resistance.** *Nature* 2007, **447:**1116-1120.

4. Odegaard JI, Ricardo-Gonzalez RR, Red Eagle A, Vats D, Morel CR, Goforth MH, Subramanian V, Mukundan L, Ferrante AW, Chawla A: **Alternative M2 activation of Kupffer cells by PPARδ ameliorates obesity-induced insulin resistance.** *Cell Metab* 2008, **7:**496-507.

5. Patel PS, Buras ED, Balasubramanyam A: **The role of the immune system in obesity and insulin resistance.** *J Obes* 2013, **2013:**616193.

6. Nio Y, Yamauchi T, Iwabu M, Okada-Iwabu M, Funata M, Yamaguchi M, Ueki K, Kadowaki T: **Monocyte chemoattractant protein-1 (MCP-1) deficiency enhances alternatively activated M2 macrophages and ameliorates insulin resistance and fatty liver in lipoatrophic diabetic A-ZIP transgenic mice.** *Diabetologia* 2012, **55:**3350-3358.

7. Charo IF: **Macrophage polarization and insulin resistance: PPARgamma in control.** *Cell Metab* 2007, **6:**96-98.

8. Murphy S, Xu J, Kochanek K, Statistics DoV: **Deaths: Final data for 2010.** *National Vital Statistics Reports* 2013, **61:**2013.

9. Huo Y, Guo X, Li H, Xu H, Halim V, Zhang W, Wang H, Fan Y-Y, Ong KT, Woo S-L, et al: **Targeted overexpression of inducible 6-phosphofructo-2-kinase in adipose tissue increases fat deposition but protects against diet-induced insulin resistance and inflammatory responses.** *J Biol Chem* 2012, **287:**21492-21500.

10. Huo Y, Guo X, Li H, Wang H, Zhang W, Wang Y, Zhou H, Gao Z, Telang S, Chesney J, et al: **Disruption of inducible 6-phosphofructo-2-kinase ameliorates diet-induced adiposity but exacerbates systemic insulin resistance and adipose tissue inflammatory response.** *J Biol Chem* 2010, **285:**3713-3721.

11. Weisberg SP, McCann D, Desai M, Rosenbaum M, Leibel RL, Ferrante AWJ: **Obesity is associated with macrophage accumulation in adipose tissue.** *J Clin Invest* 2003, **112:**1796-1808.

12. Lumeng CN, Deyoung SM, Bodzin JL, Saltiel AR: **Increased inflammatory properties of adipose tissue macrophages recruited during diet-induced obesity.** *Diabetes* 2007, **56:**16-23.

13. Kang K, Reilly SM, Karabacak V, Gangl MR, Fitzgerald K, Hatano B, Lee C-H: **Adipocyte-derived Th2 cytokines and myeloid PPARδ regulate macrophage polarization and insulin sensitivity.** *Cell Metab* 2008, **7:**485-495.

14. Huo Y, Guo X, Li H, Wang H, Zhang W, Wang Y, Zhou H, Gao Z, Telang S, Chesney J, et al: **Disruption of inducible 6-phosphofructo-2-kinase ameliorates diet-induced adiposity but exacerbates systemic insulin resistance and adipose tissue inflammatory response.** *J Biol Chem* 2010, **285:**3713-3721.

15. Guo X, Xu K, Zhang J, Li H, Zhang W, Wang H, Lange AJ, Chen YE, Huo Y, Wu C: **Involvement of inducible 6-phosphofructo-2-kinase in the anti-diabetic effect of PPARγ activation in mice.** *J Biol Chem* 2010, **285:**23711–23720.

16. Saberi M, Woods N-B, de Luca C, Schenk S, Lu JC, Bandyopadhyay G, Verma IM, Olefsky JM: **Hematopoietic cell-specific deletion of toll-like receptor 4 ameliorates hepatic and adipose tissue insulin resistance in high-fat-fed mice.** *Cell Metab* 2009, **10:**419-429.

17. Odegaard JI, Chawla A: **Mechanisms of macrophage activation in obesity-induced insulin resistance.** *Nat Clin Pract End Met* 2008, **4:**619-626.

18. Chinetti-Gbaguidi G, Staels B: **Macrophage polarization in metabolic disorders: functions and regulation.** *Curr Opin Lipidol* 2011, **22:**365-372.

19. Mantovani A, Sica A, Sozzani S, Allavena P, Vecchi A, Locati M: **The chemokine system in diverse forms of macrophage activation and polarization.** *Trends Immunol* 2004, **25:**677-686.

20. Liang C-P, Han S, Senokuchi T, Tall AR: **The macrophage at the crossroads of insulin resistance and atherosclerosis.** *Circ Res* 2007, **100:**1546-1555.

21. Bouhlel MA, Derudas B, Rigamonti E, Dievart R, Brozek J, Haulon S, Zawadzki C, Jude B, Torpier G, Marx N, et al: **PPARγ activation primes human monocytes into alternative M2 macrophages with anti-inflammatory properties.** *Cell Metabolism* 2007, **6:**137-143.

22. Sag D, Carling D, Stout RD, Suttles J: **Adenosine 5'-monophosphate-activated protein kinase promotes macrophage polarization to an anti-inflammatory functional phenotype.** *J Immunol* 2008, **181:**8633-8641.

23. Dnlap J, Loros, JJ, and DeCoursey, PJ.: *Chronobiology: Biological Timekeeping.* Sunderland, MA, US: Sinauer Associates; 2004.

24. Bass J: **Circadian topology of metabolism.** *Nature* 2012, **491:**348-356.

25. Green CB, Takahashi JS, Bass J: **The meter of metabolism.** *Cell* 2008, **134:**728-742.

26. Gimble JM, Sutton GM, Bunnell BA, Ptitsyn AA, Floyd ZE: **Prospective influences of circadian clocks in adipose tissue and metabolism.** *Nat Rev Endocrinol* 2011, **7:**98-107.

27. Frank A.J.L. Scheer MFH, Christos S. Mantzoros, and Steven A. Shea.: **Adverse metabolic and cardiovascular consequences of circadian misalignment.** *PNAS* 2009, **106:**4453-4458.

28. Kohsaka A, Laposky AD, Ramsey KM, Estrada C, Joshu C, Kobayashi Y, Turek FW, Bass J: **High-fat diet disrupts behavioral and molecular circadian rhythms in mice.** *Cell Metab* 2007, **6:**414-421.

29. Bass J, Takahashi JS: **Circadian integration of metabolism and energetics.** *Science* 2010, **330:**1349-1354.

30. Eve Van Cauter KSP, Andre J. Scheen: **Roles of circadian rhythmicity and sleep in human glucose regulation.** *Endocrine Reviews* 1997, **18:**716-738.

31. Shi SQ, Ansari TS, McGuinness OP, Wasserman DH, Johnson CH: **Circadian disruption leads to insulin resistance and obesity.** *Curr Biol* 2013, **23:**372-381.

32. Chesney J, Telang S, Yalcin A, Clem A, Wallis N, Bucala R: **Targeted disruption of inducible 6-phosphofructo-2-kinase results in embryonic lethality.** *Biochem Biophys Res Commun* 2005, **331:**139-146.

33. Okar DA, Lange AJ: **Fructose-2,6-bisphosphate and control of carbohydrate metabolism in eukaryotes.** *Biofactors* 1999, **10:**1-14.

34. Okar DA, Manzano A, Navarro-Sabate A, Riera L, Bartrons R, Lange AJ: **PFK-2/FBPase-2: maker and breaker of the essential biofactor fructose-2,6-bisphosphate.** *Trends Biochem Sci* 2001, **26:**30-35.

35. Atsumi T, Chesney J, Metz C, Leng L, Donnelly S, Makita Z, Mitchell R, Bucala R: **High expression of inducible 6-phosphofructo-2-kinase/fructose-2,6-**

bisphosphatase (iPFK-2; PFKFB3) in human cancers. *Cancer Res* 2002, **62:**5881-5887.

36. Chesney J, Mitchell R, Benigni F, Bacher M, Spiegel L, Al-Abed Y, Hee Han J, Metx C, Bucala R: **An inducible gene product for 6-phosphofructo-2-kinase with an AU-rich instability element: role in tumor cell glycolysis and the Warburg effect.** *Proc Natl Acad Sci USA* 1999, **96:**3047-3052.

37. Atsumi T, Nishio T, Niwa H, Takeuchi J, Bando H, Shimizu C, Yoshioka N, Bucala R, Koike T: **Expression of inducible 6-phosphofructo-2-kinase/fructose-2,6-bisphosphatase/PFKFB3 isoforms in adipocytes and their potential role in glycolytic regulation.** *Diabetes* 2005, **54:**3349-3357.

38. Stienstra R, Duval C, Keshtkar S, van der Laak J, Kersten S, Muller M: **Peroxisome proliferator-activated receptor γ activation promotes infiltration of alternatively activated macrophages into adipose tissue.** *J Biol Chem* 2008, **283:**22620-22627.

39. Hossain P, Kawar B, El Nahas M: **Obesity and diabetes in the developing world--a growing challenge.** *N Engl J Med* 2007, **356:**213-215.

40. Angulo P: **Nonalcoholic fatty liver disease.** *N Engl J Med* 2002, **346:**1221-1231.

41. Jensen MK, Chiuve SE, Rimm EB, Dethlefsen C, Tjonneland A, Joensen AM, Overvad K: **Obesity, behavioral lifestyle factors, and risk of acute coronary events.** *Circulation* 2008, **117:**3062-3069.

42. Weisberg SP, McCann D, Desai M, Rosenbaum M, Leibel RL, Ferrante AW, Jr.: **Obesity is associated with macrophage accumulation in adipose tissue.** *J Clin Invest* 2003, **112:**1796-1808.

43. Kang K, Reilly SM, Karabacak V, Gangl MR, Fitzgerald K, Hatano B, Lee CH: **Adipocyte-derived Th2 cytokines and myeloid PPARdelta regulate macrophage polarization and insulin sensitivity.** *Cell Metab* 2008, **7:**485-495.

44. Guo X, Xu K, Zhang J, Li H, Zhang W, Wang H, Lange AJ, Chen YE, Huo Y, Wu C: **Involvement of inducible 6-phosphofructo-2-kinase in the anti-diabetic effect of peroxisome proliferator-activated receptor gamma activation in mice.** *J Biol Chem* 2010, **285:**23711-23720.

45. Qatanani M, Lazar MA: **Mechanisms of obesity-associated insulin resistance: many choices on the menu.** *Genes Dev* 2007, **21:**1443-1455.

46. Kahn BB, Flier JS: **Obesity and insulin resistance.** *J Clin Invest* 2000, **106:**473-481.

47. Rosen ED, Spiegelman BM: **Adipocytes as regulators of energy balance and glucose homeostasis.** *Nature* 2006, **444:**847-853.

48. Badman MK, Flier JS: **The adipocyte as an active participant in energy balance and metabolism.** *Gastroenterology* 2007, **132:**2103-2115.

49. Hotamisligil GS, Peraldi P, Budavari A, Ellis R, White MF, Spiegelman BM: **IRS-1-mediated inhibition of insulin receptor tyrosine kinase activity in TNF-alpha- and obesity-induced insulin resistance.** *Science* 1996, **271:**665-668.

50. Cheung AT, Ree D, Kolls JK, Fuselier J, Coy DH, Bryer-Ash M: **An *in vivo* model for elucidation of the mechanism of tumor necrosis factor-alpha (TNF-alpha)-induced insulin resistance: evidence for differential regulation of insulin signaling by TNF-alpha.** *Endocrinology* 1998, **139:**4928-4935.

51. Cheung AT, Wang J, Ree D, Kolls JK, Bryer-Ash M: **Tumor necrosis factor-alpha induces hepatic insulin resistance in obese Zucker (fa/fa) rats via interaction of leukocyte antigen-related tyrosine phosphatase with focal adhesion kinase.** *Diabetes* 2000, **49:**810-819.

52. Boden G, Cheung P, Stein TP, Kresge K, Mozzoli M: **FFA cause hepatic insulin resistance by inhibiting insulin suppression of glycogenolysis.** *Am J Physiol Endocrinol Metab* 2002, **283:**E12-19.

53. Berg AH, Combs TP, Du X, Brownlee M, Scherer PE: **The adipocyte-secreted protein Acrp30 enhances hepatic insulin action.** *Nat Med* 2001, **7:**947-953.

54. Kabir M, Catalano KJ, Ananthnarayan S, Kim SP, Van Citters GW, Dea MK, Bergman RN: **Molecular evidence supporting the portal theory: a causative link between visceral adiposity and hepatic insulin resistance.** *Am J Physiol Endocrinol Metab* 2005, **288:**E454-461.

55. Xu H, Barnes GT, Yang Q, Tan G, Yang D, Chou CJ, Sole J, Nichols A, Ross JS, Tartaglia LA, Chen H: **Chronic inflammation in fat plays a crucial role in the development of obesity-related insulin resistance.** *J Clin Invest* 2003, **112:**1821-1830.

56. Stienstra R, Duval C, Keshtkar S, van der Laak J, Kersten S, Muller M: **Peroxisome proliferator-activated receptor gamma activation promotes infiltration of alternatively activated macrophages into adipose tissue.** *J Biol Chem* 2008, **283:**22620-22627.

57. Todoric J, Löffler M, Huber J, Bilban M, Reimers M, Kadl A, Zeyda M, Waldhäusl W, Stulnig T: **Adipose tissue inflammation induced by high-fat diet in obese diabetic mice is prevented by n-3 polyunsaturated fatty acids.** *Diabetologia* 2006, **49:**2109-2119.

58. Lumeng CN, Bodzin JL, Saltiel AR: **Obesity induces a phenotypic switch in adipose tissue macrophage polarization.** *J Clin Invest* 2007, **117:**175-184.

59. Odegaard JI, Ricardo-Gonzalez RR, Goforth MH, Morel CR, Subramanian V, Mukundan L, Red Eagle A, Vats D, Brombacher F, Ferrante AW, Chawla A: **Macrophage-specific PPARgamma controls alternative activation and improves insulin resistance.** *Nature* 2007, **447:**1116-1120.

60. Odegaard JI, Ricardo-Gonzalez RR, Red Eagle A, Vats D, Morel CR, Goforth MH, Subramanian V, Mukundan L, Ferrante AW, Chawla A: **Alternative M2 activation of Kupffer cells by PPARdelta ameliorates obesity-induced insulin resistance.** *Cell Metab* 2008, **7:**496-507.

61. Saberi M, Woods NB, de Luca C, Schenk S, Lu JC, Bandyopadhyay G, Verma IM, Olefsky JM: **Hematopoietic cell-specific deletion of toll-like receptor 4 ameliorates hepatic and adipose tissue insulin resistance in high-fat-fed mice.** *Cell Metab* 2009, **10:**419-429.

62. Solinas G, Vilcu C, Neels JG, Bandyopadhyay GK, Luo JL, Naugler W, Grivennikov S, Wynshaw-Boris A, Scadeng M, Olefsky JM, Karin M: **JNK1 in hematopoietically derived cells contributes to diet-induced inflammation and insulin resistance without affecting obesity.** *Cell Metab* 2007, **6:**386-397.

63. Han MS, Jung DY, Morel C, Lakhani SA, Kim JK, Flavell RA, Davis RJ: **JNK expression by macrophages promotes obesity-induced insulin resistance and inflammation.** *Science* 2013, **339:**218-222.

64. Turek FW, Joshu C, Kohsaka A, Lin E, Ivanova G, McDearmon E, Laposky A, Losee-Olson S, Easton A, Jensen DR, et al: **Obesity and metabolic syndrome in circadian Clock mutant mice.** *Science* 2005, **308:**1043-1045.

65. Marcheva B, Ramsey KM, Buhr ED, Kobayashi Y, Su H, Ko CH, Ivanova G, Omura C, Mo S, Vitaterna MH, et al: **Disruption of the clock components CLOCK and BMAL1 leads to hypoinsulinaemia and diabetes.** *Nature* 2010, **466:**627-631.

66. Paschos GK, Ibrahim S, Song WL, Kunieda T, Grant G, Reyes TM, Bradfield CA, Vaughan CH, Eiden M, Masoodi M, et al: **Obesity in mice with adipocyte-specific deletion of clock component Arntl.** *Nat Med* 2012, **18:**1768-1777.

67. Keller M, Mazuch J, Abraham U, Eom GD, Herzog ED, Volk H-D, Kramer A, Maier B: **A circadian clock in macrophages controls inflammatory immune responses.** *Proc Natl Acad Sci USA* 2009, **106:**21407-21412.

68. Gibbs JE, Blaikley J, Beesley S, Matthews L, Simpson KD, Boyce SH, Farrow SN, Else KJ, Singh D, Ray DW, Loudon ASI: **The nuclear receptor REV-**

ERBa mediates circadian regulation of innate immunity through selective regulation of inflammatory cytokines. *Proc Natl Acad Sci USA* 2012, **109:**582-587.

69. Castanon-Cervantes O, Wu M, Ehlen JC, Paul K, Gamble KL, Johnson RL, Besing RC, Menaker M, Gewirtz AT, Davidson AJ: **Dysregulation of inflammatory responses by chronic circadian disruption.** *J Immunol* 2010, **185:**5796-5805.

70. Yoo S-H, Yamazaki S, Lowrey PL, Shimomura K, Ko CH, Buhr ED, Siepka SM, Hong H-K, Oh WJ, Yoo OJ, et al: **PERIOD2::LUCIFERASE real-time reporting of circadian dynamics reveals persistent circadian oscillations in mouse peripheral tissues.** *Proc Natl Acad Sci USA* 2004, **101:**5339-5346.

71. Bae K, Jin X, Maywood ES, Hastings MH, Reppert SM, Weaver DR: **Differential functions of mPer1, mPer2, and mPer3 in the SCN circadian clock.** *Neuron* 2001, **30:**525-536.

72. Wu C, Okar DA, Newgard CB, Lange AJ: **Overexpression of 6-phosphofructo-2- kinase/fructose-2,6-bisphosphatase in mouse liver lowers blood glucose by suppression of hepatic glucose production.** *J Clin Invest* 2001, **107:**91-98.

73. Wu C, Kang JE, Peng L, Li H, Khan SA, Hillard CJ, Okar DA, Lange AJ: **Enhancing hepatic glycolysis reduces obesity: Differential effects on lipogenesis depend on site of glycolytic modulation.** *Cell Metab* 2005, **2:**131-140.

74. Ko ML, Shi L, Tsai JY, Young ME, Neuendorff N, Earnest DJ, Ko GY: **Cardiac-specific mutation of Clock alters the quantitative measurements of physical activities without changing behavioral circadian rhythms.** *J Biol Rhythms* 2011, **26:**412-422.

75. Farnell YF, Shende VR, Neuendorff N, Allen GC, Earnest DJ: **Immortalized cell lines for real-time analysis of circadian pacemaker and peripheral oscillator properties.** *Eur J Neurosci* 2011, **33:**1533-1540.

76. Prieur X, Mok CYL, Velagapudi VR, Núñez V, Fuentes L, Montaner D, Ishikawa K, Camacho A, Barbarroja N, O'Rahilly S, et al: **Differential lipid partitioning between adipocytes and tissue macrophages modulates macrophage lipotoxicity and M2/M1 polarization in obese mice.** *Diabetes* 2011.

77. Huo Y, Guo X, Li H, Xu H, Halim V, Zhang W, Wang H, Fan YY, Ong KT, Woo SL, et al: **Targeted overexpression of inducible 6-phosphofructo-2-kinase in adipose tissue increases fat deposition but protects against diet-induced insulin resistance and inflammatory responses.** *J Biol Chem* 2012, **287:**21492-21500.

78. Guo X, Li H, Xu H, Halim V, Thomas LN, Woo SL, Huo Y, Chen YE, Sturino JM, Wu C: **Disruption of inducible 6-phosphofructo-2-kinase impairs the suppressive effect of PPARgamma activation on diet-induced intestine inflammatory response.** *J Nutr Biochem* 2013, **24:**770-775.

79. Guo X, Li H, Xu H, Halim V, Zhang W, Wang H, Ong KT, Woo SL, Walzem RL, Mashek DG, et al: **Palmitoleate induces hepatic steatosis but suppresses liver inflammatory response in mice.** *PLoS ONE* 2012, **7:**e39286.

80. Herzig S, Hedrick S, Morantte I, Koo SH, Galimi F, Montminy M: **CREB controls hepatic lipid metabolism through nuclear hormone receptor PPAR-g.** *Nature* 2003, **426:**190-193.

81. Zhang J, Fu M, Cui T, Xiong C, Xu K, Zhong W, Xiao Y, Floyd D, Liang J, Li E, et al: **Selective disruption of PPARg2 impairs the development of adipose tissue and insulin sensitivity.** *Proc Natl Acad Sci USA* 2004, **101:**10703-10708.

82. Kamei N, Tobe K, Suzuki R, Ohsugi M, Watanabe T, Kubota N, Ohtsuka-Kowatari N, Kumagai K, Sakamoto K, Kobayashi M, et al: **Overexpression of monocyte chemoattractant protein-1 in adipose tissues causes macrophage recruitment and insulin resistance.** *J Biol Chem* 2006, **281:**26602-26614.

83. Spengler ML, Kuropatwinski KK, Comas M, Gasparian AV, Fedtsova N, Gleiberman AS, Gitlin II, Artemicheva NM, Deluca KA, Gudkov AV, Antoch MP: **Core circadian protein CLOCK is a positive regulator of NF-kB-mediated transcription.** *Proc Natl Acad Sci USA* 2012, **109:**E2457â≠“E2465.

84. Fontaine C, Rigamonti E, Pourcet B, Duez Hln, Duhem C, Fruchart J-C, Chinetti-Gbaguidi G, Staels B: **The nuclear receptor Rev-erba is a liver X receptor (LXR) target gene driving a negative feedback loop on select LXR-induced pathways in human macrophages.** *Mol Endocrinol* 2008, **22:**1797-1811.

85. Bouhlel MA, Derudas B, Rigamonti E, Dievart R, Brozek J, Haulon S, Zawadzki C, Jude B, Torpier G, Marx N, et al: **PPARgamma activation primes human monocytes into alternative M2 macrophages with anti-inflammatory properties.** *Cell Metab* 2007, **6:**137-143.

86. Hevener AL, Olefsky JM, Reichart D, Nguyen MT, Bandyopadyhay G, Leung HY, Watt MJ, Benner C, Febbraio MA, Nguyen AK, et al: **Macrophage PPARg is required for normal skeletal muscle and hepatic insulin sensitivity and full antidiabetic effects of thiazolidinediones.** *J Clin Invest* 2007, **117:**1658-1669.

87. **Diabetes Surveillance.** Atlanta, GA: Centers for Disease Control and Prevention. Dept. of Health and Human Services; 1993: 87-93

88. Lloyd-Jones D, Adams R, Carnethon M, De Simone G, Ferguson TB, Flegal K, Ford E, Furie K, Go A, Greenlund K, et al: **Heart disease and stroke statistics--2009 update: a report from the American Heart Association Statistics Committee and Stroke Statistics Subcommittee.** *Circulation* 2009, **119:**e21-181.

89. Chesney J, Telang S, Yalcin A, Clem A, Wallis N, Bucala R: **Targeted disruption of inducible 6-phosphofructo-2-kinase results in embryonic lethality.** *Biochem Biophys Res Commun* 2005, **331:**139-146.

90. Wu C, Khan SA, Peng LJ, Li H, Camela S, Lange AJ: **Perturbation of glucose flux in the liver by decreasing fructose-2,6-bisphosphate levels causes hepatic insulin resistance and hyperglycemia.** *Am J Physiol Endocrinol Metab* 2006, **291:**E536-543.

91. Xu H, Li H, Woo SL, Kim SM, Shende VR, Neuendorff N, Guo X, Guo T, Qi T, Pei Y, et al: **Myeloid cell-specific disruption of Period1 and Period2 exacerbates diet-induced inflammation and insulin resistance.** *J Biol Chem* 2014, **289:**16374-16388.

92. Payne VA, Arden C, Wu C, Lange AJ, Agius L: **Dual role of phosphofructokinase-2/fructose bisphosphatase-2 in regulating the compartmentation and expression of glucokinase in hepatocytes.** *Diabetes* 2005, **54:**1949-1957.

93. Wang H, Zhang W, Zhu C, Bucher C, Blazar BR, Zhang C, Chen J-F, Linden J, Wu C, Huo Y: **Inactivation of the adenosine A2A receptor protects apolipoprotein E-deficient mice from atherosclerosis.** *Arterioscler Thromb Vasc Biol* 2009, **29:**1046-1052.

94. Lumeng CN, Deyoung SM, Saltiel AR: **Macrophages block insulin action in adipocytes by altering expression of signaling and glucose transport proteins.** *Am J Physiol Endocrinol Metab* 2007, **292:**E166-174.

95. Zhuang G, Meng C, Guo X, Cheruku PS, Shi L, Xu H, Li H, Wang G, Evans AR, Safe S, et al: **A novel regulator of macrophage activation: miR-223 in obesity-associated adipose tissue inflammation.** *Circulation* 2012, **125:**2892-2903.